CONTENTS — H through L

ON THE DYNAMICAL EVOLUTION OF A NEBULA AND ITS EFFECT ON DUST COAGULATION AND THE FORMATION OF CENTIMETER-SIZED PARTICLES. N. Haghighipour, *Institute for Astronomy, and NASA Astrobiology Institute, University of Hawaii, Honolulu HI 96822, USA (nader@ifa.hawaii.edu).*

A planet-forming nebula is a dynamic environment with properties and structure that vary with time. The time-varying structure of such a dynamic environment has considerable effects on the dynamics of its solid particles and the formation of larger objects. Among such structures, regions where the pressure of the gas is locally enhanced are of particular interest. The appearance of such regions along with the combined effects of gas-drag and pressure gradients causes solid particles in their vicinities to migrate toward their centers, and accumulate in that region. While migrating, solid particles sweep up smaller objects and grow in size. In this paper, the effects of the appearance of pressure-enhanced structures on collision and coalescence of micron-sized particles are studied. The effects of gas-drag and pressure gradients on the rate of accumulation of centimeter-sized objects in the regions of local maximum pressure on the midplane are investigated, and the role that changes in physical properties of the gas play in variation of the sticking velocities of particles in the neighborhood of such structures are discussed.

Motivation

It is widely accepted that planet formation starts in a protostellar disk of gas and dust by collisional coagulation of dust particles to larger objects. Processes such as differential settling, turbulence, relative orbital decay, and transverse and Brownian motions have been suggested as means of generating relative velocities, and causing collisions among such particles [1,2].

Solid particles, at beginning of the planet formation process, are strongly coupled to the gas, and their dynamics are governed by the gravitational attraction of the central star, and also by their interaction with the nebula through gas-drag. This interaction is quite dynamic and varies as the nebula evolves. During the evolution of the nebula, while the physical properties of the gas, such as its density, pressure and temperature, vary with time, the gas-particle interaction manifests itself differently, and causes the gas to exert different drag forces on solid particles. This affects the motions of grains, their relative velocities, and their sedimentation on the midplane, and will ultimately affect their collision and coagulation to larger objects.

The time variations of the physical properties of the gas are results of variations in the structure of the nebula. For instance, in a dynamically evolving nebula, regions may appear where the pressure, or density of the gas is locally enhanced. In the vicinity of such regions, the pressure gradients-induced velocity-difference between solids and gas molecules causes solid particles to undergo inward and outward migrations, and accumulate around the pressure-enhanced regions [3,4]. The effect that such accumulations can have on the mutual interactions of small solids, and also possible increase in their rates of collisions and coagulation to larger objects, call for a clear understanding of the dynamical evolution of solids around such regions, and the effects that the appearance of such structures may have on the growth and settling of particles during the structures' life-times. The focus of this paper is to address and study such issues. In order to focus attention on the role that different physical phenomena, and values of different parameters of the system play in the growth and sedimentation of particles in the neighborhood of a pressure maximum region, the collision and coalescence of small particles are studied in a heuristic model. The details of this model are explained below.

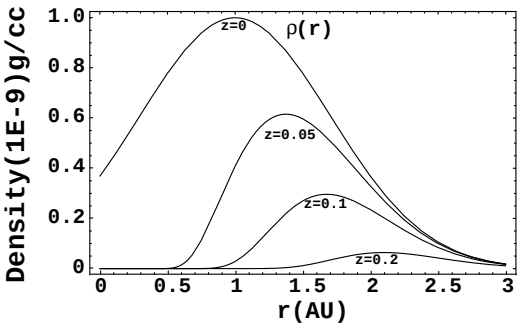

Figure 1.

Physical Model

The model nebula considered here consists of a turbulence free, isothermal rotating gaseous disk of pure molecular hydrogen and a background material of submicron sized particles. The spatial density of this particulate material is considered to be proportional to the gas distribution function given that submicron particles are strongly coupled to the gas and their gas-drag induced migrations are negligible. The density of the gas has been chosen such that on the midplane it has an azimuthally symmetric maximum (figure 1) and along the

z-axis, the vertical component of the gravitational attraction of the central star is balanced by the vertical component of the pressure gradients.

Since molecular hydrogen is an ideal gas, in such a nebula, locations of density enhancements correspond to the locations of maximum pressure. The motions of solids, subject to the gravitational attraction of the central star and also the drag force of the gas, for different values of solids' radii and densities, and also for different values of the gas temperature, have been studied. Presented below are the results of a sample run.

Numerical Results

Equation of motion of a solid particle with a radius of 1 micron was integrated numerically. The solid/gas ratio, f, was chosen to be 0.0034, and the density of the particle was 1 gcm^{-3}. Figure 2 shows the results of this simulation for a nebula with a temperature of 300 K. The particle was initially given a Keplerain circular velocity with no initial velocity along the z-axis. The top graph of figure 2 shows the growth of this object as a result of a sweeping up of the particles of the background. The middle and bottom graphs show the radial and vertical motions of this particle during the same time. These figures demonstrate that as the object approaches (1,0) AU, the location of maximum pressure on the midplane, it grows to a few centimeters in size by sweeping up the smaller particles of the background material. As a point of comparison, the motion of the object without mass-growth has also been plotted. As shown in figure 2, due to growth in size, small dust grains can rapidly descend to the midplane and, as a result, increase the density of centimeter-sized objects in that region. The maximum velocity of such objects required for their sticking to the particles of the background is also affected by their growth and migration. Figure 3 shows the graph of the sticking velocity of the 1 micron object above during its descent. As shown here, as the object grows, its maximum velocity required for a perfect inelastic collision with the 0.1 micron particles of the background also increase. The results of a comprehensive study of this process are presented and the effect of interactions among such centimeter-sized solids on the rate of their accumulation, as well as their growth to larger objects in the vicinity of the midplane is discussed.

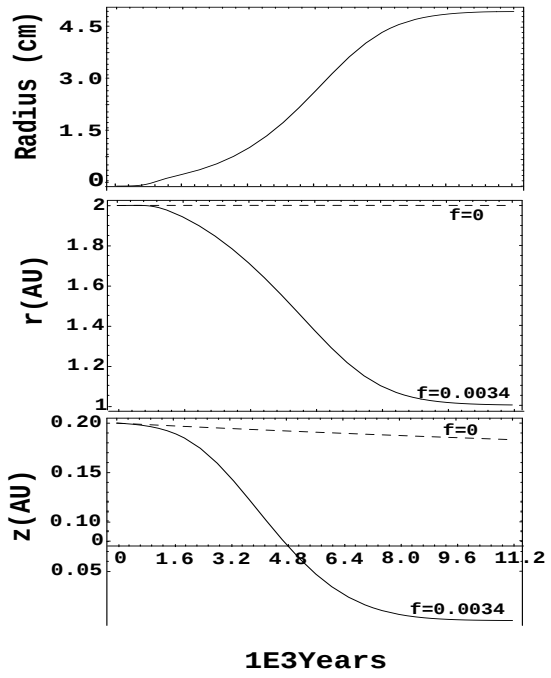

Figure 2

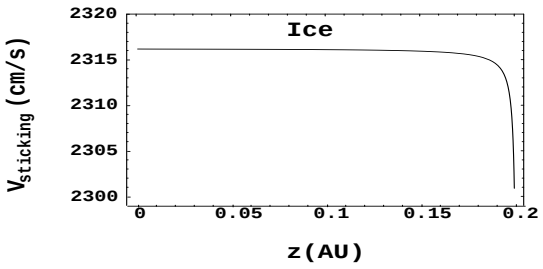

Figure 3

References

[1] Weidenschilling S. J., 1988, in *Meteorites and the Early Solar System* (J. Kerridge and M. S. Matthews, Eds.), pp. 348-371, Univ. Arizona Press, Tucson. [2] Weidenschilling S. J., and Cuzzi J. N., 1993, in *Protostars and Planets* (E. H. Levy and J. I. Lunine, Eds.), pp. 1031-1060, Univ. Arizona Press, Tucson. [3] Haghighipour N., and Boss A. P., ApJ, **583**, 996. [4] Haghighipour N., and Boss A. P., ApJ, **598**, 1301.

THE MINERALOGY AND GRAIN PROPERTIES OF THE DISK SURFACES IN THREE HERBIG Ae/Be STARS D. E. Harker[1], D. H. Wooden[2], and C.E. Woodward[3], [1]University of California, San Diego, Center for Astrophysics and Space Sciences, 9500 Gilman Dr., La Jolla, CA 92093-0424, [2]NASA Ames Research Center, MS 245-3, Moffett Field, CA 94035-1000, [3]University of Minnesota, Astronomy Department, School of Physics and Astronomy, 116 Church Street, S.E., Minneapolis, MN 55455.

Introduction: The ubiquity of accretion disks around pre-main sequence and young main sequence stars having the potential to form planetary systems is now well established [1]. However, unknown is an accurate estimate of the fraction of single stars with disks that have produced planetary systems. Theoretical models of particle aggregation show that if particles can grow from submicron to mm to cm in size, then the formation of planetesimals is possible in the time before the disk dissipates [2]. The problem remains to understand how grains condense from nebular gases, and how relic interstellar grains survive and are modified by their transport in the disk. If grains are lofted above the disk photosphere by processes such as winds, turbulent convection, or changes in vertical structure, the evolution of dust can be investigated by observing the properties of the small ($\leq 1\mu m$) grains in the optically thin disk surface layer or atmosphere.

In this work, we examine the thermal emission from three Herbig Ae/Be stars of similar spectral type: HD150193 (A1V), HD100546 (B9V), and HD179218 (B9). The stellar ages of the objects are: 2×10^6 yrs, 10×10^6 yrs, and 0.5×10^6 yrs for HD150193, HD100546 and HD179218, respectively [3]. We chose these objects for study because they are isolated (not belonging to any know star forming region), have little to no active accretion, possess possible processing circumstellar disks, and have varying degrees of silicate crystallinity [4]. We assemble and model SEDs for each system using a passive reprocessing circumstellar disk to constrain the amount of crystals and flaring of the disk in each of the systems.

Observations: Spectrophotometry of HD150193, HD100546, and HD179218 was obtained using the NASA Ames Research Center *HI*gh efficiency *F*aint *O*bject *G*rating *S*pectrometer (HIFOGS) [5]. The spectrum of HD179218 was obtained on the 2.34-m telescope at the Wyoming Infrared Observatory using 32-bit FORTH telescope software. The spectra of HD150193 and HD100546 were obtained on the 4-m Blanco telescope at the National Optical Astronomical Observatories Cerro Tololo Inter-American Observatory in Chile.

We also obtained 1.2 – 23.0 μm IR broad- and narrow-band photometric observations of HD179218 on 2001 April 30.42 UT using the University of Minnesota Mount Lemmon Observing Facility 1.52 m telescope and the UM multi-filter bolometer [6].

SED Assembly: Data from the European Space Agency Infrared Space Observatory (*ISO*) Short-Wavelength Spectrometer (SWS) and the Infrared Astronomical Observatory(IRAS) are used to expand the wavelength coverage of the spectral energy distribution (SED) of each of our three HAEBEs. All of the data sets for each object were scaled to the HIFOGS spectra.

Disk Model: We use a mineralogically enhanced version of the radiative, hydrostatic models of passively irradiated circumstellar disk [7] (hereafter CG97) that had been developed to include some discrete minerals [8] (hereafter C01). The CG97 disk is composed of two parts: an optically thin surface layer and an optically thick interior. C01 updated the CG97 model by adding a range of grain sizes and incorporating a simple mineralogy through the use of laboratory determined optical constants, including water ice, amorphous olivine, and metallic Fe. In this work, we use the updated model of C01 with our own enhanced feature of adding crystalline olivine grains into the optically thin surface layer. We also divide the disk into an inner and outer region in which we can independently vary the crystalline to amorphous silicate ratio to provide the best fit to the SED.

Crystalline Silicates: It is difficult to model the thermal emission from crystalline silicate grains [9]. In this work, we choose to calculate the crystalline silicate emission from ellipsoids by elongating the crystals along one of the three crystalline axes [10]. Based on the location of the resonance peaks in the HIFOGS and *ISO* SWS spectra of HD150193 and HD179218, we use an axis ratio of 10:1:1 to compute the optical efficiencies of the crystals. The crystalline silicates are not coated with ice since to do so requires mixing theory which eliminates the distinctive crystalline resonances. We compute the thermal emission from the crystals in the disk surface layer of each object. By dividing the disk into two regions, (inner and outer) we can vary the crystalline to amorphous silicate ratio to fit the model to the SED.

Results: Our model results are displayed in Fig. 1. To produce the best-fit model to the SEDs, HD100546 and HD179218 are both modeled with a disk 150 AU in radius, while HD150193 is modeled with a disk 5 AU in radius. The best fit SEDs for HD 100546 uses a

photosphere to gas scale height (*H/h*) of 4, *H/h* = 3 for HD150193, and *H/h* = 1 for HD179218. This means at a disk radius of 5 AU the disk around HD100546 flares about 80% more than the disk around HD179218, and about 25% more than the disk around HD150193. The model fits suggests that the measured emission from HD150193 is dominated by warm dust in a flaring disk close to the central star, and that the emission from grains in an extended disk (> 5 AU) is relatively small compared to the other two objects.

HD100546 and HD179218 show evidence of crystalline silicates, while the emission from HD150193 is dominated by amorphous silicates. For the two objects with crystalline silicates, we find that a better fit is produced to the observed SEDs of the objects if we use a model in which a higher ratio of crystalline to amorphous silicates is located in the inner regions of the disk (< 5 AU) compared to the outer regions of the disk (5 – 150 AU). The inner region of HD100546 has 30% more crystalline silicates compared to the outer region. This is contrary to the findings of [11] who used a spherical shell model to calculate a factor of almost 10 higher fraction of crystalline silicates in regions greater than 10 AU. The inner region of HD 179218 has 76% more crystalline silicates compared to the outer region.

All three SEDs are best fit using a grain size distribution with a slope of $q = -3.5$ (i.e., $a^{-3.5}$) .

Discussion: It is difficult to make any statistically significant conclusions about disk evolution from modeling only three objects. However, we can make some interesting observations based on our results. Although there is no evidence for grain growth (all three SEDs are modeled with the same grain size distribution) there is a difference in the radial distribution of crystalline silicates. A possible evolutionary scenario is one in which when circumstellar disks form around young stars, they are thought to be primarly composed of amorphous ISM grains [12]. As the disk evolves, crystalline silicates are condensed [13] or annealed [14] in the inner radial regions of the disk, either through heating [15] or through shocks in the disk [16]. The crystals are then transported to the outer regions of the disk [17]. Therefore, from this scenario, we can conclude that the disk around HD150193 is the least evolved since it does not contain any crystals, followed by HD179218 which has an even larger amount of crystals in the inner radial region compared to the outer radial region, and finally HD100546 which has a larger amount of crystals in the outer regions of its disk compared to HD179218.

References: [1] Koerner, D. E. (2001) *ASP Conf.~Ser.~231: Tetons 4: Galactic Structure, Stars and the Interstellar Medium, eds. C.E. Woodward and M.D. Bicay [ASP: San Fransico]*, 563. [2] Habing, H. J. (1999) *Nature*, 401, 456. [3] van den Ancker, M.E. et al. (1998), *A&A*, 330, 145. [4] Meeus, G. et al. (2001), *A&A*, 365, 476. [5] Witteborn, F. C. (1991), *in Airborne Astronomy Symposium on the Galactic Ecosystem: From Gas to Stars to Dust, ASP Conf. Ser., Vol. 73, ed. M. R. Haas et al. (San Fransisco: Astron. Soc. Pac.)*, 573. [6] Hanner, M. S. et al. (1990), *ApJ*, 348, 312. [7] Chiang, E. I. and Goldreich, P. (1997), *ApJ*, 490, 368. [8] Chiang, E. I. et al. (2001), *ApJ*, 547, 1077. [9] Yanamandra-Fisher, P. and Hanner, M. S. (1999), *Icarus*, 138, 107. [10] Fabian, D. et al. (2001), *A&A*, 378, 228. [11] Bouwman, J. et al. (2003), *A&A*, 401, 577. [12] Wooden. D. H. et al. (2004) *in Comets II ed. M. Festou, et al. (Tucson: Univ. Arizona Press)*, 33. [13] Grossman, L. (1972), *Geochim. Cosmochim. Acta.*, 38. [14] Rietmeijer, F. J. M. et al. (2002), *Icarus*, 156, 269 [15] Bockelée-Morvan, D. et al. (2002), *A&A*, 384, 1107[16] Harker, D. E. and Desch S. J. (2002), *ApJL*,

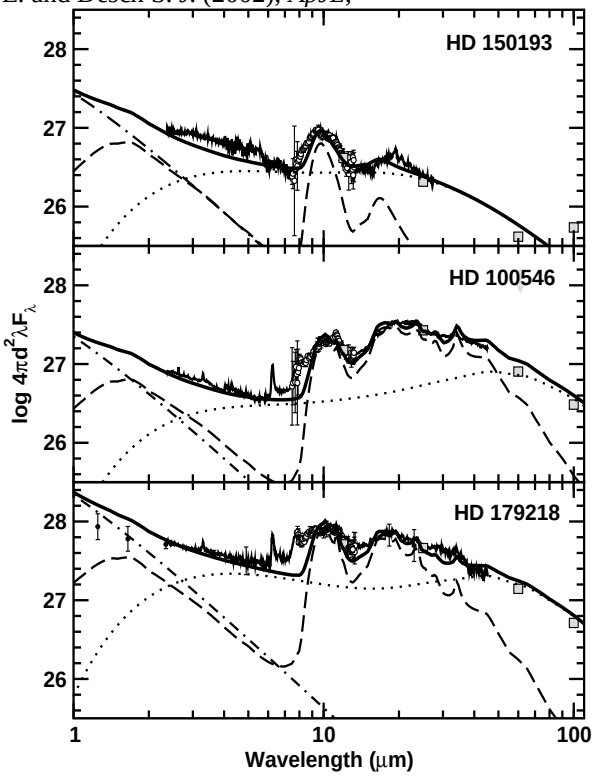

Figure 1. C01 model computed for HD150193, HD100546 and HD179218. The disk interior (dotted line), disk surface (dashed line), and stellar blackbody (dot-dash line) are co-added to produce the model SED (solid line). The model SED is compared to the assembled data sets including: *ISO* SWS spectra (solid, jagged line), HIFOGS spectra (open circles) and IRAS photometry points (gray squares). HD 179218 also has MLOF photometry points (filled circles).

ASTROPHYSICAL OBSERVATIONS OF DISK EVOLUTION AROUND SOLAR MASS STARS

Lee Hartmann, Center for Astrophysics, 60 Garden St., Cambridge, MA 02138

The time evolution of protoplanetary disks provides important clues to physical processes in disks including planet formation. I will review the implications of very short timescale variability of disks for disk structure, suggesting that the standard picture of surface density distributions may require significant modification. I will also consider the implications of the decay of disk accretion as a function of age for understanding angular momentum transport. Special emphasis will be placed on reviewing the very latest observational results, especially those from the Spitzer Space Telescope, on disk structure, gap clearing, and dust evolution. The wealth of new data now arriving from modern instruments emphasizes previous findings that a wide variety of behaviors and evolutionary timescales are seen in protoplanetary disks. Determining where the solar system fits within this increasing range of possibilities poses a major challenge to those attempting to bridge the gap between meteoritic and astrophysical disciplines.

THE SYSTEMATIC PETROLOGY OF CHONDRITES: A CONSISTENT APPROACH TO ASSIST CLASSIFICATION AND INTERPRETATION. Herd, R.K., Hunt, P.A., and Venance, K.E.[1], [1]Geological Survey of Canada, Natural Resources Canada, 601 Booth Street, Ottawa Canada K1A 0E8. herd@nrcan.gc.ca; pahunt@nrcan.gc.ca; kvenance@nrcan.gc.ca.

Introduction: Chondrites of all kinds comprise about 84 percent of known meteorites; they are a major class of extraterrestrial rocks whose detailed provenance has yet to be ascertained. Understanding their origin is critically dependent on understanding the origin of their chondrules and other constituents (matrix, CAIs, clasts, pre-solar grains etc.), how these have become associated, and what processes are documented by their lithology and petrology, including isotope chemistry. They can be compared to terrestrial rocks; they contain evidence that extraterrestrial "igneous"(melting, quenching, crystallization, re-melting), "sedimentary" (agglomeration) and "metamorphic" (cataclasis, re-crystallization) processes have acted upon them. They contain structures and textures produced by these processes. Petrological expertise used to describe and interpret terrestrial rocks can be adapted to derive important data from chondrites, but the chondrites and their components need to be imaged in detail before other analyses are done. Currently the nomenclature of chondrules is based in part upon their texture and in part upon their chemistry [1].

Background: With experience in mapping, collecting, examining and interpreting igneous, sedimentary and metamorphic terrestrial rocks, petrologists can contribute to the systematic study of chondrites. While the "field occurrence" of chondrites is still unknown (?as part of asteroids, comets or other planetesimals), space exploration will eventually provide a context for their Solar System setting, and laboratory work on chondritic meteorites will then help determine the origin of their parent bodies. So far this has generally been bulk analyses, mineralogy and mineral chemistry, and isotope studies on bulk samples, individual chondrules or other components, and on mineral phases. Textural documentation and interpretation have often been neglected; critical observational data on their physical properties or on the petrography of the rocks may not have been recorded before destructive chemical analyses.

Method: Our petrological studies on Canadian meteorites and comparative samples began in 1999 [2-10]. We have utilized polished thin sections and examined them with polarized-light petrographic microscopes and scanning-electron microscopes (SEM). Digital colour photomicrographs, and digitized back-scattered-electron (BSE) images from the SEM, the latter compiled into photomosaics of the polished thin sections, served to define the lithology and structure of the meteorites; they are the maps within the context of which detailed textural and analytical studies proceeded. The fine-grained texture of the chondrules and other components was documented with BSE images at magnifications up to 3000X. An energy-dispersive spectra (EDS) system on the SEM allowed qualitative identification of mineral phases prior to electron-microprobe analyses. All of the data collected during this systematic approach is available as digital files for future research. While our experience of many meteorites is limited (there are about 1100 different ones in the National Meteorite Collection of Canada [6]), we have examined the following in great detail: Kitchener, a veined L6 [2]; Tagish Lake, an anomalous C-chondrite [3]; an unnamed Antarctic L/LL3 [4,5,7,8]; Saratov, L4 [7,8,9]; and most recently other ordinary chondrites (OCs) of petrologic grade 4 – 6: these have been imaged and await mineral analyses.

Results: Textural and mineralogical similarities and contrasts among the different meteorites and their components were readily identified using our systematic approach to surveying the polished thin sections. By analogy with terrestrial metamorphic rocks, granoblastic-polygonal textures were recognized in the L6 samples; veined L6 OCs have been shocked and recrystallized at the tens of microns scale even though chondrule shape has been well preserved [2]. Within even small fragments of Tagish Lake, photomosaics revealed regions with primary porosity, and the BSE photos showed the boundary between carbonate-rich and carbonate-poor lithologies; apparently new phosphate phases were identified with EDS and probable pre-solar silicate grains were found in a magnesian olivine chondrule [3]. Chondrule textural types in the primitive OCs were grouped into those that occur frequently, whatever their size, and those that were rare or atypical; archetypical examples of the former were imaged and analyzed in detail, and all of the latter. In the studies of the L/LL3 and L4 all conventionally recognized chondrule types were found; textural variations within each type allowed many sub-types to be defined. A sequence of textural changes within chondrules in the L/LL3 and L4 samples indicated variable recrystallization between petrologic grades and within the same meteorites; some chondrules in both showed textures indicative of higher petrologic grade than their associated chondrules: they have been recrystallized prior to incorporation into their present host [4,5,7,8,9].

Variable recrystallization within the L/LL3 was taken to be indicative of a metamorphic age overprint [5]. By analogy to smelter particles, some porphyritic olivine-pyroxene chondrules (POP) in the L/LL3 and L4 have textures that suggested the large olivines were xeno-crystic [10]. Textures modified by progressive recrystallization from those seen within chondrules of petrologic grade 3-4 OCs have been recognized within OCs of petrologic grade 4, 5 or even 6, implying the ultimate origin of the higher grade meteorites by modification of the more primitive materials.

Conclusions: A systematic petrographic study of chondritic meteorites yields valuable data and should always precede detailed chemical or isotopic analyses. This documentation sets the context within which all other analyses are undertaken, just as the field context of terrestrial rocks sets the framework for subsequent study. The homogeneity or variability of the samples may be a major factor in interpreting the detailed analytical results. To facilitate consensus on textural terminology and interpretation, there is a need for an atlas of chondritic meteorites as a reference point for research [cf. 11]. The advent of digital imaging techniques means that digital photomicrographs and scanning-electron microscope images derived from systematic textural studies could be readily shared, compared and discussed among interested researchers. This could be done interactively through a dedicated web site and list.

References: [1] Brearley, A.J. and Jones, R.H. (1998) *MSA Reviews in Mineralogy, 36*.[2] Herd, R. K. (2000) *Meteoritics & Planet. Sci., 35, A70.* [3] Herd, R. K. et al. (2001) *LPS XXXII, #1928.* [4] Herd, R. K. et al. (2001) *Meteoritics & Planet. Sci., 36, A79*. [5] Herd, R. K. et al. (2002) *LPS XXXIII, #1957*. [6] Herd, R. K. (2002) *Meteoritics & Planet. Sci., 37, A62*. [7] Herd, R. K. (2003) *LPS XXXIV, #2058*. [8] Herd, R. K. et al. (2003) *Meteoritics & Planet. Sci., 38, A 145*. [9] Herd, R. K. et. al. (2004) *LPS XXXV, #2070.* [10] Knight, R.D. et al. (2004) *LPS XXXV, #1734*. [11] Corfu, F. et al. (2003) *Reviews in Mineralogy & Geochemistry, 53*.

UNDERSTANDING OUR ORIGINS: FORMATION OF SUN-LIKE STARS IN H II REGION ENVIRONMENTS. **Jeff Hester**, Dept. Physics and Astronomy, Arizona State University, Tempe, AZ 85287 (jhester@asu.edu).

In the introduction to their paper on modes of star formation, Adams & Meyers[1] note that, "If most star formation takes place within sufficiently dense environments, then the current theory of star formation could require substantial modification, or perhaps even a new paradigm." There is a great deal of truth in that statement.

Studies of low-mass star formation have historically focussed on regions in which low-mass stars form in relative isolation. The reasons for this emphasis are twofold. First, the Taurus-Auriga molecular cloud (the poster child for this mode of star formation) is nearby (140 parsecs), allowing disks and other structures in circumstellar environments to be studied in detail. Second, star formation in isolation has been considered to be the easier mode of star formation to understand [2].

There are many lines of evidence that this common bias about the environment in which most low-mass stars form is incorrect. One recent study of star formation within 2 kpc of the Sun found that a substantial majority ($\sim 70-90\%$) of young low-mass stars form instead in relatively dense clusters[3]. Of these, 90% or more form in relatively rich clusters of 100 or more members. It is especially important to note that 75% of the stars in this sample are in clusters that currently contain known O and/or early B stars. These results give the unambiguous impression that most low-mass Sun-like stars form in association with massive stars.

This conclusion differs dramatically from some earlier studies, which concluded that formation of low-mass Sun-like stars occurs predominately in much smaller groups[1,2]. This discrepancy can be attributed to the fact that the earlier studies underestimate the cluster formation rate by an order of magnitude. Quoting Lada & Lada[3], this difference "represents an enormous discrepancy and is of fundamental significance for understanding cluster formation an evolution." Previous studies have also argued that planetary systems would be disrupted in rich environments[4]. But this conclusion assumes that low-mass stars remain in their rich natal environments for a billion years or longer – an assumption that is not supported by more recent studies which show that over 90% of clusters disperse before reaching an age of 10 million years, and fewer than 4% of clusters remain intact for longer than 100 million years[3]. Disruption by close stellar encounters does not pose a problem for formation of planetary systems in cluster environments.

Low-mass star formation in rich environments containing massive stars is a significantly different process than low-mass star formation in environments such as Taurus-Auriga. A simple comparison of *HST* images of large, isolated disks in Taurus [5] with the "proplyds," "EGGs," and other manifestations of low-mass star formation in H II regions [6,7] makes this point in a clear and visible fashion. Massive stars deposit enormous amounts of energy into their environments during their brief lives. Most of this energy is in the form of ultraviolet radiation. A 60 $M_\odot$ O5 star has a luminosity of nearly 800,000 $L_\odot$ for most of its $\sim$360,000 year lifetime. This radiation ionizes and heats the gas around a star. (The volume of photoionized gas around a massive star is called an H II region.) Supernovae and stellar winds also deposit large amounts of energy into the environment around massive stars. Once a massive star forms, its radiative and mechanical luminosity quickly comes to dominate the structure and dynamics of the surrounding interstellar environment.

The decay products of a number of short-lived radionuclides with half-lives typically of order 10^6 years have been found in meteorites. Because of their short lifetimes, these radionuclides cannot be explained as simply the result of the integrated nucleosynthesis that had taken place prior to the birth of the Solar System. Instead, these short-lived radionuclides require a nucleosynthetic source in or near the solar nebula. Following the discovery of the decay products of ^{26}Al[8], it was suggested that a nearby supernova might have injected the ^{26}Al into the solar nebula, and that the shock from the supernova might even have been responsible for triggering the Sun's formation. An alternative suggestion was that spallation by cosmic ray protons accelerated in solar flares could account for the ^{26}Al. Over the intervening years the second of these suggestions found fairly broad acceptance, in large part because spallation would occur even in isolated star-forming environments like Taurus-Auriga. This is a central aspect of the "X-wind" model for the formation of the Sun[9]. This view was strengthened by the discovery of decay products of ^{10}Be in meteorites. ^{10}Be has no stellar nucleosynthetic source, but is formed readily by spallation. ^{10}Be seemed a "smoking gun" favoring spallation as a source for short-lived radiounclides, and Taurus-Auriga as representative of the environment in which the Sun was born.

This situation has changed dramatically over the last few years, largely due to two results. The first is the discovery of decay products of ^{60}Fe in meteorites[10]. ^{60}Fe is a neutron-rich isotope that cannot be readily formed

by spallation, but is a common product of nucleosynthesis in evolved massive stars. On its face, the presence of ^{60}Fe in meteorites requires that the young Solar System was near a supernova explosion. Models of supernova nucleosynthesis indeed show that a nearby supernova explosion can account for all of the short-lived radionuclides found, with the exception of ^{10}Be. This puzzle was answered by calculations showing that ^{10}Be would have been captured from the Galactic cosmic ray flux in just the right amounts to explain the meteorite results[11]. *We can now say with a high level of confidence that supernova nucleosynthesis provided the source for most of the short-lived radionuclides in the young Solar System, and that the Sun, like most low-mass stars, formed in the presence of luminous, massive stars.*

If one looks at a cluster containing massive stars one sees large numbers of young low-mass objects, many of which show evidence of surrounding disks, all sitting in the warm ($\sim 10^4$ K) ionized interior of the H II region. *These stars did not form in the low-density environments in which we see them today!* Rather, these stars *must* have formed in dense interstellar gas that was subsequently eroded away by the radiation and winds from massive stars, and by supernovae themselves. It is illustrative to consider the well-defined sequence of stages through which a low-mass star in an H II region must have passed[7,12]. As noted, a low-mass star forms in dense molecular gas around the periphery of an H II region. It is likely that the formation of this star was triggered by the expansion of the H II region[13], although this is not essential to our understanding of what comes next. Sometime within a few hundred thousand to a few million years after the star begins to form, it is overrun by the advancing ionization front. As the star is uncovered it will likely still be surrounded by the remnants of the dense core from which it formed and from which it may still be accreting mass. This is the "evaporating gaseous globule" or EGG phase of evolution, seen most clearly in *HST* observations of the Eagle Nebula[7]. (While not all EGGs contain stars, a signficant fraction do.) Within a few 10^4 years the EGG will evaporate, exposing the disk within. The object has become a "proplyd" – a photoevaporating circumstellar disk – like those seen in the Orion Nebula[6]. There are now a number of objects that are observed undergoing the transition from EGG to proplyd[12]. Proplyds themselves are short-lived. Within $\sim 10^4$ years radiation from the massive stars erodes the circumstellar disk down to a size of ~ 50 AU[14]. It is this state – a young low-mass star surrounded by a disk of roughly Solar System proportions, bathed in the UV radiation of a nearby massive star – in which the star remains until the nearby massive star undergoes a supernova explosion. Ejecta from that explosion will hit the preexisting disk. While the disk itself should survive the passage of the supernova ejecta, grains carrying newly synthesized elements including short-lived radionuclides should be injected efficienty into the disk. Preliminary simulations suggest that this process, which we are calling the "aerogel model", is capable of explaining the abundances of short-lived radionuclides found in meteorites[15].

Evolution in an H II region environment has numerous consequences for our understanding of the evolution of the Solar System, ranging from the myriad effects of the UV-rich environments in which the early stages of planet formation must take place, to the role of the decay of ^{26}Al in the differentiation of planetesimals. The scenario presented here is offered as a framework for understanding the ties between the astrophysical environment of star formation and the properties of planetary systems.

References: [1] Adams, F.C., & Meyers, P. C. 2001, *Ap.J.*, 553, 744 [2] Shu, F. H., Adams, F. C., & Lizano, S. 1987, *Ann. Rev. Astr. Astroph.*, 25, 23 [3] Lada, C. L., & Lada, E. A. 2003, *Ann. Rev. Astr. Astroph.*, 41, 57 [4] Adams, F. C. & Laughlin, G. 2001, *Icarus*, 150, 151 [5] e.g., Krist, J. E., et al. 1998, *Ap.J.*, 501, 841 [6] e.g., Bally, J., O'Dell, C. R., & McCaughrean, M. J. 2000, *Astron. J.*, 119, 2919 [7] Hester, J. J., et al. 1996, *Astron.J.*, 111, 2349 [8] Lee, T., Papanastassiou, D. A., & Wasserburg, G. J. 1976, *Geophys. Res. Lett.*, 3, 41 [9] Shu, F. H. et al. 2001, *Ap.J.*, 548, 1029 [10] Tachibana, S., & Huss, G. R. 2003, *Ap. J.*, 588, L41 [11] Desch, S. J., Connolly, H. C., Jr, & Srinivasan, G. 2004, *ApJ*, 602, 528 [12] Hester, J. J., Desch, S. J., Healy, K. R., & Leshin, L. A. 2004, *Science*, 304, 1116 [13] e.g., Healy, K. R., Hester, J. J., & Claussen, M. J. 2004, *Ap. J.*, 610, 835 [14] Johnstone, D., Hollenbach, D., & Bally, J. 1998, *Ap. J.*, 499, 758 [15] Ouellette, N., Desch, S. J., & Hester, J. J. 2004, this volume

CHONDRULE CRYSTALLIZATION EXPERIMENTS. R. H. Hewins[1], H. C. Connolly Jr.[2], G. E. Lofgren[3] and G. Libourel[4], [1]Geological Sciences, Rutgers University, Piscataway, NJ08816 [2]KBCC-CUNY, New York, [3]ST NASA Johnson Space Center, Houston, TX 77058, [4]CRPG-CNRS, 15 Rue Notre-Dame des Pauvres (BP 20), 54501 Vandoeuvre les Nancy, France.

Introduction: Given the great diversity of chondrules, laboratory experiments are invaluable in yielding information on chondrule formation process(es) and for deciphering their initial conditions of formation together with their thermal history. In addition, they provide some critical parameters for astrophysical models of the solar system and of nebular disk evolution in particular (partial pressures, temperature, time, opacity, etc). Most of the experiments simulating chondrules have assumed formation from an aggregate of solid grains, with total pressure of no importance and with virtually no gain or loss of elements from or to the ambient environment. They used pressed pellets attached to wires and suffered from some losses of alkalis and Fe.

Conventional Experiments: The hierarchy of chondrule textures has been well established. Skeletal crystals found in barred olivine and some porphyritic olivine (PO) chondrules require rapid growth rates (but not necessarily rapid cooling rates), and hence formation by undercooling of a completely melted liquid. Equant crystals found in most PO chondrules indicate formation from a liquid with abundant nuclei and/or, depending on the amount of relict grains, a partially melted precursor. The textures of some porphyritic chondrules in ordinary chondrites can be duplicated by low degrees of melting of chondritic material. Partial melting of very fine-grained starting material produces dominantly very fine-grained porphyritic chondrules. Production of normal porphyritic chondrules from such a precursor would require multiple remelting events to coarsen them.

The olivine phenocrysts of type II (ferroan) chondrules show normal Fe-Mg zonation which has been simulated with cooling rates of a few to a few hundred degrees per hour. The size of pyroxene exsolution features in charges constrains cooling rates around 1200ºC to less than 45º/hr. Reverse zoning on relict grains can be shown from diffusion experiments to require many minutes for the dissolution process. Large olivine grains introduced as seeds into finely ground mixture showed barred overgrowths when the mixture was totally melted, but no overgrowths in the case of incomplete melting where new growth was on nuclei surviving in the melt. Thus overgrowths must be used with caution as indicators of chondrule thermal history. Element partitioning experiments yield information about approach to equilibrium and cooling rate.

Heating times are much more difficult to constrain than cooling times, because longer times and higher temperatures have similar effects. However, extremely short heating times coupled with high cooling rates are inappropriate for chondrules: they produce mixtures of relict grains and skeletal crystals unlike the natural case.

Complex experiments: Totally glassy spheres can easily be made by total melting, though similar chondrules are rare. If crystalline dust is injected into a cooling totally molten droplet, crystallization ensues forming normal chondrule textures. In some experiments, the starting material was a powder blown into the furnace, instead of a pellet pressed on a wire. Chondrule-like droplets charged with crystals were accreted; the textures were heterogeneous and aggregational, resembling particularly some chondrules in CR chondrites. Igneous rims on chondrules might have formed by accretion of such a mist, though formation by melting of solid dust mantles has also been demonstrated to be feasible. Partially melted charges that incorporated C in a form such as graphite contain olivine grains in which much of the FeO was reduced to Fe metal. These crystals resemble the dusty olivine relict grains found in many chondrules. Forsteritic olivine and pyroxene have also been made in graphite crucibles.

Condensation/Evaporation experiments: Relatively few experiments have been designed to study evaporation or condensation of silicate melt. Condensation of a chondritic vapor at high temperature results in the sequence of phases seen in CAI. High partial pressures of K and SiO in the ambient gas have been shown to result in condensation into silicate melt droplets. The resulting zonation in silica-rich phases resembles what is seen in some layered chondrules. When chon-

dritic or IIA chondrule compositions are heated at 1580ºC with a pH_2 of 10^{-5}, sequential evaporative losses are seen, with S lost first and then all alkalis in less than one hour. With loss of FeO to the vapor, type IAB compositions are approached, and as loss of Si also becomes important, type IA compositions with Ca-rich forsteritic olivine are reached. Loss of FeO by evaporation takes 18 hours for 4mm charges. Silica-rich IIB and IB compositions cannot be reached by evaporation from these precursors. Experimental residues with IA compositions have porphyritic textures and show strong isotopic mass fractionations. Heating in graphite crucibles in evacuated silica tubes produces forsteritic olivine by reduction of FeO to Fe metal and migration of metal blebs out of the silicate sphere. The loss of FeO is more rapid than by pure evaporation, taking less than 4 hours.

Constraints on chondrule formation: If formed as closed systems, the peak temperatures of chondrules with skeletal crystals would have been relatively close to their liquidus temperatures. These have an enormous range, but because the most Mg-rich were incompletely melted and the most Mg-poor were completely melted, the range of maximum peak temperatures may have been restricted to 1450-1750ºC. If chondrules were heated for extremely short durations, the temperatures would be higher than this to achieve the same amount of melting and the same density of nuclei at the onset of crystallization. Within the range of peak temperatures, the liquidus temperature correlates with bulk composition, and there is the apparent problem that each chondrule must be heated to the temperature appropriate to its composition if indeed it were heated to its liquidus temperature. However, if most chondrules were incompletely melted, as were many porphyritic chondrules, or if they were open systems, the temperatures need not be near-liquidus. Experimental evaporation residues have porphyritic textures produced at up to 200ºC below the final liquidus temperatures of the residues.

Consideration of textures and mineral features requires cooling rates of several to several hundred degrees per hour. Chondrules were probably self-buffered at oxygen fugacities a few log units below the I-W buffer, and many contained solid carbon. Some type II chondrules contain suprachondritic alkalis and can have experienced little or no evaporation. Type I could have experienced ~40%, the lack of isotopic mass fractionation being explained by exchange with a gas containing high pressures of the lithophile elements. Similarly an important role for condensation in chondrule formation requires high pSiO, due to evaporation of locally concentrated dust. Chondrules that are condensates or evaporation residues formed in very restricted volumes. If type I chondrules did form by evaporation of partially melted crystalline precursors, they were heated about three hours, and their alkalis are secondary.

It is likely that different kinds of chondrules formed in different ways. In some, the dominant process may have been condensation, in others evaporation, or accretion of a mist of droplets and dust, or melting of aggregates with little change in composition. If chondrules formed inheterogeneous turbulent clouds, many may have experienced all of these processes to some extent. Therefore, more specific experiments of crystallization, evaporation or condensation, involving the control of complex gas partial pressures, are needed.

FORMATION OF SiO_2-RICH CHONDRULES BY FRACTIONAL CONDENSATION. D. C. Hezel, H. Palme and F. E. Brenker, D. C. Institut für Geologie und Mineralogie, Universität zu Köln, Zülpicherstraße 49b, 50674 Köln, Germany d.hezel@uni-koeln.de.

Introduction: Chondrules are a major component in most chondritic meteorites. It is known since long that these once molten droplets vary in bulk chemical composition, ranging between olivine and pyroxene-normative (Fig. 1); however, so far chondrules did not seem to exceed pyroxene-normative bulk composition. This cut-off is consistent with compositions predicted by equilibrium condensation calculations [e.g. 1], during which no minerals more silica-rich than pyroxene can condense.

A simple explanation for the range in chondrule bulk compositions was given by [2]: These authors considered chondrules to be mixtures of two end-members, (1) refractory, olivine-normative and FeO-free material and (2) non-refractory, SiO_2- and FeO-rich material.

However, there are chondrules and fragments in all types of chondritic meteorites, that are very SiO_2-rich with bulk silica-concentrations of up to 100wt.% SiO_2 [e.g. 3,4,5]. These compositions can no longer be explained by precursors resulting from equilibrium condensation. Suggested explanations for these silica rich components (SRC) are (i) fractional condensation [e.g. 3,4,5], which leads to SiO_2-condensation at temperatures around 1215 K (at 10^{-4} bar) [6] due to incomplete reaction of early condensed solids – especially olivine – with the cooling nebula, (ii) fractional crystallization of a melt or magma on a parent body [e.g. 7], (iii) extreme reduction of chondritic olivine and pyroxene [8]

To better understand the origin of these objects we began a comprehensive chemical and mineralogical study of SRCs in various types of chondritic meteorites by determining the major element composition, rare earth elements (REE) and silica polymorphs in SRCs. We studied 35 thin sections from 27 different ordinary chondrites (OC), including 9 H-, 13 L- and 5 LL-chondrites comprising all petrologic types. SRCs were identified in half of the samples studied. In earlier work we reported analyses of SRCs in the CH carbonaceous chondrite Acfer 182 [4].

Results: *Petrography:* SiO_2-rich objects occur either as chondrules or fragments. The size of the fragments may be up to 1.6 cm in diameter [7]; however, most fragments and none of the chondrule like objects exceed the size of average chondrules in the same meteorite. The appearances of SRCs are quite different, even in a single section all SRCs can be different. The SRCs are most easily distinguished by their paragenesis. (I) The common paragenesis in nearly all chondrites is pyroxene-SiO_2, (II) in the Seres-meteorite SRCs contain pyroxene, SiO_2, ±olivine ±spinel. In the latter one the objects are often zoned with SiO_2 in the center, surrounded by pyroxene, which itself is encircled by a thin rim of olivine, (III) one unusually large clast in Parnallee contains pyroxene-SiO_2-plagioclase earlier described by [7].

Mineral compositions: The pyroxene in typical pyroxene-SiO_2 chondrules is virtually pure orthopyroxene (opx) with only traces of other elements, usually below 1 wt.%. However, the opx can have variable amounts of ferrosilite-components. In some SRCs opx is zoned, with decreasing MgO-concentrations from core to rim. In other SRCs no individual opx grains can be identified, but there are domains with more MgO- and more FeO-rich opx. Even within one thin section FeO-concentrations in opx can differ between one SRC and another. SiO_2 is usually very pure with occasional traces of FeO of up to 0.52 wt.%. REE in opx are very low, between 0.1-1 times CI-chondritic with absolute flat patterns. REE in SiO_2 are below the detection limit.

In Seres pyroxenes in SRCs have Fs_{18} and olivines $Fa_{18\text{-}19}$; all other elements are below 1 wt.%. One SRC contains Cr-rich spinel. Rare earth elements were only measured in pyroxenes. Olivines and spinels are too small and SiO_2 usually does not contain these elements in detectable amounts. The concentrations are again between 0.1-1 times CI-chondritic and REE patterns are flat.

SiO_2-polymorphism: We used Micro-Raman technique to analyze SiO_2-polymorphs in-situ. The dominant polymorph is tridymite, followed by cristobalite; however, we never encountered SiO_2-glass. The SiO_2-rich clast in Parnallee mentioned above contains more quartz than tridymite and only traces of cristobalite.

Discussion: The SRCs exceed the chondrule field in Fig. 1 to more SiO_2-rich compositions. This indicates that SRCs are part of the normal chondrule suite and not some exotic components. A magmatic origin as mechanism for the unusual high SiO_2-concentrations can be excluded, because of (1) feldspar-free parageneses, (2) very low Al and Na contents and the absence of fractionation between Al and Ca and (3) flat REE-patterns. In magmatic systems pyroxene should fractionate light from heavy REE. The production of SiO_2 by reduction can also be rejected because metal is not present in SRCs. Evaporation during chndrule formation would likewise lead to Al, Ca-rich objects. Recondensation of earlier evaporated SiO_2 may produce some SiO_2-enrichment but is unlikely to lead to SiO_2 pure objects as the vapor phase

will contain many other species. Therefore, we favor fractional condensation to produce silica rich precursors, which can then form SRCs. The combination of this process with the suggestion of [2], that chondrules are mixtures of an olivine-normative and a SiO_2-rich component – formed by fractional condensation – seems to provide a good explanation for the formation of all chondrule bulk compositions, including SRCs. Fig. 1 illustrates this result. The bulk SiO_2-concentration of chondrules is plotted against the Mg/Si-ratio of bulk chondrules: The green line is a mixing line of forsterite (Fo) and SiO_2. The brown line is a mixing line of Ol_{Fa40} and SiO_2. The vertical solid line at 60wt.% SiO_2 is the phase boundary between olivine + pyroxene and pyroxene + SiO_2-praragenesis. Black dots represents bulk chondrule compositions from various OC. Open circles are SRC bulk compositions from this study. We conclude that: (1) SRCs are simply very silica rich chondrules and (2) all chondrules can be considered as mixtures between an olivine normative component and SiO_2.

Conclusion: The SRCs provide insight in the precursor forming process predating chondrule formation. Our proposed scenario for SRC formation is as follows: (1) Fractional condensation produced precursors with variable chemical compositions. (2) These precursors were then mixed and reheated to high temperatures, thereby forming chondrules. The reheating is documented in the high temperature SiO_2-polymorphs tridymite and cristobalite. After reheating, the SRCs were incorporated in their parent bodys. The comparatively high FeO content of chondrules requires condensation of precursors in an environment more oxidizing than the canonical solar nebula. Complete evaporation and recondensation of an earlier generation of solid objects cannot be excluded.

Fig. 1 suggests that SRCs extend compositional trends in chondrule compositions to higher SiO_2 contents. Complex models of igneous fractionation of large melt pools as envisioned by [7] are not required.

References: [1] Ebel D. S. and Grossman L. (2000) GCA 64:339-366; [2] Grossman J. N. and Wasson J. T. (1983) GCA 47:759-771; [3] Brigham C. A. et al. (1986) GCA 50:1655-1666; [4]; Hezel D. C. et al. (2003) MAPS 38:1199-1216; [5] Krot A. N. (2003) LPSC XXXIV, Abstract #1451; [6] Petaev M. I. and Wood J. A. (1998) MAPS 33:1123-1137; [7] Bridges J. C. et al. (1995) *Meteoritics* 30:715-727; [8] Brandstätter, F. and Kurat, G. (1985) MAPS, 20:615-616; [9] Dodd (1978) EPSL 39:52-66; [10] Hezel D. C. et al. (in prep.); [11] Huang S. et al. (1996) Icarus 122:316-346; [12] Jones R. H. (1990) GCA 54:1785-1802; [13] Jones R. H. (1994) GCA 58:5325-5340; [14] Jones R. H. (1996) GCA 60:3115-3117; [15] Kimura M. and Yagi K. (1980) GCA 44:589-595; [16] Matsunami S. et al. (1993) GCA 57:2101-2110; [17] McCoy T. J. et al. (1991) GCA 55:601-619; [18] Olsen (1983) Chondrules and their origins 223-234; [19] Rubin A. E. and Pernicka E. (1989) GCA 53:187-195; [20] Ruzicka A. et al. (1995) Meteoritics 30:57-70; [21] Sears D. W. G. et al. (1984) GCA 48:1189-1200; [22] Tachibana S. et al. (2003) MAPS 38:939-962.

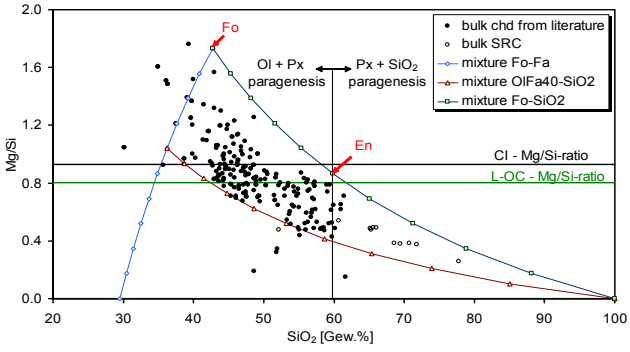

Fig. 1: Bulk chondrule- and SRC-composition in OC. Fo: forsterites, En: enstatite, chd: chondrules. Bulk chondrule data are taken from: Bridges et al. (1995); Dodd (1978); Grossman and Wasson (1983); Hezel et al. (2004); Huang et al. (1996); Jones (1990); Jones (1994); Jones (1996); Kimura & Yagi (1980); Matsunamie et al. (1993); McCoy et al. (1991); Olsen (1983); Rubin & Pernicka (1989); Ruzicka et al. (1995); Sears et al. (1984); Tachibana et al. (2003).

REFRACTORY FORSTERITES FROM MURCHISON (CM2) AND YAMATO 81020 (CO3.0) CHONDRITES: CATHODOLUMINESCENCE, CHEMICAL COMPOSITIONS AND OXYGEN ISOTOPES. H. Hiyagon[1], N. Sugiura[1], M. Kimura[2] and A. Miyazaki[1], [1]Department of Earth and Planetary Science, Graduate School of Science, University of Tokyo, Tokyo 113-0033, Japan. (hiyagon@eps.s.u-tokyo.ac.jp), [2]Faculty of Science, Ibaraki University, Mito 310-8512, Japan.

Introduction: Forsteritic olivine (FeO <1 wt%) with bright (blue) cathodoluminescence (CL) often occurs as isolated grains surrounded by matrix or as grains within chondrules. It is common in carbonaceous chondrites (CCs), but is also found in unequilibrated ordinary chondrites (UOCs) and even in R-chondrites. It has high concentrations of refractory lithophile elements (RLEs: Ca, Al, Ti, etc.) and is referred to as refractory forsterite (RF). The origin of RF is still controversial whether it formed through direct condensation from the solar nebula [e.g., 1-3] or formed from chondrule melts [e.g., 4-6]. Recently, Pack et al. [7] proposed a model, in which RF crystallized in a RLE-rich melt directly condensed from a solar nebula under a dust-enriched condition. In order to better understand the origin of RFs, we conducted chemical, CL, and O-isotopic studies on RFs from Murchison (CM2) and Yamato 81020 (CO3.0) chondrites. A preliminary study for Murchison RFs was reported in [8].

Samples : A 9.85 gram piece of the Murchison meteorite was freeze-thaw disaggregated and isolated olivine grains, both FeO-poor (RFs) and FeO-rich, as well as chondrules were handpicked, mounted on a slide glass (25mm in dia.) with epoxy together with San Carlos olivine and synthetic forsterite for O-isotope standards, and polished together. In the present study, 13 isolated RF grains were analyzed. Their shapes are euhedral, rounded or fragmental, and their size is ~200 to ~500μm in diameter. For comparison, some RFs, both as isolated grains and found within chondrules, on thin sections of Yamato 81020 (CO3.0) were also studied. Among them, Y81-Ch1, a porphyritic olivine-pyroxene chondrule of 150μm x 160μm in size, contains euhedral, apparently *in situ*-grown, RF grains (Fig.1).

Analytical conditions: The samples were first examined with a SEM (JEOL-5310) –EDS (Oxford Co.) for petrography and major element chemistry. Cathodo-luminescence images were taken with the MiniCL (Gatan Inc.) attached to the SEM using red/green/blue filters. Oxygen isotopes were analyzed with a CAMECA ims-6f ion microprobe using analytical conditions similar to those described in [9]. The beam size was ~10μm in diameter. The samples were further analyzed with an EPMA for more precise determinations of minor element abundances in olivine (Ca, Al, Ti, Cr, Mn, V, etc.).

Results:

CL images: All the RFs show bright CL emission. Many of the isolated RF grains show zoning in CL images with darker CL regions in the margin. Some of them show irregular-shaped sharp boundaries between bright/dark CL regions [8]. Some of them contain spinel grains in the bright CL region [8]. Olivine phenocrysts in a chondrule Y81-Ch1, on the other hand, show brighter CL in the margin. The cause for this enhanced CL brightness is not certain at present, but may be due to slight enrichment of Mn and Cr in the margin.

Minor element chemistry: Bright CL regions of RFs from Murchison show high concentrations of CaO (up to 0.75 wt%), Al_2O_3 (up to 0.66 wt%), TiO_2 (up to 0.14 wt%) and V_2O_3 (up to 0.19 wt%), and low concentrations of FeO (0.0-0.3 wt%), Cr_2O_3 (0.01-0.2 wt%) and MnO (0.00-0.06 wt%). A CaO-FeO daigaram is shown in Fig.2. One RF, MCFH-24, shows extremely low concentrations of FeO, Cr_2O_3, MnO and V_2O_3 (below detection limits of EPMA: <0.017, <0.006, <0.015 and <0.009 wt%, respectively), which are different from the trend of other RFs, and should be discussed separately. Darker CL regions tend to show lower Ca, Al, Ti, V and higher Fe, Cr, Mn concentrations. In some cases, however, no clear difference is observed in Fe and Cr concentrations between the bright/dark CL boundaries.

RFs in Y81020 show chemical compositions very similar to those of Murchison RFs, but tend to have higher concentrations of FeO (0.3-0.1.6 wt% for CaO >0.4 wt%) and Cr_2O_3 (0.06-0.36 wt% for CaO >0.4 wt%) (Fig.2). Euhedral olivine phenocrysts in Y81-Ch1 show the highest concentrations of CaO (up to 0.88 wt%) and V_2O_3 (up to 0.064 wt%) among all RFs, but their chemical composition as a whole is consistent with those for the other RFs.

Oxygen Isotopes of Murchison RFs: The obtained oxygen isotopic compositions for Murchison RFs are summarized in Fig.3. Both bright and dark CL regions and spinel grains enclosed in RFs were analyzed. Also shown for comparisons are terrestrial fractionation (TF) line and carbonaceous chondrite anhydrous minerals (CCAM) line. All the data fall in a surprisingly narrow region approximately on the CCAM line with $\delta^{17}O$ and $\delta^{18}O$ = -8±3 and -5±3 permil, respectively. No difference is observed in O isotopes among the bright CL regions, dark CL regions and even spinel grains. This suggests that all RFs in Murchison formed from a single O-isotopically homogeneous reservoir. Spinel is not relict but formed *in situ* with olivine.

Discussion: We have not yet reached a conclusion whether RFs formed through direct condensation from the nebula or they formed within a RLE-rich melt (18-20 wt% CaO) as proposed by Pack et al. [8]. Apparently many RFs seem to have experienced remelting (suggested by rounded-type RFs) or complex thermal histories (suggested by complex zoning in CL images). The problem for the latter model is lack of abundant melt phases around RFs. It seems also difficult to understand concentration profiles of CaO and other RLEs within RF grains: they are rather homogeneous for some RFs or they decrease toward the margin. The concentration profiles are inconsistent with those expected from a closed system crystallization model. An open system crystallization model [8] may be possible, but still has difficulties in explaining rather constant profiles for some RFs. The discovery of *in situ*-grown RFs in a chondrule Y81-Ch1 will cast new insights into the formation process of RFs. It contains a melt phase, which has long been missing. However, CaO content of the mesostasis is at most 15 wt%, which is not high enough for a melt phase in equilibrium with olivine with >0.8 wt% CaO. The bulk CaO content of this chondrule is even much lower. The formation process of Y81-Ch1 and its relation to other RFs has key importance to better understand the formation process of RFs.

References: [1] Grossman L. and Olsen E. (1974) *GCA*, *38*, 171-187. [2] Steele I. M. (1989) *GCA*, *50*, 1379-1395. [3] Weinbruch S., Palme H. and Spettel B. (2000) *Meteorit. Planet. Sci., 35,* 161-171. [4] McSween H. Y. Jr. (1977) *GCA, 41*, 411-418. [5] Jones R. H. (1992) *GCA, 56*, 467-482.[6] Jones R. H., Saxton J. M., Lyon I. C. and Turner G. (2000) *Meteorit. Planet. Sci., 35,* 849-857. [7] Pack A., Yurimoto H. and Palme H. (2004) *GCA, 68*, 1135-1157. [8] Hiyagon H. and Kimura M. (2004) *Antarctic Meteorites XXVIII,* (Abstract) 15-16. [9] Hiyagon H. and Hashimoto A. (1999) *Science, 238*, 828-831.

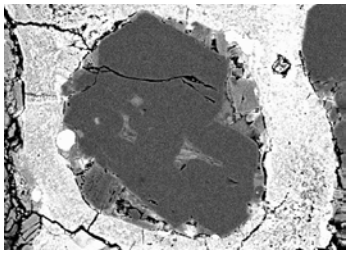

Fig.1 A backscattered electron image of a chondrule, Y81-Ch1, in Yamato 81020.

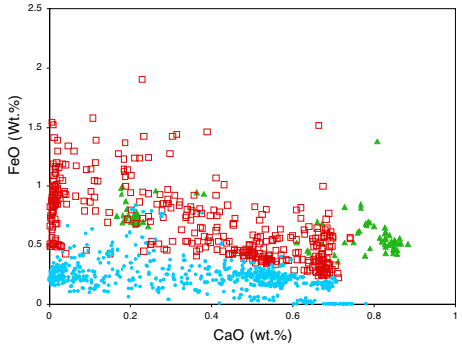

Fig.2 Correlation between FeO and CaO for isolated RF grains in Murchison (blue dots), in Y81020 (red squares), and RFs within chondrules in Y81020.

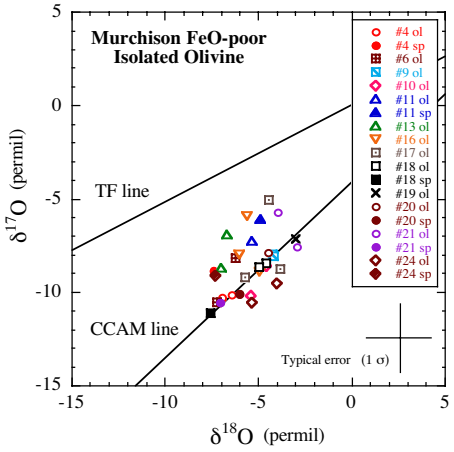

Fig.3 Oxygen isotopic compositions of isolated RF grains from Murchison.

Apparent I-Xe cooling rates of chondrules compared with silicates from the Colomera iron meteorite. C. M. Hohenberg, A. P. Meshik, O. V. Pravdivtseva Washington University, Physics Department, CB1105, One Brookings Drive, Saint Louis, MO 63130, USA, cmh@wustl.edu.

Introduction: In I-Xe dating, a regular pattern of increasing $^{*129}Xe/^{*128}Xe$ ratio with increasing extraction temperature is often observed. If one makes the crude assumption that the temperatures at which the Xe is extracted in the laboratory is approximately the same as the temperature at which those sites closed 4.6 Ga ago, a (zeroth order) model cooling rate can be found. In order to test and refine this model we can apply the cooling theory of Dodson [1] to those extraction steps approaching the I-Xe isochrons. Using an Arrhenius plot for these temperature fractions, and assuming that an only single phase is involved, the effective diffusion parameters can be estimated (frequency factor and activation energy). From the apparent (zeroth order) cooling rate, the closure temperature can be estimated from the Dodson equation [1]. This model closure temperature can then be compared with the actual laboratory temperature at which the isochron begins. The ratio of the closure temperature and the temperature corresponding to the start of the isochron provides the ratio of the two temperature scales, incorporation and extraction. The actual cooling rate is then given by the apparent (zeroth order) cooling rate times the temperature scale factor.

Figure 1 shows Arrhenius plots for I-Xe data for a silicate inclusion (K-feldspar) from the Colomera iron meteorite [2], and three individual chondrules from Allende. The activation energy found for the Colomera inclusion is 55 Kcal/mol, and the corresponding closure temperature about 400ºC. The change in model I-Xe age for points approaching the isochron, divided by the extraction temperature interval provides the first approximation of the cooling rate, $4 < \Delta T/\Delta t < 16$ ºC/Ma [2]. Since the isochron for the Colomera silicate begins at about 1500ºC, about 3.8xs the estimated closure temperature, the corrected cooling rate should be about 1/4 of this first approximation, or $1 < \Delta T/\Delta t < 4$ ºC/Ma [2].

Previous studies of Allende chondrules also suggest a regular pattern of increasing model I-Xe age as the extraction temperatures approach the isochron [3]. Arrhenius plots of a representative set of these chondrules are also shown in Figure 1. Chondrules 3, 6 and 9 have apparent activation energies of 185, 89 and 174 kCal/mol, respectively, and apparent closure temperatures 900 °C, 700 °C and 900 °C (about 1.3 xs lower than the temperature at which the isochron begins). We interpret this as indication that the laboratory extraction temperature approximates the corresponding temperature in the rate equation. If true, this implies that the apparent $\Delta T/\Delta t$ in approach to the isochron approximately gives the actual cooling rate of these chondrules. Apparent cooling rates for chondrules 3, 6 and 9 are shown in Table 1 as a function of extraction temperature. Included are the temperature fractions approaching the isochron. Lower temperature fractions do not fit the single phase model in the Arrhenius plot, presumably corresponding to lower temperature phases or iodine contamination. Although there is still some scatter, most of these Allende chondrules a surprisingly consistent apparent cooling rate of 50 – 350 ºC/Ma as the isochron is approached.

Whether this rate applies to cooling in the nebula or the Allende parent body, consistency of this apparent cooling rate among these Allende chondrules is suggestive of the latter, and one to two order of magnitude greater that that inferred for K-feldspar inclusions in the Colomera iron meteorite.

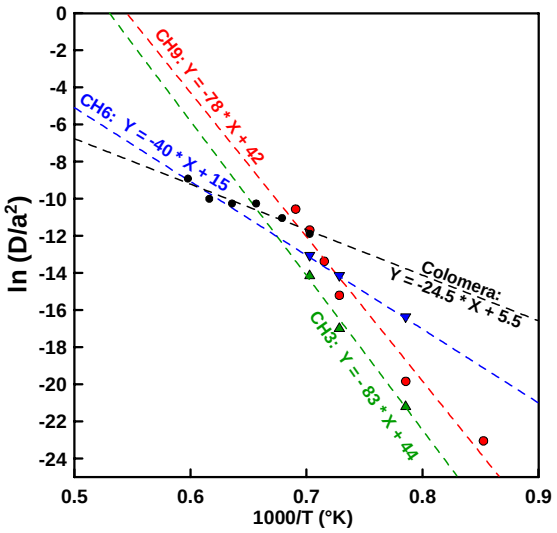

Fig.1 Arrhenius plots (Colomera silicate inclusion and Allende chondrules CH#3, CH#6, CH#9.

Table 1. Model cooling rates for Allende chondrules #3, #6, #9.

T, °C	#3	#6	#9
1200	636	36	41
1300	128	28	67
1325			209
1350	270	94	560
1375			165
1400			70
Average	345	53	185

Acknowledgments: This work supported by NASA grant NAG5-12776.

References: [1] Dodson M. H. (1973) *Contr. Mineral. Petrol.* **40**, 259-274. [2] Pravdivtseva O. V. et al. (2000) ***LPSC XXXI*, #1929**. [3] Swindle T. D. et al. (1983) *GCA* **47**, 2157-2178.

CHONDRULE FORMATION IN PLANETESIMAL BOW SHOCKS: PHYSICAL PROCESSES IN THE NEAR VICINITY OF THE PLANETESIMAL. L. L. Hood[1], F. J. Ciesla[2], and S. J. Weidenschilling[3], [1]Lunar and Planetary Lab, University of Arizona, 1629 E. University Blvd., Tucson, AZ 85721; lon@lpl.arizona.edu; [2]NRC Research Associate, NASA Ames Research Center, MS 245-3, Moffett Field, CA 94035; [3]Planetary Science Institute, 1700 E. Ft. Lowell Rd., #106, Tucson, AZ 85719.

Introduction: Currently, gas dynamic shock waves in a low-temperature (< 650 K) nebula are considered to be a leading candidate mechanism for providing the repetitive, short-duration heating events that are believed to have been responsible for the formation of chondrules in chondrites [e.g., 1,2]. It can be shown, for example, that shocks with Mach numbers greater than 4 or 5 would be capable of thermally processing and melting 0.1-1 mm sized precursor aggregates as required by meteoritic data [3, 4, 5, 6]. Near the nebula midplane, possible energy sources for generating multiple shocks include mass concentrations in a gravitationally unstable nebula [7, 8], tidal interactions of proto-Jupiter with the nebula [9, 10], and bow waves upstream of planetesimals scattered gravitationally into eccentric / inclined orbits by proto-Jupiter [11, 12, 13]. In this paper, we reconsider the planetesimal bow shock model and analyze physical processes occurring in the near vicinity of the planetesimal.

Analysis: Figure 1 shows a simulation of gas flow around a planetesimal using the piecewise parabolic method (PPM) to solve the hydrodynamic equations [14]. The planetesimal is represented as a high-density, low-pressure fluid with no velocity and a radius of 1000 km (white object in the center). The gas is initially assumed to be flowing left to right at 8 km/s with a density of 10^{-9} gm cm^{-3} and a temperature of 400 K. The gas density distribution resulting from the shock wave is shown in the figure. In a recent study, we have found that chondrule precursors that are melted following passage through a planetesimal bow shock would likely cool at rates that are too rapid to be consistent with meteoritic evidence [13]. However, that study was limited to the bowshock exterior to about 1.5 planetesimal radii (measured perpendicular to the symmetry axis) to avoid complications interior to this distance where large pressure gradients and lateral flow occur as the gas flows around the planetesimal. Here, we reconsider the near flow regime and identify several physical effects that may yield less rapid cooling rates and that may have resulted in the accretion of formed chondrules onto meteorite parent bodies.

As seen in Figure 1, immediately upstream of the planetesimal, the shock front forms at a distance of approximately one planetesimal radius above the surface. For large planetesimals, this distance will be greater than the stopping distance of formed chondrules moving downstream from the shock front. For

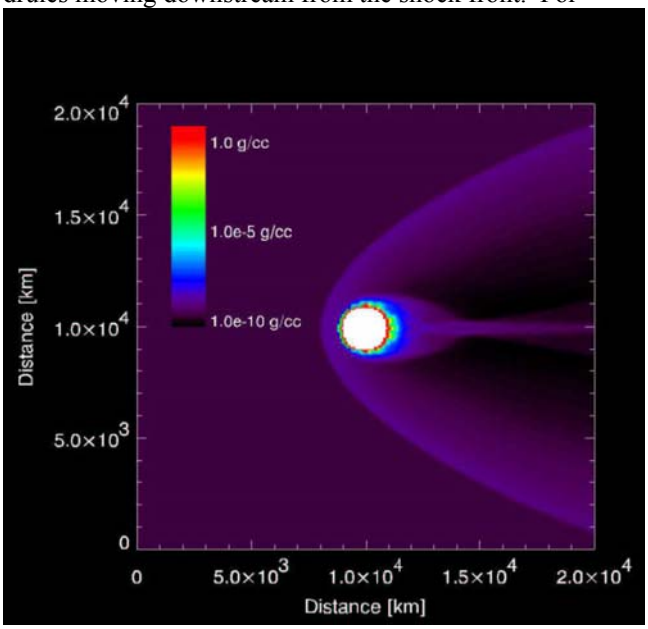

example, for an adiabatic shock and for the upstream gas density considered in this simulation, the stopping distance of 1 mm diameter chondrules in the shocked gas is about 450 km. Therefore, in this example, for planetesimals larger than about 450 km in radius, most mm-sized chondrules would form and be accelerated by the shocked gas as it moves laterally around the planetesimal. Most of these chondrules would not accrete to the planetesimal and their cooling rates would likely be too rapid to be consistent with laboratory experiments (see, e.g., ref. 13). For planetesimals smaller than about 450 km, most mm-sized chondrules forming upstream of the planetesimal would impact it at a significant relative velocity and be damaged or destroyed. Accretion of large numbers of intact chondrules would only occur for planetesimals with radii near the critical radius where the thickness of shocked gas ahead of the planetesimal is approximately equal to the stopping distance. For a radiative shock, the downstream gas cools by line emission and increases in density compared to the adiabatic shock case [15, 4]. Therefore, the actual critical radius for mm-sized chondrules in a nebula with the above gas parameters

may be less than 450 km if line emission cooling is accounted for.

An increase in the efficiency of accretion of formed chondrules on planetesimals moving supersonically relative to the nebula would occur if a significant impact-induced planetesimal atmosphere [16, 17] is present. To avoid being swept away by the incident nebula, such an atmosphere must have a pressure at least as large as that of the solar nebula dynamic pressure, which is about 0.6 millibars for the parameters adopted in the simulation of Figure 1. As formed chondrules and/or larger particulates impact the planetesimal at velocities greater than about 5 km/s, partial vaporization of the impacting particles and the planetesimal surface will occur, thereby releasing silicate vapor to supply the transient atmosphere. The net result will be the formation of a quasi-stationary atmospheric layer composed of silicate vapor between the planetesimal surface and the incident shocked solar nebula gas. If the transient atmospheric pressure becomes larger than the solar nebula dynamic pressure, the stand-off distance will increase. At some point, the transient atmospheric density and stand-off distance will become large enough to stop incident formed chondrules and other particles so that the atmospheric supply rate decreases. An equilibrium would therefore be reached such that most formed chondrules are stopped in the transient atmosphere before impacting the planetesimal. Accretion of intact chondrules would then occur for a wider range of planetesimal radii.

The capture of formed chondrules and other particulates in a transient atmosphere on the upstream side of a planetesimal moving supersonically relative to the solar nebula gas may be consistent with meteoritic evidence that chondrules experienced relatively slow cooling rates and formed in regions with enhanced solids-to-gas mass ratios (e.g., ref. 18). The effective cooling rates will be slowed by radiation from hot chondrules near the shock front, which is maintained at a distance of approximately one planetesimal radius from the chondrules in the transient atmosphere. It will also be slowed by radiation from surrounding chondrules and from the planetesimal surface. The solids-to-gas mass ratio will be increased by accumulation in the transient atmosphere to values much larger than that in the solar nebula upstream of the shock front. This would allow a solar ratio of solids to gas upstream of the shock front as is suggested by recent simulations of the collisional destruction of chondrules during passage through nebular shocks [19]. A complete quantitative evaluation of this mechanism requires at least a two-dimensional numerical simulation similar to that shown in Figure 1 but including detailed shocked gas physics and accounting for the formation of a transient atmosphere.

Discussion: A remaining difficulty for the planetesimal bow shock mechanism is whether it is capable of processing sufficient solid material in the region of the early solar system now occupied by the asteroid belt to explain the abundance of chondrules in chondrites. However, the required efficiency may not be as great as is usually assumed. Although ordinary chondrites (containing 60-80% by volume of chondrules) account for about 80% of observed falls, their durability during atmospheric entry is high so their abundance relative to other chondrites outside of the atmosphere may be much lower. It has been estimated, for example, that the abundance of ordinary chondrites outside the atmosphere may be as small as 3% [20]. To some extent, the efficiency problem may be reduced by the fact that chondrule formation in the near vicinity of a planetesimal would make it easier for chondrules formed in this manner to be accreted to certain chondrite parent bodies. In particular, it is possible that the ordinary chondrite parent bodies, which contain abundant chondrules, are among those former planetesimals that were excited into eccentric / inclined orbits by proto-Jupiter.

References: [1] Boss, A. P., in *Chondrules and the Protoplanetary Disk*, R. H. Hewins et al., eds., pp. 257-264, Cambridge Univ. Press, 1996; [2] Jones, R. H. et al., in *Protostars and Planets IV*, V. Mannings et al., eds., pp. 927-946, Univ. of Arizona Press, Tucson, 2000; [3] Hood, L. and Horanyi, M., *Icarus, 93*, 259-269, 1991; [4] Iida, A. et al., *Icarus, 153*, 430-450, 2001; [5] Desch, S. and Connolly, H., *Meteorit. Planet. Sci., 37*, 183-207, 2002; [6] Ciesla, F. and Hood, L., *Icarus, 158*, 281-293, 2002; [7] Wood, J. A., *Meteorit. Planet. Sci., 31*, 641-645, 1996; [8] Boss, A., *Astrophys. J., 576*, 462-472, 2002; [9] Bryden, G. et al., *Astrophys. J., 514*, 344-367, 1999; [10] Rafikov, R. R., *Astrophys. J., 572*, 566-579, 2002; [11] Hood, L. L., *Meteorit. Planet. Sci., 33*, 97-107, 1998; [12] Weidenschilling, S. J. et al., *Science, 279*, 681-684, 1998; [13] Ciesla, F. J. et al., *Meteorit. Planet. Sci*., in press, 2004; [14] Colella, P. and Woodward, P. R., *J. Comp. Phys., 54*, 174-201, 1984; [15] Ruzmaikina, T. and Ip., W., *Icarus, 112*, 430-447, 1994; [16] Podolak, M. et al., *Icarus, 84*, 254-260, 1990; [17] Podolak, M. Et al., *Icarus, 104*, 97-109, 1993; [18] Ciesla, F. et al., *Meteorit. Planet. Sci., 39*, 531-544, 2004; [19] Nakamoto, T. and Miura, H., *Lunar Planet. Sci. XXXV*, Abstract #1847, 2004; [20] Sears, D. W. G. (abstract), *Lunar Planet. Sci., XXVIII*, 1273-1274, 1997.

GENETIC RELATIONSHIPS BETWEEN CHONDRULES, RIMS AND MATRIX. G. R. Huss[1], C. M. O'D. Alexander[2], H. Palme[3], P. A. Bland[4] and J. T. Wasson[5], [1]Department of Geological Sciences, Arizona State University, Box 871404, Tempe, AZ 85287-1404, USA [gary.huss@asu.edu], [2]Department of Terrestrial Magnetism, Carnegie Institution of Washington, 5241 Broad Branch Road NW, Washington, D.C. 20015, USA, [3]Universität Köln, Institut für Mineralogie und Geochemie, 50674 Köln, Germany, [4]Department of Earth Science and Engineering, Imperial College London, South Kensington Campus, London SW7 2AZ, UK, [5]Institute of Geophysics and Planetary Physics, University of California, Los Angeles, CA 90095-1567, USA.

Introduction: The most primitive chondrites are composed of chondrules and chondrule fragments, various types of inclusions, discrete mineral grains, metal, sulfides, and fine-grained materials that occur as interchondrule matrix and as chondrule/inclusion rims. Understanding how these components are related is essential for understanding how chondrites and their constituents formed and were processed in the solar nebula. For example, were the first generations of chondrules formed by melting of matrix or matrix precursors? Did chondrule formation result in appreciable transfer of chondrule material into the matrix? Here, we consider three types of data: 1) compositional data for bulk chondrites and matrix, 2) mineralogical and textural information, and 3) the abundances and characteristics of presolar materials that reside in the matrix and rims. We use these data to evaluate the roles of evaporation and condensation, chondrule formation, mixing of different nebular components, and secondary processing both in the nebula and on the parent bodies. Our goal is to identify the things that are reasonably well established and to point out the areas that need additional work.

Compositional Data: The bulk compositions of chondrites exhibit systematic elemental fractionations compared to CI chondrites, the meteorites that most closely represents the bulk composition of the solar system. The most important are: 1) volatility-controlled depletions of volatile and moderately volatile elements, 2) variations in refractory element abundances, perhaps sited in CAIs, 3) variations in Mg/Si ratios, and 4) metal-silicate fractionation [1].

There are data to suggest that fractionations of the first three types occurred in large part prior to chondrule formation [e.g., 2, 3]. Incomplete nebular condensation has long been considered a primary mechanism for these fractionations [e.g., 1, 4, 5], but differential sublimation of the dust inherited from the sun's parent molecular cloud, which in many ways is indistinguishable from incomplete condensation, may have played a substantial role [e.g., 6]. Chondrule formation superimposed additional fractionations. Volatile elements were lost during chondrule melting, although the time scale for chondrule melting was most likely too short to permit complete loss [7, 8]. Volatile elements lost from chondrules may have recondensed onto chondrule surfaces [e.g., 3] or in the matrix [8]. There is a complimentary relationship in the compositions of matrix and chondrules in CR and CV chondrites, which suggests that the two components originated in the same material reservoir [8-10]. Metal may be largely a by-product of chondrule formation, either due to reduction of FeO during melting and ejection of the immiscible metal melt from the chondrule, or through evaporation of iron and recondensation as metal [e.g., 3, 8]. This implies that at least some metal-silicate fractionation could have post-dated most chondrule formation.

Mineralogy and Petrology of Matrix and Rims: Matrices and fine-grained rims on chondrules and CAIs differ significantly in mineralogy among the meteorite classes, in large part due to parent-body processing. Aqueous alteration and/or thermal metamorphism has destroyed or significantly modified the primary mineralogies of rims and matrix in most chondrites, but in a few, such as Bishunpur (LL3.1) and ALH77307 (CO3.0), there is an abundance of amorphous and nanocrystalline material [11, 12]. Amorphous material is very susceptible to alteration and recrystallization, so its preservation suggests that some of the primary material has survived in these meteorites. The amorphous material could be chondrule glass fragments, nebular/chondrule condensates or interstellar material accreted directly into the meteorites.

Rims are generally thought to have accreted onto chondrules in the nebula, although their low porosity (~10%) remains problematic. In some instances, it seems that the rims accreted while the host chondrules were still hot [13]. If so, then at least some fine-grained dust was present during or shortly after chondrule formation, and it may have acted as an important site for recondensation of material that evaporated from chondrules. However, the majority of rim and matrix material cannot have experienced the high temperatures of chondrule formation, because it is in them that presolar materials (circumstellar grains and interstellar organics) are found [e.g., 14].

Abundances and Characteristics of Presolar Grains: The known types of presolar materials exhibit a broad range of chemical and thermal resistance. Thus, their relative abundances provide a means of probing the conditions that they and any accompanying

material experienced, both on the meteorite parent bodies and prior to accretion [6, 14]. There are clear correlations between the volatile abundances of primitive chondrites and the complex of presolar grains that are present in their matrices [6]. The CI chondrites and CM matrices have the highest abundances of most presolar components and these components show the widest range of thermal stability. The most primitive members of the other classes show varying depletions of labile components in the order CI+CM<OC<CO<CR <CV. These depletions can best be understood in terms of thermal processing of the mixture of components represented by CI chondrites and CM matrices [6].

Insoluble organic material (IOM) constitutes the bulk of the organic material in chondrites. The matrices of all chondrite classes seem to have started out with roughly the same CI-like IOM abundances [15]. However, unlike for the presolar grains, the most primitive IOM is preserved in the CR chondrites [16]. The IOM in aqueously altered meteorites (type 1-2) appears to have undergone low temperature oxidation, perhaps associated with the melting of irradiated ices. The IOM in other meteorites of petrologic type ≥3 have experienced varying degrees of thermal maturation.

Discussion: In order to successfully evaluate questions like those posed in the introduction, it is important to consider the extent to which parent-body processing has altered the original record. In CM chondrites, aqueous alteration has altered both matrix and chondrules, significantly changing the mineralogy and moving elements between them [e.g., 17]. The oxidized CV chondrites also show considerable evidence of elemental mobilization [e.g., 18]. Even the most primitive UOCs show evidence of exchange of alkalis between matrix and chondrules [19]. The nature and extent of these processes must be understood before we can get a clear picture of the original state of the various types of chondrites. CR chondrites, CO3.0 chondrites, and the most primitive UOCs may be the best samples to work with.

Returning to our original questions: Were the first generations of chondrules formed by melting of matrix or matrix precursors? Compositional studies indicate that much of the chemical fractionation that produced the various classes of chondrites from bulk solar-system material occurred prior to chondrule formation [e.g., 2, 3]. Data for presolar grains in the least metamorphose members of each class combined with bulk compositional data for the host meteorites indicate that the precursors of matrix and chondrules experienced the same nebula processing [6]. And the complementarity of the compositions of matrix and chondrules, particularly in CR chondrites, indicates that they formed from a common reservoir [8-10]. These observations suggest that the answer may be yes, but there are problems. The melting temperature of chondrules is ~600 K above the evaporation temperatures of chondritic silicates, and matrix heated to these temperatures will have experienced extensive evaporation [20]. Also, the bulk compositions of rims and matrix in most chondrite classes do not appear to be consistent with a simple exchange model and the IOM, particularly in CR chondrites, seems to have escaped significant nebular heating [13, 16].

Did chondrule formation result in appreciable transfer of chondrule material into the matrix? This question is difficult to answer because redistribution of elements by parent body processes can mimic this transfer. However, metal and silicates in CR and OC chondrites make a relatively convincing case that material evaporated from chondrules during melting partially recondensed on fine-grained matrix precursors and on the surfaces of chondrules [3, 8-10, 13]. A major challenge for the future will be to understand the details of the processes and material transfers that generated the observed effects.

References: [1] Palme H. (2001) *Phil. Trans. R. Soc. 359*, 2061-2075. [2] Grossman J. N. (1996) In *Chondrules and the Protoplanetary Disk* (Ed. R. H. Hewins, R. H. Jones, and E. R. D. Scott), Cambridge Univ. Press, pp. 243-253. [3] Connolly H. C., Jr., Huss G. R. and Wasserburg G. J. (2001) *GCA 65*, 4567-4588. [4] Larimer J. W. and Anders E. (1967) *GCA 31*, 1239-1270. [5] Alexander C. M. O'D., Boss A. P. and Carleson R. W. (2001) Science 293, 64-68. [6] Huss G. R., Meshik A. P., Smith J. B. and Hohenberg C. M. (2003) *GCA 67*, 4823-4848. [7] Yu. Y and Hewins R. H. (1998) *GCA 62*, 159-172. [8] Kong P. and Palme H. (1999) *GCA 63*, 3673-3682. [9] Klerner S., Palme H. (1999) *MAPS 34*, A64-A65. [10] Klerner S. and Palme H. (1999) LPSC XXX (CD-ROM, #1272. [11] Alexander C. M. O., Barber D. J., and Hutchison R. H. (1989) *GCA 53*, 3045-3057. [12] Brearley, A. (1993) *GCA 57*, 1521-1550. [13] Alexander C. M. O'D. (1995) *GCA 59*, 3247-3266. [14] Huss G. R. and Lewis R. S. (1995) *GCA 59*, 115-160. [15] Alexander C. M. O'D., Russell S. S., Arden J. W., Ash R. D., Grady M. M. and Pillinger C. T. (1998) MAPS 33, 603-622. [16] Cody, G. D., and Alexander C. M. O'D. (2004) GCA, in press. [17] McSween H. Y., Jr. (1979) *GCA 43*, 1761-1770. [18] Krot A. N., Scott E. R. D., and Zolensky M. E. (1995) *Meteoritics 30*, 748-775. [19] Grossman J. N. (2004) *MAPS*, in press. [20] Wasson J. T. and Trigo-Rodriguez J. M. (2004) *LPS XXXV*, abstract #2140.

Supported by NASA grants NAG5-11543 (GRH), NAG5-12887 (JTW), NAG5-13040 (CMO'DA).

CHONDRITE FRACTIONATION WAS COSMOCHEMICAL; CHONDRULE FRACTIONATION WAS GEOCHEMICAL. R. Hutchison, Mineralogy Department, Natural History Museum, London SW7 5BD, U.K. marobh@btopenworld.com

Introduction: Following Larimer and Anders [1], the compositions of chondrite groups are related to elemental volatility and independent of chondrule/matrix ratio. Chondrite compositions were established before chondrule formation. Chondrules are objects that were partially or wholly melted before or during accretion of chondrite parent bodies. Chondrules range from metal-sulfide types to silicate-rich ferromagnesian types. Chemical differences between textural or chemical types of ferromagnesian chondrule are unrelated to elemental volatility and probably were caused by crystal-liquid fractionation. The quasi-solar composition of each chondrite may be reconciled with the chemical diversity of its constituents if its parent body formed by fragmentation and reaccretion of partly molten pre-existing bodies [2]. Is there evidence against this, such as positive evidence for a nebular origin of chondrules?

Fractionation between chondrite groups: Relative to the `solar', CI group composition, other groups gained or lost refractory lithophile elements (Al,Ti,Ca) which were coherent during fractionation. The groups also gained or lost Mg and metal (Fe,Ni,Co) relative to Si. Compositional differences were interpreted as the loss from CI of different proportions of solids that had condensed and separated from nebular gas at different, falling temperatures [1]. It subsequently proved that the CV, CK, CO and CM groups had gained refractory lithophile elements [see 3], but the three fractionations continued to be interpreted in terms of fractional condensation from a hot solar nebula, with insignificant lateral transport of matter. Equilibrium condensation was extended to include volatiles (Tl,Bi,In), supported by the assumption that magnetite in chondrites formed by oxidation of metal at low nebular temperature. We now know that magnetite formed on parent bodies [see 4], which discredits part of the condensation model.

More recently Shu et al. [see 5] proposed that severe heating of solids in a protosolar accretion disk only occurred close to a T Tauri protosun and that residual refractory-rich solids or solidified liquids were carried outwards by x-winds and returned to the disk at asteroidal distances. The bulk of the disk remained cold. The former presence of spallation-produced ^{10}Be, $T_{½}$=1.5 Ma, in a Ca-, Al-rich inclusion (CAI) indicates that the Sun did go through a T Tauri phase [6]. Hutchison [7] reinterpreted the major and some minor element abundances of the chondrite groups in terms of an x-wind model. Precursors of each group occupied annular zones at different heliocentric distances in a cold accretion disk. To each zone was added material that had been heated and partially vaporized by the protosun, then carried outwards by the x-wind as condensates or residues. Different aliquots of Si, Mg and Fe,Ni metal were added to CI to produce non-carbonaceous chondrite groups (EH, EL, H, L, LL and R). Refractory-rich carbonaceous groups (CV, CK, CO and CM) represent CI disk that gained refractory residues as CAIs. CR and CH groups have unfractionated refractory lithophiles, but CH gained metal, probably by a secondary process. Most chondritic material, including sulfur, volatile elements and presolar grains, ± ices, is thought to have been derived directly from disk solids. The bulk composition of each chondrite group is the product of cosmochemical processing.

Fractionation between ferromagnesian chondrules: As defined above, chondrules range widely in chemistry and mineralogy. Other definitions, however, exclude all but ferromagnesian silicate objects that were wholly or partially melted before or during the aggregation that formed a chondrite. Even within this restricted definition, however, compositional variation among chondrules strongly constrains theories of their origin.

The abundances of Al and Ca relative to Si, and the Ca/Al ratios (Fig. 1) are particularly significant. The ranges are more limited in chondrites than in ferromagnesian chondrules. The atomic Ca/Al ratio of the CI group is 0.72. Among chondrites, the minimum ratio is 0.65 (EL) and the maximum is 0.76 (R group). Fig 1 shows that barred olivine (BO) chondrules have a higher Al/Si ratio and radial pyroxene (RP) chondrules a lower ratio than any chondrite group. The reverse is true of the respective Ca/Al ratios. FeO-poor, olivine-rich type IA chondrules have superchondritic Ca/Al ratios (mean=0.96), but FeO- and olivine-rich type IIA chondrules have subchondritic Ca/Al ratios (mean=0.64).

In kinetic heating experiments on CI analogue, Wang et al. [8] found that Ca and Al do not begin to evaporate until 95 percent of the mass has been lost. The residue has an Fe-free, Si- and Mg-poor composition like CAIs, not ferromagnesian chondrules. This indicates that the range in Ca/Al ratios in chondrules was not produced by fractional volatilization, nor could chondrule compositions have been produced by condensation of solar gas or gas plus dust [9]. Type IA chondrules cannot have been produced by volatile loss from type IIA chondrule starting material. In contrast,

different degrees of partial melting of a chondritic precursor can produce melts with a range of Ca/Al ratios [10], and it is proposed that such a geochemical process is required for chondrule formation.

References: [1] Larimer J. W. and Anders E. (1970) *GCA*, 34, 367-387. [2] Hutchison R. (2004) *Meteorites: A petrologic, chemical and isotopic synthesis*. Cambridge University Press, UK. [3] Larimer J. W. and Wasson J. T. (1988) *MESS* 394-415. [4] Krot A. N. et al. (1997) *GCA*, 61, 219-237. [5] Shu F. H. et al. (2001) *Ap. J.* 548, 1029-1050. [6] McKeegan K. D. et al. (2000) *Science, 289,* 1334-1337. [7] Hutchison R. (2002) *MAPS*, 37, 113-124. [8] Wang J. et al. (2001) *GCA*, 65, 479-94. [9] Ebel D. S. and Grossman L. (2000) *GCA*, 64, 339-366. [10] Jurewicz A. J. G. et al. (1995) *GCA,* 59, 391-408. [11] Wasson, J. T. and Kallemeyn, G. W. (1988) *Phil. Trans. R. Soc. Lond.,* A325, 535-544. [12] Bischoff A. et al. *Meteoritics,* 29, 264-274. [13] Jones R. H. and Scott E. R. D. (1989) *Proc. LPSC*, 19, 523-536. [14] Jones R. H. (1990) *GCA*, 54, 1785-1782. [15] Lux G. et al. (1981) *GCA*, 45, 675-685.

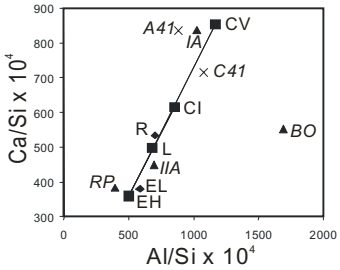

Figure 1. Ca/Si vs Al/Si atomic ratios, x 10^4. Selected chondrite groups and chondrule types are plotted to show maxima and minima in ranges. CV, CI, EH and EL data [11]; R group [12]. Type IA [13] and IIA [14] are means of 11 chondrules each, from Semarkona, LL3.0; A41 and C41 are individuals with the highest and lowest Ca/Al ratios in type IA chondrules [13]. BO and RP, means of 7 and 8 chondrules, respectively, from H3 chondrites [15].

CHONDRULE FORMATION AND ACCRETION OF CHONDRITE PARENT BODIES: ENVIRONMENTAL CONSTRAINTS. R. Hutchison[1] and J. C. Bridges[2], [1]Mineralogy Department, Natural History Museum, London SW7 5BD, UK, marobh@btopenworld.com, [2]Planetary and Space Sciences Research Institute, The Open University, Milton Keynes MK76AA, UK j.bridges@open.ac.uk.

Introduction: At the 1994 conference it was argued that theories of the origin of chondrules are constrained by the nature of the materials that co-existed with chondrules during accretion [1]. Subsequent advances, in chronology and isotopic systematics of chondrules, CAIs and presolar grains, have tightened these constraints. Chondrules are not viewed in isolation but as a constituent in a turbulent environment that prevailed for >10 Ma after Solar System formation. We summarise the properties and accretional relationships of chondrules deemed critical in determining their genesis and propose a scenario for chondrule and chondrite origin.

Selected properties of chondrules:

- Chondrules range in size from 5 cm - 1μm.
- Chondrules range from silicate-rich to metal-sulfide-rich.
- Co-existing chondrules commonly have different redox states.
- Silicate (ferromagnesian) chondrules:
  - have fractionated Ca/Al ratios.
  - commonly are enriched in refractory Al and moderately volatile Na.
  - commonly have unfractionated rare earth elements at (1-3) x chondritic.
  - may contain troilite with igneous rare earth element abundances.
  - may contain grains that were out of equilibrium with the host melt.
  - were heated to sub-liquidus temperatures (1550-1900°C).
  - cooled at rates ranging from 5000°C/hr to 2-10°C/hr.
  - have ages (2±1) - 10 Ma younger than CAIs and Solar System origin.

Accretional relationships of chondrules:

- Compound chondrules formed by chondrule-chondrule collision.
- From textures, some semi-molten chondrules clumped into groups.
- Chondrules constitute <80 percent of an ordinary chondrite.
- Chondrule fragments and mineral clasts are abundant.
- Solid and semi-molten chondrules co-existed with clastic dust.
- Fine-grained matrix may occur within chondrules.
- Chondrule formation and igneous activity overlapped in time.
- Chondrules and polymict breccias formed at the same time.
- Chondrules accreted with presolar grains.
- Chondrules accreted with CAIs.
- Chondrules accreted with metamorphosed chondrite.
- Some chondrules were aqueously altered before or after accretion.
- Accreted assemblages have quasi-solar compositions.

Ages of chondrules and associated high-temperature objects: A chronology of the first 10 Ma of the Solar System links relative ages from short-lived radionuclides (^{26}Al, ^{53}Mn and ^{129}I) to precise U-Pb ages of rapidly cooled igneous meteorites [2-4]. This is compatible with U-Pb ages of chondrules and Ca-, Al-rich inclusions (CAIs) [5]. A troctolitic igneous pebble with H group oxygen isotopic signature was metamorphosed with its L group (Barwell) host within ~2 Ma of Solar System origin. In Semarkona, LL3.0, an igneous clast with extreme partitioning of its rare earth elements had cooled to isotopic closure when $^{26}Al/^{27}Al$ was $(7.7\pm2.1)\times10^{-6}$ [6], near the maximum of the range in chondrules. Excavation of the clast and mixing between H and L parent body zones require hypervelocity impact. This implies the existence of a large, gravitationally perturbing mass - a protojupiter - within ~2 Ma of Solar System origin.

Chondrites and associated low-temperature material: Presolar grains occur in all chondrite groups, which suggests the former presence of a low-temperature, disk-wide reservoir [7]. Hydrous minerals, bleached chondrules [8] and oxygen isotopic systematics of chondrules [9] and associated cristobalite-bearing inclusions [10] indicate that, apart from EH and EL groups, chondrite precursors contained water-bearing material, presumably ice.

Chondrites and CAIs: CAIs commonly have rim sequences and alteration products indicative of chemical reaction at sub-solidus temperatures [11]. It is

likely that CAIs formed (2±1) Ma before chondrules and before the accretion of chondrites [4, 5], which requires `storage' of CAIs during this interval. Because the ages of many CAIs were not reset during storage, CAIs probably were present in bodies large enough to escape capture by the protosun but small enough to avoid internal heating.

Chondrite precursors: Chondrite groups formed from chemically fractionated precursor material in a series of annular zones at different heliocentric distances in a protoplanetary accretion disk. Chemical fractionation preceded chondrule formation [12]. Present within the disk were: 1) Layered bodies >100 km in diameter, with surface regolith, metamorphosed shells and partly molten interiors ± metal-sulfide cores. 2) Unlayered bodies of low-temperature, hydrated or icy disk solids and CAIs. 3) Fine-grained presolar disk material. 4) Residual gas.

Accretion of chondrites: Gravitational perturbation by protojupiter pumped up relative velocities and caused hypervelocity impact between bodies, with some mixing between heliocentric zones. Unlayered bodies were absent from the zones of the dry EH and EL groups. Repetitive break-up and reaccretion caused ferromagnesian chondrules to form from melt and associated solid olivines or pyroxenes. The observed mixture of igneous and metamorphic lithic clasts, mineral clasts and clast chondrules was produced, together with newly formed chondrules, some with relict grains, and liberated CAIs. Matrix was derived from the dusty disk, from regolith or from disintegrating unmelted primary bodies. Near total reaccretion of disrupted bodies maintained quasi-solar bulk chemical compositions [13].

Origin of protojupiter: To form protojupiter in <2 Ma suggests that the process was `top down' by gravitational collapse, not `bottom up' by grain accretion and capture of gas. To account for the 7.2° tilt of the Sun's spin axis relative to the ecliptic, protojupiter may have been captured on a low inclination. This would have disrupted the disk and ended T Tauri activity in the early Sun [14].

References: [1] Hutchison R. (1996) *Chondrules Protoplanet. Disk,* 311-318. [2] Lugmair G. W. and Shukolyukov A. (2001) *MAPS*, 36, 1017-1026. [3] Huss G. R. et al. (2001) *MAPS*, 36, 975-997. [4] Gilmour J. D. and Saxton J. M. (2001) *Phil. Trans. R. Soc. Lond.*, A359, 2037-2048. [5] Amelin Y. et al. (2002) *Science*, 297, 1678-1683. [6] Hutcheon I. D. and Hutchison R. (1989) *Nature*, 337, 238-241. [7] Huss G. R. and Lewis R. S. (1995) *GCA*, 59, 115-160. [8] Grossman J. N. et al. (2000) *MAPS*, 35, 467-86. [9] Bridges J. C. et al. (1999) *GCA*, 63, 945-951. [10] Bridges J. C. et al. (1995) *Meteoritics*, 30, 715-727. [11] Wark D. A. and Lovering J. F. (1977) *Proc. LSC*, 8, 95-112. [12] Larimer J. W. and Anders E. (1970) *GCA*, 34, 367-387. [13] Hutchison R. (2004) *Meteorites: A petrologic, chemical and isotopic synthesis*. Cambridge University Press, UK. [14] Hutchison R. et al. (2001) *Phil. Trans. R. Soc. Lond.*, A359, 2077-2091.

AMOEBOID OLIVINE AGGREGATES FROM THE SEMARKONA LL3.0 CHONDRITE. S. Itoh[1], S. S. Russell[1] and H. Yurimoto[2] [1]Department of Mineralogy, The Natural History Museum, Cromwell Road, London SW7 5BD, UK (s.itoh@nhm.ac.uk, sarr@nhm.ac.uk), [2]Department of Earth and Planetary Sciences, Tokyo institute of Technology, Meguro, Tokyo 152-8551, Japan (yuri@geo.titech.ac.jp).

Introduction: Amoeboid olivine aggregates (AOAs) are major types of refractory inclusions in carbonaceous chondrites (CC). However, AOAs from ordinary chondrites (OC) have not been reported, even though fine-grained Ca-Al-rich inclusions (FGIs) from OC have been found [e.g. 1].

Chemical and isotopic compositions of refractory inclusions have been disturbed by aqueous alteration or thermal metamorphism, even in the refractory inclusions from the relatively low petrologic type CO3.2 Kainsaz chondrite [2]. Many petrologic and isotopic studies of FGIs, AOAs, chondrules and matrix pointed out that chondritic components from the 3.0 petrologic subtypes in UOC and CO3 chondrites show the smallest degree of disturbance due to metamorphism and alteration [e.g. 2-5]. Thus, the Semarkona LL3.0 is a good target for studying pristine chemical and isotopic compositions of chondritic components.

We report the petrography and oxygen isotopic compositions of AOAs from the Semarkona LL3.0 chondrite, in order to compare the petrography and oxygen isotopic compositions of AOAs in OC and CC, and establish the genetic relationships between AOAs and FGIs in the early solar system.

Analytical procedure: We carried out a petrographic study of three AOAs from a thin section of Semarkona LL3.0 chondrite. They were examined with a petrographic microscope and by X-ray microanalysis using the JEOL 5900LV scanning electron microscope (SEM) and the Leo 1455 SEM with Oxford INCA EDX system, the Phillips XL-30 FE-SEM and the Cameca SX-50 electron microprobe at the Natural History Museum, London.

In-situ oxygen isotopic analyses were performed by the TiTech Cameca ims-1270 SIMS instrument. A 20keV Cs^+ primary ion beam for oxygen isotope analysis focused to a 2 μm spot. Oxygen isotopes were measured as negative secondary ions with M/ΔM of ~6000. Other analytical conditions for O isotope analysis have been described elsewhere [8]. We carefully evaluated overlapping of primary beam among mineral phases by scanning electron microscope after SIMS analysis.

Results and discussion: The AOAs were irregularly shaped and 50-300 μm across in size, composed of olivine ($Fo_{99\text{-}100}$) and Ca-Al-rich components consisting of diopside (TiO_2= ~ 0.5wt%; Al_2O_3= ~ 1wt%) and anorthite (Fig. 1). The core of the Ca-Al-rich regions consist of anorthite enclosed by and/ or attached to diopside, surrounded by a mantle of olivine.

AOA1: AOA1 is irregularly shaped and 250 μm in size (Fig. 1a). There abundance of olivine is large relative to that of diopside and anorthite (Olivine; ~80 vol.%). The anorthite is partly attached to olivine but almost enclosed by diopside.

AOA2: AOA2 is irregularly shaped and 300 μm in size (Fig. 1b). There abundance of olivine is large relative to that of diopside and anorthite (Olivine; ~80 vol.%). The anorthite is partly attached to olivine but almost enclosed by diopside. The texture of AOA2 is similar to that of AOA1.

AOA3: AOA3 is irregularly shaped and 50 μm in size (Fig. 1c). There abundance of olivine is small relative to that of diopside and anorthite (Olivine; ~50 vol.%).

AOAs from the Semarkona LL3.0 chondrite have similar sizes to AOAs from CO3.0 chondrites [e.g. 6, 7]. No AOA has alteration minerals or fayalitic olivine. This suggests that Semarkona AOAs have not been altered or metamorphosed, that is, they have a similar texture to those from CO3.0 chondrites.

The O-isotopic compositions of each phase, all minerals (diopside, anorthite and olivine) comprising the AOAs are enriched in ^{16}O ($\delta^{17,\,18}O_{SMOW}$= ~ −50‰) (Fig. 2). These results are similar to those of AOAs from the Y-81020 CO3.0 chondrite [7].

The relationship between OCs AOAs and CCs AOAs: The petrography and oxygen isotopic compositions of Semarkona LL3.0 AOAs straightforwardly show no difference to those from CO3.0 chondrites and they may have formed in a similar environment. With respect to the O isotopic distributions of AOAs from LL3.0 and CO3.0 chondrites, they were formed from the same reservoir in the early solar system. As results, we conclude that ^{16}O-rich components are dominant in the forming region of AOAs in the solar nebula.

The relationship between AOAs and FGIs: The oxygen isotope distributions of AOAs from OCs and CCs are consistent with those of FGIs from OCs and CCs [e.g. 1, 2, 7]. With respect to the O isotopic distributions of fine-grained refractory inclusions (AOAs and FGIs) from LL3.0 and CO3.0 chondrites, they seem to be formed from the same reservoir in the early solar system. As results, we conclude that ^{16}O-rich components are also dominant in the forming region of fine-grained refractory inclusion in the solar nebula.

The petrography of AOAs continuously changes to those of FGIs (the abundance of olivine changes continuously from 0 to 100 vol.%[7]). The oxygen isotopic distributions of AOAs and FGIs have also been recognized as a similar. However, it is still unclear whether the AOA-forming environment is similar to that of FGI. A preliminary study of REE measurements from AOAs and FGIs in the reduced type CV3 chondrites shows that AOAs are unfractionated REE pattern (Group III and IV) but FGIs are both fractionated (Group II) and unfractionated [9,10]. That means these reservoirs of each components might be different [9]. The systematic study of REE pattern from AOAs and FGIs combined with petrography study could be given some constraints for the difference of environment between AOAs and FGIs.

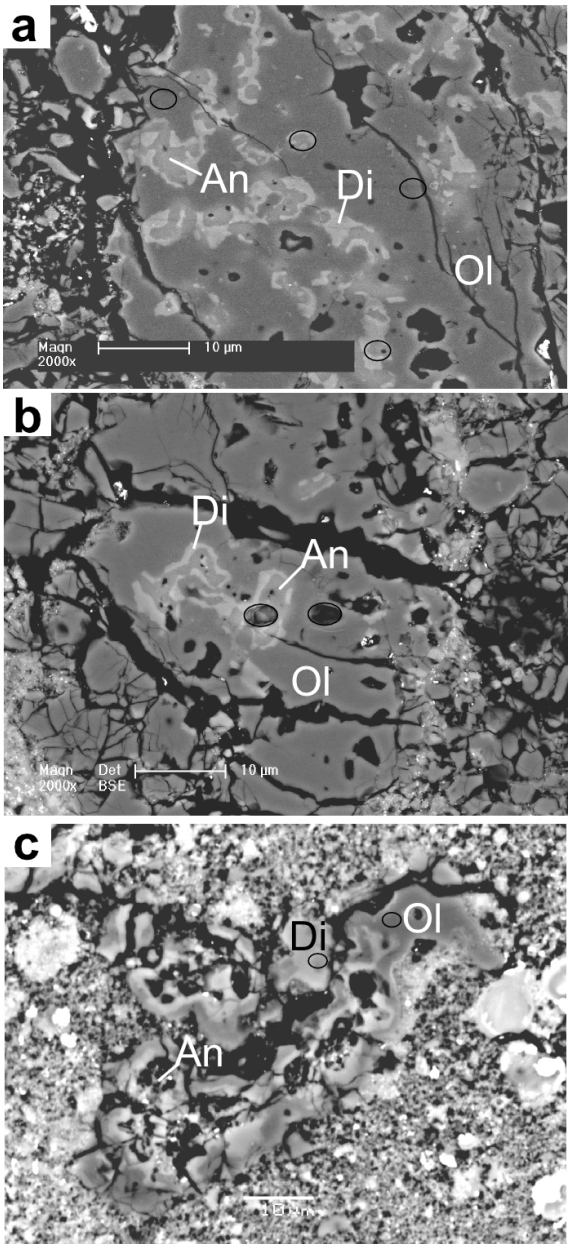

Fig 1. Backscattered electron images of Semarkona AOAs. (a) Close up of AOA1. (b) Close up of AOA2. (c) AOA3. Black circles denote the SIMS spots. The scale bar is 10 microns in each image. Di, diopside; An, anorthite; Ol, olivine.

Acknowledgement: We thank EMMA staff for technical assistant for SEM and EPMA at NHM. We also thank K. Nagashima and Yurimoto lab members for technical assistant for SIMS at Titech. This study has been partly supported by the JSPS Research Fellow and the Royal Society/Daiwa Anglo-Japanese foundation fellowship.

References: [1] McKeegan K. D. et al. (1998) *Science,* **280**, 414-418. [2] Itoh S. et al. (2004) *Geochim. Cosmochim. Acta,* **68**, 183-194. [3] Kojima T. et al. (1995) *Proc. NIPR Symp. Antact Meteorites*, **8**, 79-96. [4] Russell S. S. et al. (1998) *Geochim. Cosmochim. Acta,* **62**, 689-714. [5] Grossman J. N. et al. (1999) *Lunar & Planet. Sci.,* **30,** abs. #1639**.** [6] Chizmadia L. J. et al. (2002) *Meteorit. Planet. Sci.* **37**, 1781-1796. [7] Itoh S. et al. (2002) *Lunar Planet. Sci. XXXIII* abs. 1490. [8] Yurimoto H. et al. (1998) *Science*, **282**, 1874-1877. [9] Russell S. S. et al. (2003) *Lunar Planet. Sci. XXXIV* abs. 1631. [10] Russell et al. (2004) *MAPS,* **67th,** 5139.

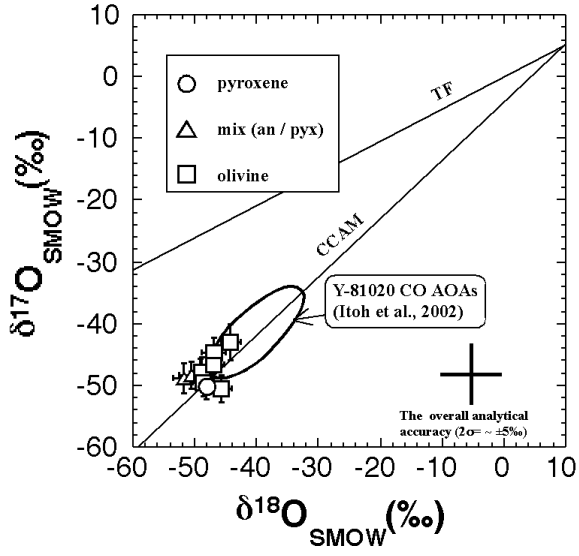

Fig. 2 A three O isotope diagram of Semarkona AOAs.

THE EVOLUTION OF SOLIDS IN PROTO-PLANETARY DISKS. S. B. Jacobsen[1], M. I. Petaev[1,2], D. D. Sasselov[2] and E. R. Adams[2], [1]Department of Earth and Planetary Sciences, Harvard University, Cambridge, 02138, USA (jacobsen @ neodymium.harvard.edu), [2]Harvard-Smithsonian Center for Astrophysics, 60 Garden Street, Cambridge, MA 02138, USA.

Introduction: We are working on a model for the evolution of solids in the Solar Nebula that takes into account: 1) astronomical observations of proto-planetary disks, 2) thermal/dynamical models of proto-planetary disks, 3) isotopic and chemical data from meteorites, 4) thermodynamic models of condensation/evaporation, 5) timescales established from extinct nuclides, 6) isotopic fractionation.

Equilibrium Condensation Cannot Explain Chemical Variations in Chondrites: There are well documented volatile element depletions in most primitive meteorites as well as in terrestrial planets. One of the major shortcomings of the equilibrium condensation model is its inability to account for the observed mineralogy of primitive meteorites; the very presence of high-temperature condensates in them requires an isolation of at least a portion of such condensates from further reactions with the residual nebular gas. To take into account effects of condensate isolation, the CWPI condensation model was developed [1]. The model assumes that as condensation proceeds, a specified fraction (*isolation degree* ξ) of condensed phases is steadily withdrawn from reactive contact with the residual nebular gas, presumably as a result of growth and aggregation of condensed mineral grains (*inert or coarse* dust), while the rest (*reactive or fine* dust) continues to react with the gas. It was also found that the segregation of coarse condensates from the fine dust and residual gas could result in volatility-based fractionation patterns similar to those observed in primitive meteorites. Here we used a newer version of the CWPI model [2] to test this effect quantitatively. Figure 1 shows our results for four elements of different volatility (Al, Si, Cr, Mn) which condense in the system of solar composition at different conditions. We assume that chondritic meteorites represent accreted coarse dust, while fine dust and gas were somehow lost. It is obvious that equilibrium condensation (red curve) fails to account for the bulk chemistry of most chondrites. Bulk chemistry of the CM, CO, CV, and CK carbonaceous chondrites, enriched in refractory elements, requires significant isolation of condensates (green curve corresponding to ξ = 0.7%) during condensation. It is interesting that bulk Earth plots very close to this curve. We note that chondritic meteorites with obvious metal/silicate fractionation (H, L, LL, CR and CH) have been shifted from the CV-CK-CO-CM-CI trend. On the other hand, enstatite chondrites, which are depleted in refractories, could have formed in residual systems, which then must have been re-processed later. The curves for fine dust corresponding to ξ = 0.1 to 0.15 % show that the enstatite chondrites cannot be the complement to the coarse dust trend corresponding to the CV-CK-CO-CM-CI trend. Fine dust from ξ = 0.7% ends up with much higher Si/Al ratios (~70) and has not been identified in meteorites.

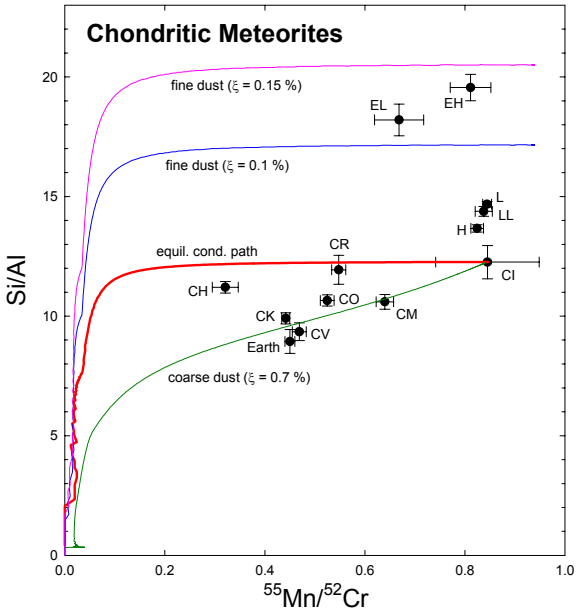

Figure 1.

Mn-Cr Chronology Requires a Short Time Scale for the Solar Nebula: The ^{53}Mn-^{53}Cr extinct nuclide chronometer with its 3.5 Myr half-life is currently the only such chronometer that involves elements with substantial fractionation due to volatility (^{55}Mn/^{52}Cr variations in Figure 1) and for which there is an adequate set of high precision measurements (see Figure 2). All carbonaceous chondrites plot on a single fossil isochron corresponding to a ^{53}Mn/^{55}Mn ratio of 8.4 x 10^{-6}; the ordinary chondrites are slightly above this line while the E-chondrites are significantly below and correspond to a ^{53}Mn/^{55}Mn ratio of 5.6 x 10^{-6}. This yields a time ~ 2 Ma after the formation of the C-chondrites. The Earth's mantle also plots below the C-chondrite isochron but it is possible that the bulk Earth is on this isochron if there is substantial Cr in the Earth's core. The time-scale from this chronometer is consistent with the observation that the dust disappears from accretion disks around young stellar objects within ~2 Myr.

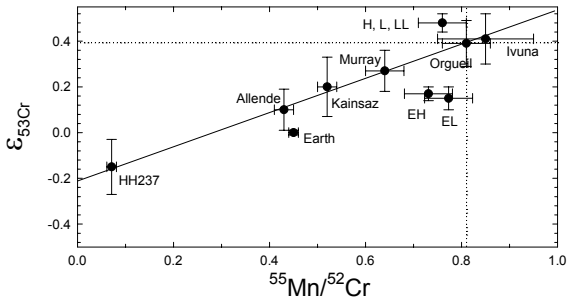

Figure 2. Data from [3,4,5].

Isotopic Heterogeneity Requires Open System Evolution of the Solar Nebula: Variations in the isotopic composition of primitive meteorites demonstrate that the presolar material aggregating to make the chondrite parent bodies and the terrestrial planets was not completely homogenized (for Cr see Figure 3), nor was it processed at temperatures high enough to erase signatures of diverse presolar stellar sources. This is in accord with astronomical observations, which indicate that accretion disks of young stellar objects are at relatively low temperatures.

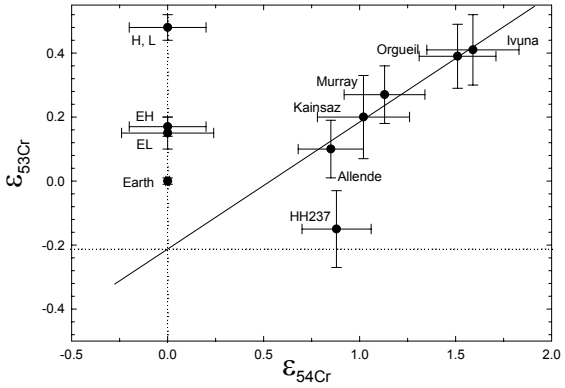

Figure 3. Data from [3,4,5].

The data in Figure 3 show that the ^{53}Cr isotope variations in C-condrites (except for CH) correlate with ^{54}Cr isotope variations. The ^{54}Cr anomalies are most likely of nucleosynthetic origin and result from incomplete homogenization of the material that formed the C-chondrites. If these meteorites represent successive coarse dust fractions as suggested in Figure 1 this means the new material of different Cr isotopic composition was added to the Solar Nebula as condensation was proceeding in the region where the C-chondrites formed. Also, Yin et al. [6] reported the isotopic composition of Mo in bulk CM and CV carbonaceous chondrites and showed that it is distinctly different from what is considered to be the average solar isotopic composition. Bulk CI chondrites appear to be normal in Mo isotopes [7]. The anomalies are most likely in CAIs or matrix of primitive meteorites, since chondrules appear to be isotopically normal.

Thermal Evolution Model of the Nebula: Figure 4 illustrates radial temperature distributions in accreting circumstellar disks using observational input from Hartmann et al. [8]. The three solid lines represent three different ages in the development of a disk: from (1) the hottest at high accretion rates (10^{-6} $M_\odot$/yr) and age of 10^5 yrs, to the oldest, passive protoplanetary disk at $5x10^6$ yrs (3). The upper dotted horizontal line (at 1350K) shows the radial location of the dust coagulation/evaporation front for each disk.

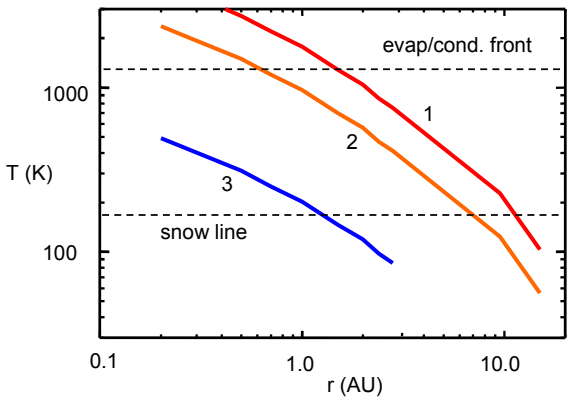

Figure 4.

Conclusions: The following observations demonstrate that the traditional closed system equilibrium condensation models are inadequate for the Solar Nebula: (1) the volatile element pattern in primitive meteorites and the terrestrial planets, (2) isotopic anomalies in bulk samples of chondritic meteorites. The short time scale obtained by extinct nuclide chronology is broadly consistent with astronomical observations as well as with disk models. The gas in the inner solar system must by gone by 5 Myr when the snow line reaches 1 AU, otherwise the Earth would have accreted large quantities of volatiles. This is broadly consistent with noble gas evidence for nebular gas free accretion of the last ~ 20% of the Earth giving rise to the oxidized nature of Earth's mantle.

References: [1] Petaev M.I. and Wood J.A. (1998) *MAPS 33*, 1123-1137. [2] Petaev M. I. et al. (2003) *GCA 67*, 1737-1751 [3] Lugmair G. W. and Shukolykov A. (1998) *GCA*, *62*, 2863-2886. [4] Shukolyukov A. et al. (2003) *LPS XXXIV*, Abstract #1279. [5] Shukolyukov A. and Lugmair G. W. (2004) *GCA*, *68*, 2875-2888. [6] Yin Q-Z. et al. (2002) *Nature*, *415*, 881-883. [7] Dauphas N. et al. (2002) *ApJ*, *569*, L139-L142. [8] Hartmann et al. (1998) *ApJ*, *495*, 385.

NEW NICKEL VAPOR PRESSURE MEASUREMENTS: POSSIBLE IMPLICATIONS FOR NEBULAR CONDENSATES [1,2]N. M. Johnson, [3]A. Meibom, [1,4]F. T. Ferguson, and [1]J. A. Nuth, III, [1]NASA-Goddard Space Flight Center, Astrochemistry Branch, Code 691, Greenbelt, MD 20771, [2]National Research Council Research Associate, [3]Geological and Environmental Sciences, 320 Lomita Mall, Stanford University, CA 94305, [4]Department of Chemistry, Catholic University of America, Washington, DC.

Introduction: Temperatures high enough to vaporize even refractory solids existed in the midplane of the solar nebula during its earliest evolutionary stages and played an important role in the processing of materials that went into the formation of the inner planets and asteroids. A variety of such high-T materials have been identified in primitive chondritic meteorites [1]. These include chemically zoned FeNi metal grains that are generally believed to have formed directly by gas-solid condensation from a gas of approximately solar composition (Fig. 1) [2,3,4,5]. These FeNi particles provide important information about the times scales of formation and physical transport mechanisms in the nebula, as well as formation temperature, pressure and gas chemistry [2,3,4,5]. Currently, however, the interpretation of the chemical signatures in these FeNi particles rests on less than perfect information about the condensation sequence of siderophile elements. For example much, if not all, of the thermodynamic data for the vapor pressures of moderately refractory metals, such as Fe, Ni and Co, do not cover the desired temperature range. As a result, quite large extrapolations are needed. These extrapolations can be complex and uncertain due to factors such as oxygen fugacity or the presence of hydrogen gas [6].

In general, Fe, Ni, and Co show relatively little fractionation relative to each other in processed chondritic metals [7]. Although their vapor pressures are quite similar, they do diverge enough so that significant differences in condensation temperature are predicted (e.g., see ref. [4]) and are expected to be apparent in pristine nebula condensates. In order to make such predictions more accurate we need to have precise vapor pressure measurements relevant to the P-T regimes encountered in the solar nebula.

Recently, we have reported the vapor pressures of Fe and Co to temperatures near 2000 K under low total pressure conditions (less than 0.01 Pa) [8,9]. The resulting vapor pressure lines are shown in Fig. 2. Not surprisingly, the Fe and Co vapor pressure lines run roughly parallel to each other with cobalt having a lower vapor pressure than iron. Nickel was also measured and initial results presented [10]. However, additional and ongoing experiments suggest that the relation of nickel vapor to iron and cobalt may be a compelling indicator of formation temperature.

Experiments: We measure vapor pressure by using a commercial Thermo-Cahn Thermogravimetric system capable of vacuum (P_{TOT} less than 0.01 Pa) operation to 1975 K. This system is capable of measuring mass loss with microgram accuracy provided that the sample plus cell is 100 gram or smaller. We determined the mass loss rate of pure nickel metal under vacuum from 1100 to 1975K. The metal is placed in a simple effusion cell (constructed of alumina) that contains a small hole for vapor escape. The temperature and mass loss are recorded simultaneously. Over the past year, modifications were made to the setup to increase the signal to noise ratio. Experimental details are given in Ferguson *et al.* (2004) [8,9].

Results: Our most recent nickel data suggest that the vapor pressure line of nickel crosses that of Co at ~1900 K and that of Fe at ~1750 K such that the vapor pressure of nickel is greater than Co and Fe below these temperatures, respectively (Fig. 2). We are continuing these measurements and will present specific results at this workshop.

Discussion: The chemically zoned FeNi metal particles have Co/Ni ratios that are roughly solar, which is consistent with the interpretation that they represent direct gas-solid condensates from the solar nebula. However, from the outset it was observed that the Co/Ni ratios in the center of the particles were generally higher than predicted by the applied thermodynamic condensation models. This was initially explained as an effect of partial diffusional equilibration of the FeNi particles as they grew in the nebula [11]. The available literature suggested that the diffusion coefficient of Ni in low Ni fcc FeNi alloy was about a factor of three higher than that of Co. Diffusional equilibration would therefore tend to increase the Co/Ni ratio by allowing Ni to diffuse away from the center of the particle faster than Co [12]. However, a more recent determination of the diffusion coefficient of Ni and Co clearly show that these elements diffuse at essentially the same speed and partial diffusional equilibration can therefore not explain the higher than predicted Co/Ni ratios [13]. The vapor pressure data obtained in this study are relevant to this issue. We will address this problem and explore the more general issue of how the new vapor pressure data for Ni, Co and Fe influence the interpretation of the chemical zonation observed in chondritic FeNi metal grains.

References: [1] Kerridge J. F. and Matthews M. S. (1988) *MESS*,Univ. Ariz. Press. [2] Meibom A. et al. (1999) *JGR Planets, 104*, 22053-22059. [3] Meibom A. et al. (2000) *Science, 288*, 839-841. [4] Petaev et al. (2001) *MAPS, 36*, 93-106. [5] Campbell et al. (2001) *GCA, 65*, 163-180. [6] Schick H. L. (1960) *Chem. Rev., 60*, 331-362. [7] Weisberg et al. (2001) *MAPS, 36*, 401-418. [8] Ferguson F. T. et al. (2004) *J. Chem. Eng. Data, 49*, 497-501. [9] Ferguson F. T. et al. (2004) *J. Chem. Eng. Data*, submitted. [10] Johnson N. M. et al. (2004) *66th MetSoc*, Abstract #5189. [11] Weisberg et al. (1995) *Proc. NIRP Symp. Antarct. Meteorites 8*, 11-32. [12] Meibom A. et al. (2001) *JGR Planet, 106*, 23797-32801. [13] Righter J. et al. (2004) *GCA*, in press.

Acknowledgements: This work was supported by NASA's Cosmochemistry Program.

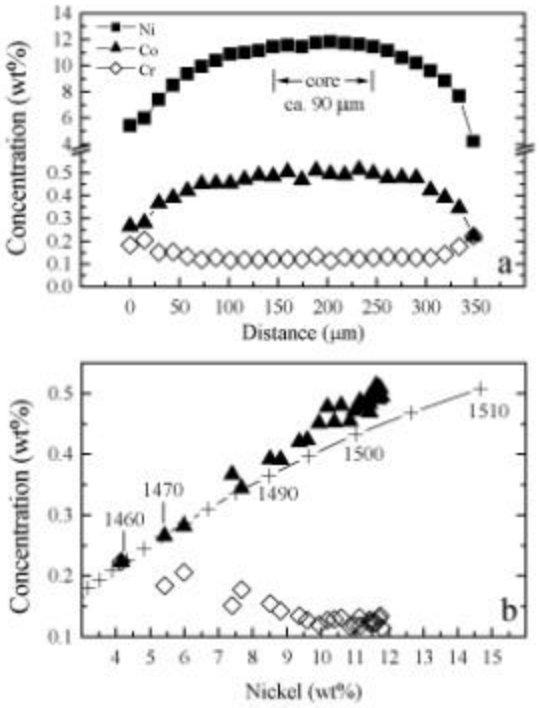

Figure 1. a) Electron microprobe traverse across a chemically zoned FeNi metal grain in the QUE 94411 metal-rich chondrite. b) Co and Cr plotted against Ni. There is a strong positive correlation between Co and Ni, in general agreement with thermodynamic calculations of metal condensation from a gas of roughly solar composition at representative nebula pressures (10 Pa) (solid lines and crosses) [4]. Note however, that in the center of the metal particle, the Co/Ni ratio is substantially higher than predicted (not depicted).

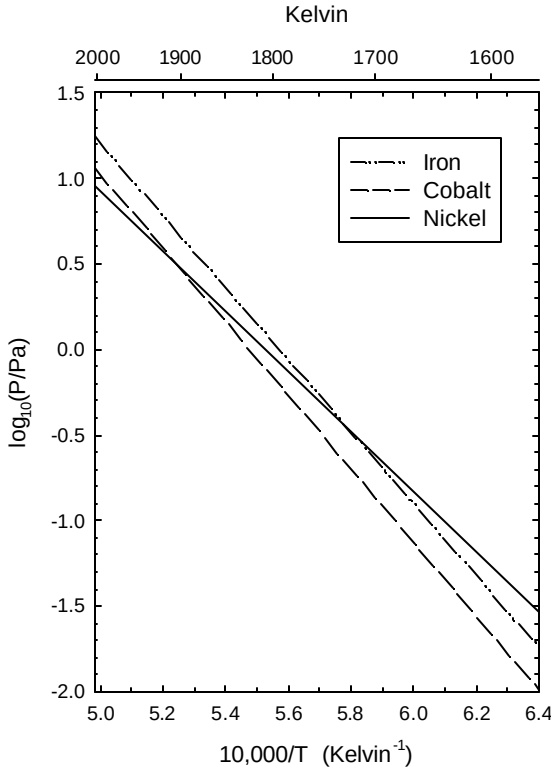

Figure 2 Vapor pressure lines of iron, cobalt, and nickel. Note the crossover of nickel line over iron at ~1750 Kelvin and that of cobalt at ~1900 Kelvin

CHEMICAL, MINERALOGICAL AND ISOTOPIC PROPERTIES OF CHONDRULES: CLUES TO THEIR ORIGIN.
R. H. Jones[1], J. N. Grossman[2] and A. E. Rubin[3], [1]Institute of Meteoritics, Department of Earth and Planetary Sciences, University of New Mexico, Albuquerque, NM 87131, USA (rjones@unm.edu), [2]US Geological Survey, 954 National Center, Reston VA20192, USA. [3]Institute of Geophysics and Planetary Physics, University of California, Los Angeles, CA 90095-1567, USA.

Introduction: The diverse chemical, mineralogical and isotopic properties of chondrules can be used to constrain models of chondrule origins. In order to place constraints on the chondrule formation environment it is important to ensure that we examine primary properties (i.e. those properties possessed by the chondrules immediately after formation) that are not compromised by the effects of secondary, parent-body processes. Chondrule properties can be used to address several fundamental questions:

1. What did chondrule precursors consist of?

The chemical composition of a chondrule gives the most direct information about the bulk chemistry of the precursor assemblage. However, there are caveats to this assumption because the chondrule formation process itself may have significantly modified the composition of the precursor assemblage: volatile elements may have been lost or gained as a result of evaporation/condensation, physical processes may have removed components such as metallic iron beads, and elements such as carbon may have reacted to gaseous components that were lost from the system. Moreover, secondary processes, including parent-body metamorphism and alteration plus terrestrial weathering, may obscure many primary chemical properties of chondrules even in fairly primitive meteorites, including all E chondrites, ordinary and CO chondrites of petrologic type ≥3.1, all CM, CV, CK and R chondrites, and most CR chondrites. Even chondrules in type 3.0 chondrites such as Semarkona, Acfer 094 and Y-81020 may have experienced some redistribution of certain elements during secondary processing.

There is considerable diversity of primary chondrule bulk compositions within each chondrite group. For example, the bulk iron content of chondrules varies by a factor of ~10. The redox state of Fe also varies widely from nearly all Fe^0 to all Fe^{2+}. Mg/Si and refractory-element/Si ratios range from at least 0.5 to 2 × solar in ferromagnesian chondrules from most chondrite groups, with even higher values found in Al-rich chondrules and much lower values in some Si-rich varieties. Primary volatile element contents also vary widely, although these elements are extremely susceptible to secondary modification and many literature data are probably misinterpreted. Low-FeO chondrules show a wide range of primary contents of alkali elements and S, whereas high-FeO chondrules probably had mostly high primary alkali contents and variable S contents. In most chondrules, refractory element contents are generally unfractionated relative to solar. The difficulty in interpreting these chemical variations comes in deciding which result from variations among precursor assemblages and which were caused by chemical fractionations during chondrule formation.

There are significant differences in the distribution of chondrule compositions among the chondrite groups. For example, in C chondrites most chondrules have a high Mg/Si ratio, whereas in E chondrites most chondrules have a low Mg/Si ratio.

Bulk oxygen isotopic compositions of chondrules are also highly variable. Differences among chondrules may reflect the extent to which they underwent isotopic exchange with nebular gas during chondrule formation. Differences among chondrite groups suggest that precursor materials for each group were derived from different isotopic reservoirs.

The physical nature of the precursor assemblage is difficult to establish. Generally, it is assumed that chondrule precursors consisted mostly of fine-grained dust, probably on the (sub-) micrometer scale. Most relict grains that survived melting were relatively coarse, i.e. ≥10 μm. Relict grains that have been identified include olivine and, less commonly, pyroxene. Relict CAI assemblages have also been observed.

Possible sources of fine-grained material include chondrite matrix and amorphous condensates such as those suggested for IDPs. However, the composition of matrix is not consistent with it being the dominant precursor material for chondrules. It is impossible to determine whether chondrule precursor materials were crystalline or amorphous from their post-formation properties. Sintered aggregates may hold more clues to the nature of precursor assemblages.

It has been proposed that chondrules did not form by melting of precursor dust aggregates at all, but rather formed by condensation of liquid droplets. One of the problems with this model is how to incorporate relict grains that were likely derived from previous generations of chondrules. Another problem is that the chondrules would have the same oxygen isotopic composition as the gas, which is inconsistent with the isotopic heterogeneity of chondrules. In addition, implausibly high gas pressures or high gas/dust ratios are required to stabilize condensation of liquids.

At least part of the diversity of chondrule compositions has been interpreted as a chemical evolution with time, as the nebula cooled and evolved chemically. Arguments for an evolution towards more Si-rich and ultimately more Fe-rich compositions with time include oxygen isotopic compositions of chondrules and overgrown igneous rims. However, other petrologic observations such as evidence from relict grains argue that this was not universally true: high-FeO relicts are observed in low-FeO chondrules and vice versa. Arguments have also been made for an evolution towards more Si-rich compositions with time, based on Mg isotopic evidence.

The overall picture of chondrule precursor information that emerges is that there was a great diversity in bulk chemical and oxygen isotopic compositions of chondrules. A given region of the solar nebula must have contained chondrule precursor aggregates with a wide range of compositions. Chondrule precursor heterogeneity occurred on a scale that allowed for different chondrule assemblages both within and among chondrite groups.

2. What was the initial redox state of chondrules?

Chondrules show a range of oxidation states: within an individual O or C chondrite, chondrules range from being extremely reduced (metal-rich, and olivine compositions of Fa<1) to relatively oxidized (no metal, and Fa>30). Chondrules therefore can potentially provide us with information about the redox state of their formation environment. However, we first need to be able to identify the conditions under which the redox state was established. Several possibilities exist, for example, redox state may have been determined by the ambient fO_2 of the gas in the chondrule forming region, by the condensation temperature of precursor materials, or by the abundance in the precursor assemblage of reducing agents such as C. We cannot determine directly whether carbon was an effective reducing agent, because it would be lost as CO gas during the reduction process.

We do not know if widespread reduction or oxidation affected chondrule precursors or chondrules during the formation event. The only grains in chondrules that show direct evidence for a reduction process are dusty relict grains that were initially FeO-rich, and these were probably reduced during final chondrule heating.

3. **What do we know about the ambient gas in the chondrule-forming region?**

Chondrules can potentially provide information about the ambient gas phase in the nebula (P, T, fO_2), because they were intimately associated with it. Considerations of evaporation during chondrule formation lead to the inference that the pressure during the chondrule forming event was higher than the canonical solar nebula, and that the chondrule-forming region was enriched in dust and possibly ice.

Bulk compositions of chondrules are depleted in volatile elements (e.g. Na, K, Mn) relative to CI chondrite abundances. This may be interpreted as volatile loss during chondrule formation, which in itself places constraints on the ambient pressures of volatile species. However, the very presence of even low abundances of volatile elements such as Na, S etc. in primary chondrule minerals places constraints on the ambient temperature of chondrule precursor material; this must have been lower than the condensation temperatures of these elements, about 650 K.

Other observations also indicate that chondrule melts were open systems with respect to the local nebula gas. Some chondrules show evidence of reaction with the gas during formation, as the chondrule cooled and gaseous species condensed onto the molten droplet. For example, the presence of low-Ca pyroxene rims on type I chondrules has been interpreted as progressive condensation of silica onto chondrule surfaces during chondrule formation. In addition, oxygen isotope heterogeneities within and among chondrules record oxygen isotopic exchange between a chondrule and the surrounding gas during chondrule formation.

4. How many times were chondrules heated?

Petrologic considerations can be used to place constraints on how many heating episodes are inferred for a given chondrule, and this has important implications for chondrule formation models.

There is widespread evidence for multiple heating events in chondrules, in the form of easily identifiable features such as relict grains, igneous rims, and compound chondrules. More than 25% of OC chondrules and more than 50% of CV chondrules contain direct evidence for this type of process. Clearly, fragmentation and recycling of material occurred commonly in the chondrule-forming region. It seems likely that most chondrules are the products of at least two heating events.

A related question is to what extent chondrules may have been heated multiple times, without recycling. Petrological interpretations of chondrule textures and mineral compositions can be ambiguous. For example, type II, FeO-rich porphyritic chondrules have been interpreted as cooling in a single, continuous cooling stage, and at the opposite extreme as resulting from many short, high-temperature pulses. Further work is necessary to resolve this ambiguity.

MAXIMAL SIZE OF CHONDRULES IN SHOCK-WAVE HEATING MODEL: STRIPPING OF LIQUID SURFACE IN HYPERSONIC RAREFIED GAS FLOW.

T. Kato[1], T. Nakamoto[2], and H. Miura[1,3], [1]Pure and Applied Sciences, Univ. of Tsukuba (kato@rccp.tsukuba.ac.jp), [2]Center for Computational Sciences, Univ. of Tsukuba (nakamoto@rccp.tsukuba.ac.jp), [3]Research Fellow of the Japan Society for the Promotion of Science (miurah@rccp.tsukuba.ac.jp).

Introduction: Chondrules have a characteristic size distribution: diameters are in a range from 0.1 to 1 mm. From mineralogical features, it is thought that chondrules were formed through melting at least once and resolidifying with rapid cooling. Many formation models for chondrules have been proposed to date, but none has been widely accepted. The shock wave heating model is one of the most plausible models since many chondrule features are accountable. When a shock wave is generated in the solar nebula, the relative velocity between dust particles and the gas in the flow is caused, and that leads to the friction and heating on the dust particles.

When the dust melts by the shock wave heating, deformation and internal flow in the molten dust (i.e. liquid sphere) may take place by surrounding rarefied gas with a hypersonic velocity. For a completely molten and uniform liquid spherical dust particle, hydrodynamical equations with linear approximation were solved, and deformation, internal flow, and pressure distribution were obtained [1, 2]. On the other hand, the possible maximal size of chondrules was estimated based on the balance between the ram pressure by the hypersonic gas flow and the surface tension of the liquid particle [3].

However, when the time scale of heat conduction in a dust particle is longer than the time scale of melting, melting of the dust particle would take place from the surface to the center, and the dust particle would melt partially. So, a dust particle that has a central solid core surrounded by a liquid mantle may be realized. If it is the case, the stability of dust particle with liquid surface and solid core against the hypersonic gas flow should be examined. In this study, we examine behavior of liquid sphere with a solid core in a hypersonic rarefied gas flow.

Results: We analytically solved hydrodynamical equations with linear approximation and obtained the deformation, internal flow, and pressure distribution. As boundary conditions, a spherical solid core is considered to be at the center of liquid sphere, and the balance of forces among the ram pressure by the gas flow, the surface tension, and the stress tensor is considered on the surface.

Figure 1 shows obtained velocity and pressure distribution in the liquid shell for a case with $p_{\mathrm{fm}} r_0$ = 1 m s^{-1}, p_{fm} =100 N m^{-2}, and the ratio of the solid core to the entire sphere is 0.1, where p_{fm} is the momentum flux of the gas flow, r_0 is the outer radius of the partilce, and is the viscosity of the liquid. In the liquid shell, a circulate motion is realized: At the surface of the liquid sphere, the melt flows backwardly, and in the vicinity of the solid core, it moves forwardly. The maximum velocity in the liquid shell is about 8 cm/s. The pressure gradient in the shell directs forward. So, the solid core is exterted forces toward upstream side of the gas flow.

Disscussions: It is expected that the solid core begin to move because of the internal flow and the pressure gradient. If the time scale of the solid core motion is shorter than the time scale of complete melting, it is expected that the solid core leave the liquid sphere. In other words, the liquid solution is stripped away from the solid core.

Following two time scales may be regarded as the characteristic time scale of the motion of the solid core: first is the acceleration time scale of the liquid mantle (t_{accel}) and second is the circulation time scale of the liquid mantle (t_{circ}). When the dust size is large, it takes long time for the solid core to in the liquid mantle. In this case, since leaving of the solid core is limited by the acceleration of the core, we regard t_{accel} as the leaving time scale of the solid core. On the other hand, when the dust size is small, the solid core easily begins to move and quickly adjusts to the surrounding liquid motion. In this case, we regard t_{circ} as the leaving time scale of the solid core. Thus, in this study, we regard $t_{\mathrm{core}} = \max(t_{\mathrm{accel}}, t_{\mathrm{circ}})$ as the stripping time scale of the liquid mantle.

The stripping is expected to occur if following two conditions are met: (1) Melting of a dust particle takes place gradually from the surface: The time scale of heat conduction (t_{cond}) is longer than the time scale of heating (t_{heat}), and (2) the liquid surface is stripped away before the dust particle entirely melts: The time scale of the solid core motion (t_{core}) is longer than the time scale of total melting ($t_{\mathrm{melt}} = \max(t_{\mathrm{cond}}, t_{\mathrm{heat}})$).

Time scales as a function of the radius are shown in Figures 2 and 3. It is found that the stripping of the liquid surface is likely to occur when the dust size is large, because the larger the dust radius is, the longer it takes to melt completely. Also, it is likely to occur when the velocity and the density of the shock waves are large, because the larger the velocity and the den-

sity of the shock are, the more intense the internal flow and the pressure gradient in the liquid shell become. Therefore, it turns out that the maximal size of chondrules can be determined by the stripping of the liquid surface. The maximal size of chondrules surviving from the stripping is estimated to be about 5 mm in radius when shock parameters for chondrule-forming shock waves are taken into consideration [4].

In the above discussion, it is assumed that the dust particle has a dense internal structure. This means that the density of both solid and liquid phases are the same. In what follows, we discuss a dust particle having a porous structure: solid phase has a lower density than the liquid phase. The porous dust may be affected by following effects: (1) The radius of the liquid sphere becomes smaller than the dense particle, if the masses are equal, (2) the circulation time scale changes because the radii ratio of the liquid shell and the solid core changes in the partial melting state, and (3) the heat conductivity becomes low and the thermal conduction time scale becomes large. In view of these effects, we have estimated the maximal size of chondrules surviving from the stripping. When the density is a half and the heat conductivity is one-third of the dense case, the maximal size of chondrules is estimated to be about 1 - 2 mm in radius. This size is smaller than the case of dense particles (5 mm). Though it is considered that chondrules have experienced several melting and resolidifying events, the maximal size of chondrules may be determined by the first melting process, i.e., when a porous dust particle was melted.

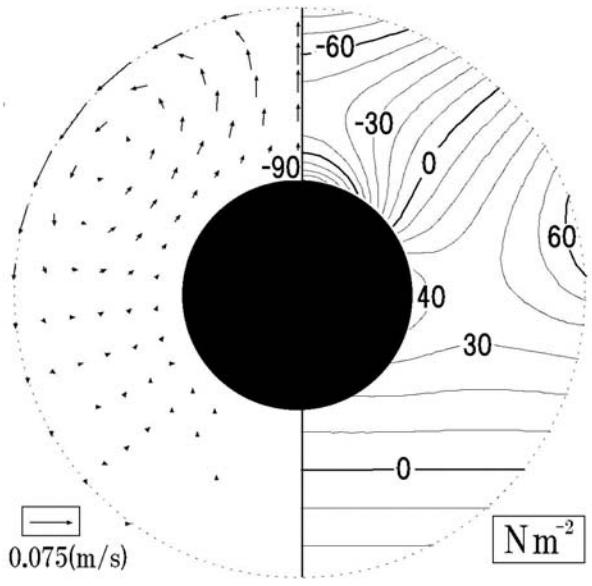

Fig. 1: The velocity and the pressure distributions in a liquid mantle are displayed on the left-hand side (velocity) and right-hand side (pressure), respectively. Parameters of the flow are $p_{fm}r_0\eta$= 1 m s^{-1} and p_{fm} =100 N m^{-2}. The ratio of the solid core to the liquid sphere is 0.1.

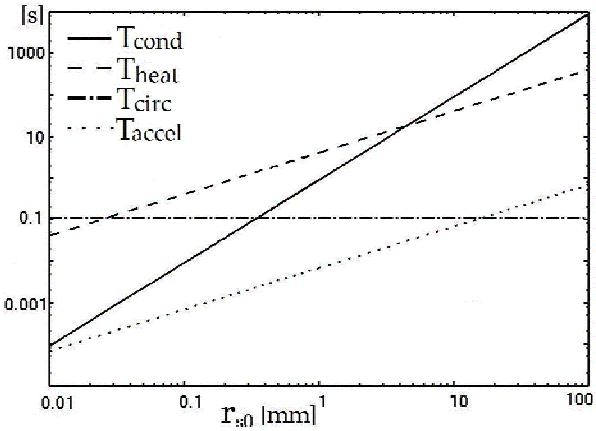

Fig. 2: Time scales as a function of radius r_0 in the case of p_{fm} = 65 N m^{-2} and v_{rel} = 25 km s^{-1}. When r_0 > 5 mm, melting and stripping of the outer part of the particle is expected to occur. When r_0 < 5 mm, the entire dust particle is expected to melt without partial melting.

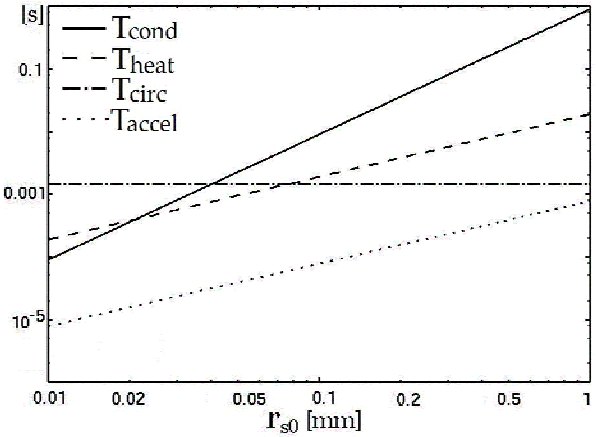

Fig. 3: Same as Fig. 2 except for p_{fm} = 5000 N m^{-2} and v_{rel} = 70 km s^{-1}. When r_0 > 0.04 mm, the stripping is expected to occur. On the other hand, when 0.02 mm < r_0 < 0.04 mm, partial melting occurs, but stripping does not take place. And when r_0 < 0.02 mm, the stripping does not occur because the entire dust particle melts uniformly.

References: [1] Sekiya M., Uesugi M., and Nakamoto T. (2003). *Progr. Theor. Phys., 109,* 717. [2] Uesugi M., Sekiya M., and Nakamoto T. (2003). *Earth Planets Space., 55,* 493-507. [3] Susa H. and Nakamoto T. (2002). *Astrophys. J., 564* L57-59. [4] Miura H. and Nakamoto T. (2004) submitted.

THE NATURE AND ORIGIN OF INTERPLANETARY DUST: HIGH TEMPERATURE COMPONENTS.

L. P. Keller and S. Messenger, Mail Code SR, NASA Johnson Space Center, Houston, TX 77058 (Lindsay.P.Keller@jsc.nasa.gov).

Introduction. The specific parent bodies of individual interplanetary dust particles (IDPs) are unknown, but the anhydrous chondritic-porous (CP) subset has been linked directly to cometary sources [1]. The CP IDPs escaped the thermal processing and water-rock interactions that have severely modified or destroyed the original mineralogy of primitive meteorites. Their origin in the outer regions of the solar system suggests they should retain primitive chemical and physical characteristics from the earliest stages of solar system formation (including abundant presolar materials). Indeed, CP IDPs are the most primitive extraterrestrial materials available for laboratory studies based on their unequilibrated mineralogy [2], high concentrations of carbon, nitrogen and volatile trace elements relative to CI chondrites [3, 4, 5], presolar hydrogen and nitrogen isotopic signatures [6, 7] and abundant presolar silicates [8].

Chondritic-porous IDPs. Typical CP IDPs are highly porous particles that consist of fine-grained crystalline silicates, GEMS (glass with embedded metal and sulfides) grains, and Fe-Ni sulfides, all encased by an organic-rich carbonaceous matrix. The constituent grains in IDPs are much finer-grained (<1 μm) than typical meteorite matrix grains. The abundance of glassy grains (e.g. GEMS grains) is also much higher in IDPs than in meteorite matrix.

Crystalline silicates in CP IDPs are predominantly olivine and low-Ca pyroxene, with lesser high-Ca pyroxene, feldspar, and rare melilite. Multiple lines of evidence suggest a high temperature nebular condensation origin for most of the crystalline silicates in CP IDPs. The olivine and pyroxene grains are typically single crystals and have Mg-rich (Mg/Mg+Fe ~ 100-90) and Mn-rich (up to 5 mol%) compositions that are consistent with condensation models [9]. Many of the enstatite grains and some of the forsterite crystals show unique whisker and platelet morphologies (Figure 1) as well as characteristic defects (axial screw dislocations) that implicate growth from the vapor phase [10]. The crystalline silicates observed in CP IDPs also show marked similarities in terms of mineralogy, size, composition, and abundance to those observed forming around young stars and in comets through astronomical infrared (IR) spectroscopic measurements [11, 12]. Additional evidence that the crystalline silicates are an early-formed component of CP IDPs includes: 1) the presence of pre-accretionally irradiated rims on many of the crystalline grains which indicates the grains were exposed as small objects prior to their accretion into their parent bodies and 2) the close association of crystalline silicates with presolar molecular cloud materials (high D/H organics) and presolar silicates.

Presolar forsterite grains have been identified in CP IDPs on the basis of their oxygen isotopic compositions. One forsterite grain appears to have originated from red giant or asymptotic giant branch (AGB) stars [8]. We have recently identified a group of polycrystalline forsterite grains whose O isotopic compositions point toward an origin from a type II supernova [13].

GEMS Grains. GEMS grains are a major component of CP IDPs and are <0.5 μm diameter grains consisting of abundant 10 to 50 nm-sized kamacite and Fe-Ni sulfide grains dispersed in a Mg-Si-Al-Fe amorphous silicate matrix (Figure 2). To date, GEMS grains have not been reported from any meteorite samples. Bradley [2] proposed that GEMS are preserved interstellar (IS) silicates based on observed preaccretional irradiation effects and IR spectral properties that closely resemble IS dust [14]. Oxygen isotopic measurements confirm that at least a small fraction (<5%) of GEMS are demonstrably presolar, while the remainder have ratios that are indistinguishable from solar values [8, 15].

GEMS with solar oxygen isotopic compositions either had their isotopic compositions "homogenized" through processing in the interstellar medium (ISM) [e.g. 16], or formed in the early solar system. We have recently measured bulk elemental compositions of GEMS grains and showed that they are systematically sub-chondritic with respect to S/Si, Mg/Si, Ca/Si, and Fe/Si [17]. For these element/Si ratios, the average GEMS compositions are ~60% of solar values, although the average Al/Si ratio in GEMS is indistinguishable from solar. The elemental and isotopic data for GEMS grains suggest that most formed in the early solar nebula either as shock melts or as direct, non-equilibrium condensates [17]. In this model, the pre-accretional irradiation effects observed in GEMS grains occurred in the solar nebula – this view is supported by the similar magnitude of irradiation effects experienced by GEMS grains and many of the crystalline silicates in CP IDPs. If most GEMS grains are condensates, then a mechanism has to exist to transport the GEMS grains (as well as some forsterite and enstatite) to the comet-forming region, perhaps through bipolar outflows during the early accretion phase of the disk [16].

Trace components. High temperature refractory phases such as those observed commonly in Ca- and Al-rich inclusions (CAIs) in meteorites also occur in

IDPs [18-20] however, the average grain size is much smaller than is observed in CAIs [19]. Fassaite, anorthite, gehlenite, spinel occur as rare isolated grains in chondritic IDPs, but entire IDPs dominated by CAI-like mineralogy are also observed [18,19].

Sulfides. Sulfides are a major constituent of CP IDPs and dominated by low-Ni pyrrhotites with a wide range of grain sizes [21]. The pyrrhotites occur as isolated single crystals as well as 10-50 nm-sized grains decorating the exterior of GEMS grains. The sulfides are believed to result from the sulfidation of pre-existing FeNi metal in the early nebula. Observational evidence suggests that Fe sulfides are likely circumstellar grains around young stars [22], although isotopically anomalous sulfides have not been detected in preliminary S isotopic measurements [23].

Discussion CP IDPs derive from fundamentally different parent bodies than meteorites. Their most probable sources are short-period comets that originate from the Kuiper belt. These particles thus sample an entirely different regime of the solar nebula, ~40 AU from the Sun, than meteorites (1.8-3.5 AU). These IDPs contain abundant crystalline grains that must have formed at high temperatures, predominantly in the solar system (as shown by their isotopic compositions). Most GEMS grains are similarly solar in O isotopic compositions and their origins appear to be linked with the solar system crystalline silicates based on complementary chemical signatures [17]. Both the crystalline silicates and GEMS are intimately mixed with thermally labile presolar organic matter. These observations are most easily explained by a substantial portion of IDP components originated in high-temperature processes near the Sun, and were subsequently transported to the Kuiper belt. Such extensive radial mixing of material in young stellar objects has been inferred from observations of bipolar outflows.

Acknowledgements. This work was supported by NASA RTOPs 344-31-40-07 (LPK) and 344-31-72-08 (SRM).

References. [1] Brownlee, D. E. et al. (1995) *LPSC* **26**, 183. [2] Bradley, J. P. (1994) *Science*, **265**, 925. [3] Thomas, K. L. *et al*. (1993) *GCA*, **57**, 1551. [4] Keller, L. P. *et al.* (2004) *GCA*, **68**, 2577. [5] Flynn, G. J. *et al.* (1993) *Meteoritics* **28,** 349. [6] McKeegan, K. D. *et al*. (1985) *GCA*, **49**, 1971. [7] Messenger, S. (2000) *Nature*, **404**, 968. [8] Messenger et al. (2003) *Science*, **300**, 105. [9] Klock, W. *et al*. (1989) *Nature*, **339**, 126. [10] Bradley, J. P. *et al*. (1983) *Nature* **301**, 473. [11] Malfait, K. *et al.* (1998) *A&A*, **332**, L25. [12] Hanner, M.S. *et al.* (1999) *Earth, Moon and Planets*, **79**, 247. [13] Messenger, S. and Keller, L. P. (2004) *MPS*, **39**, A68. [14] Bradley, J. P. *et al*. (1999) *Science*, **285**, 1716. [15] Stadermann, F. J. and Bradley, J. P. (2003) *MPS,* **38**, #5236. [16] Tielens, A.G. G. M. (2003) *Science*, **300**, 68. [17] Keller, L. P. and Messenger, S. (2004) *LPSC* **35**, #1985. [18] Christoffersen, R. C. and Buseck, P.R. (1986) *Science*, **234**, 590. [19] Zolensky, M. E. (1987) *Science*, **237**, 1466. [20] Greshake, A. *et al*. (1996) *MPS*, **31**, 739. [21] Dai, Z. and Bradley, J. P. (2001) *GCA* **65**, 3601. [22] Keller, L. P. *et al.* (2001) *Nature*, **417**, 148. [23] Mukhopadhyay, S. *et al*. (2003) *MPS*, **38**, #5289.

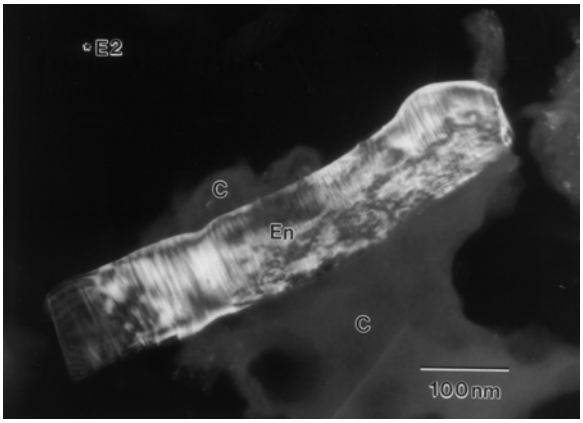

Figure 1. A darkfield transmission electron image of an enstatite whisker in IDP L2009*E2. Characterisitic elongation direction is perpendicular to the (100) stacking faults.

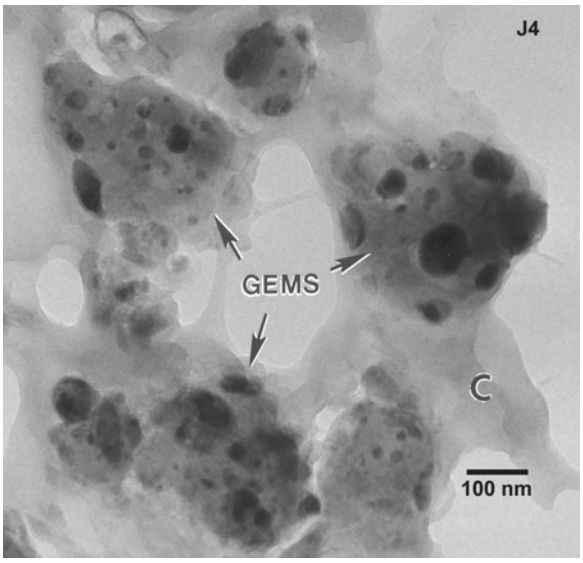

Figure 2. A brightfield TEM image of a cluster of GEMS grains and their carbonaceous matrix (L2009J4). The dark, rounded grains within the GEMS are kamacite and FeNi sulfide grains.

REFRACTORY RELIC COMPONENTS IN CHONDRULES FROM ORDINARY CHONDRITES. M. Kimura[1], H. Hiyagon[2], M. K. Weisberg[3,4] and H. Nakajima[1], [1]Faculty of Science, Ibaraki University, Mito 310-8512, Japan, makotoki@mx.ibaraki.ac.jp, [2]Dept. Earth and Planet. Science, University of Tokyo, Tokyo 113-0033, Japan, [3]Dept. Physical Sciences, Kingsborough College, City University of New York, Brooklyn, NY 11235, [4]Dept. Earth and Planetary Sciences, American Museum of Natural History, NY, NY 10024, U.S.A.

Introduction: Relic components have been found in chondrules from many chondrites. In rare cases, in carbonaceous chondrites (CC), the common ferromagnesian chondrules (FMC) and the less abundant Al-rich chondrules (ARC) contain relic Ca-Al-rich inclusions (CAI) or their constituent minerals [1-3]. However, relic CAIs have not yet been reported in chondrules of ordinary chondrites (OC). Relic components are important for reconstructing the evolution of solid material in the primitive solar nebula, for example, CAIs followed by most ARCs should have formed prior to the FMCs [4].

In this paper, we describe our study of refractory relic components in FMCs in OCs and discuss the significance of these relic components in the OCs.

Relic Spinel in FMCs: The chemistry and textural setting of spinel group minerals are good indicators of petrologic subtype, and spinel in subtypes 3.0-3.3 preserves its primary composition [5].

Kimura et al. [5] also studied the crystallization of spinel in FMCs. In many FMCs, spinel crystallized after olivine, as determined from the bulk chondrule composition and texture. However, the crystallization sequence of some FMCs expected from the bulk composition is inconsistent with the occurrence of spinel completely enclosed in olivine. Such spinel is interpreted to be a relic phase, and was probably incorporated into the chondrule precursor material before melting.

The oxygen isotopic compositions of most spinel grains in several FMCs plot around the terrestrial fractionation (TF) line, supporting *in situ* crystallization of the spinel (Fig. 1). On the other hand, the relic spinel in one FMC (WE-S3) is enriched in ^{16}O ($\delta^{17}O$ = -5.06 ± 1.64‰ and $\delta^{18}O$ = -2.47 ± 3.15‰), and has lighter oxygen than the coexisting olivine which plots on the TF line (Fig. 1).

Diffusion of oxygen into spinel is very slow [6], and it is difficult for the oxygen isotopic compositions of the relic spinel to equilibrate with that of the surrounding phases during chondrule formation by flash heating. Thus, it is expected that relic spinel would preserve a record of its primordial oxygen isotopic compositions during chondrule formation. The oxygen composition of the spinel in WE-S3 is not as ^{16}O-rich as the spinel in CAIs and refractory forsterite in OCs [7]. However, the oxygen composition of the relic spinel obtained here is similar to those of spinel grains in ARCs [8].

Relic Perovsktie in FMC: Kimura et al. [9] reported perovskite grains in a large FMC, 2.5 x 3 mm in size, in an LL3.2 chondrite (Y790448). This chondrule has barred texture in the center, and is porphyritic in the margin. It mainly consists of olivine (Fo_{76} on average), with low-Ca pyroxene ($En_{64}Fs_{24}Wo_{12}$), high-Ca pyroxene ($En_{58}Fs_{20}Wo_{22}$) and plagioclase ($An_{88}Ab_{12}$). Minor spinel and ilmenite are also present. This chondrule also contains five grains of perovskite, 3-9 μm in size (Fig. 2). Perovskite has been previously reported from CAIs in OCs [10,11]. However, this is the first discovery of perovskite in a FMC in an OC.

Although measurement of the oxygen isotopic compositions and REEs for the perovskite and the host chondrule are currently in progress, we suggest the possibility that the perovskite has been derived from a CAI, and it is another relic phase in FMCs.

Discussion and Summary: Refractory-rich relic components have been recently reported in FMCs and ARCs, especially in CCs, e.g., a CAI fragment in an FMC [1], relict spinel in an ARC [2], and a CAI component in an ARC [3]. Relic olivine has also been recognized in OC chondrules by its compositional difference from other olivine in the same chondrule, such as magnesian olivine in FeO-rich chondrules [12], and FeO-rich olivine with tiny (dusty) blebs of metal in MgO-rich chondrules [13]. Refractory relic forsterite and spinel were recently discovered in a FMC by their ^{16}O-rich oxygen isotopic compositions [7].

The discovery of relic spinel and perovskite in FMCs reported here is further evidence that OCs, as well as CCs, contain some of the earlier-formed components. These relic oxides may have been derived from ARCs and CAIs, respectively. The discovery is an indication of the complexities in the early solar nebula processes that ranged from formation of CAI, through ARC, to FMC.

However, the early-generated refractory components seem to be less common as relict components in OC chondrules, in comparison with CC chondrules. This may be related to the lower abundance of CAIs in OCs (much lower than 0.2

vol.% after [14]). CAIs may have been lower in abundance in the reservoir where the components of OCs formed. The lower abundance of refractory materials seems to be consistent with the generally heavier oxygen isotopic composition of the OC chondrules, than those of many CC chondrules. Alternatively, the chondrules in OCs may have been more thoroughly processed and recycled than those in some CCs, thus destroying the most primitive relict components and allowing more oxygen exchange with a heavier gaseous reservoir.

References: [1] Misawa K. and Fujita T. (1994) *Nature, 368*, 723-726. [2] Maruyama S. and Yurimoto H. (2003) *GCA, 67*, 3942-3957. [3] Krot A.N. et al. (2004) *GCA, 68*, 2167-2184. [4] MacPherson G.J. et al. (2000) *LPS XXXI*, #1796. [5] Kimura M. et al. (2004) *Antarctic Meteorites XXVIII*, 31-32. [6] Ryerson F.J. and McKeegan K.D. (1994) *GCA, 58*, 3713-3734. [7] Pack A. et al. (2004) *GCA, 68*, 1135-1157. [8] Russell S.S. et al. (2000) *EPSL, 184*, 57-74. [9] Kimura M. et al. (2003) *MAPS, 38*, A33. [10] Bischoff A. and Keil K. (1984) *GCA, 48*, 693-709. [11] Kimura M. et al. (2002) *MAPS, 37*, 1417-1434. [12] Jones R. (1990) *GCA, 54*, 1785-1802. [13] Nagahara H. (1981) *Nature, 292*, 135-136. [14] Kimura M. et al. (2001) *MAPS, 36*, A98-A99.

Fig. 1. The oxygen isotopic compositions of olivine and spinel in 3 chondrules in Wells (LL3.3).

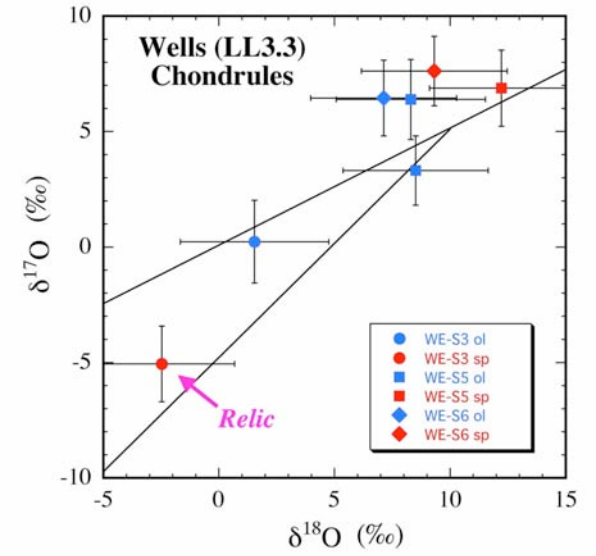

Fig. 2. A part of Y790448 (LL3.2) chondrule. A perovskite (Per) grain is encountered with olivine (Oli), plagioclase (Pla) and spinel (Spi). Width 50 μm.

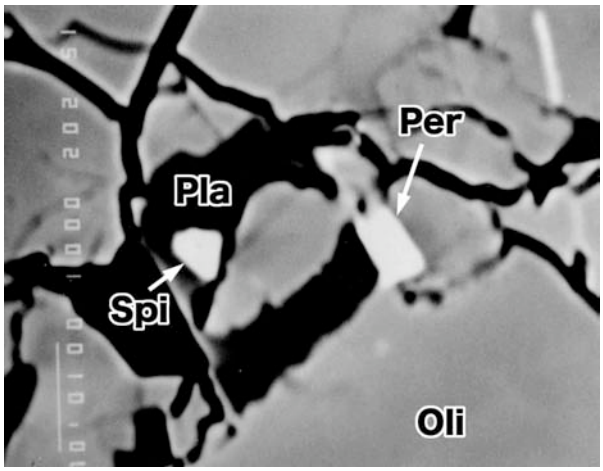

CONSTRAINTS ON THE ORIGIN OF CHONDRULES AND CAIS FROM SHORT-LIVED AND LONG-LIVED RADIONUCLIDES. N. T. Kita[1, 2], G. R. Huss[3], S. Tachibana[4], Y. Amelin[5], E. Zinner[6], L. E. Nyquist[7], and I. D. Hutcheon[8], [1]Geological Survey of Japan, AIST (noriko.kita@aist.go.jp), [2]University of Wisconsin, Madison, [3]Arizona State University, [4]University of Tokyo, [5]Geological Survey of Canada, [6]Washington University, St. Louis, [7]NASA Johnson Space Center, [8]Lawrence Livermore National Laboratory.

Introduction: In order to understand the timing of events in the early solar system, we rely on the radio-nuclide-based chronometers applied to materials in primitive meteorites. Because the time scale of early-solar system evolution was on the order of a few million years (Myr), we focus on so-called "short-lived radionuclides" with mean lives of less than 10 Myr (Table 1), as well as on the long-lived U-Pb system where high precision ^{207}Pb-^{206}Pb ages are applied. Note that the validity of some systems as chronometers (e.g., Be-B, Fe-Ni) has yet to be established. We summarize literature data for chondrules and CAIs and discuss how these chronometers constrain formation time scales in the early solar system.

Table 1. Short-lived nuclides for early solar system chronometry

Parent nuclide	Daughter nuclide	τ_{half} (Myr)	Initial abundance
^{41}Ca	^{41}K	0.1	^{41}Ca/^{40}Ca ~ 2E-8
^{26}Al	^{26}Mg	0.73	^{26}Al/^{27}Al ~ 5E-5
^{10}Be	^{10}B	1.5	^{10}Be/^{9}Be~ 1E-3
^{60}Fe	^{60}Ni	1.5	^{60}Fe/^{56}Fe~ 5E-7?
^{53}Mn	^{53}Cr	3.7	^{53}Mn/^{55}Mn~ 1E-5?

The initial abundances of short-lived nuclides in primitive meteoritic materials are determined from analyses of the excesses of daughter nuclides correlated with the stable isotope of the parent element. By assuming a homogeneous distribution of short-lived nuclides in the early solar system, variations in the estimated isotope ratios (R) can be transferred to relative ages as follows;

$$\Delta t = \ln(R/R_0) \times \tau_{half} / \ln(2) ,$$

where R_0 represents the solar system initial isotope ratio for a specific short-lived nuclide (values listed in Table 1).

The ^{26}Al-^{26}Mg system: Since the discovery of ^{26}Mg excesses, correlated with Al/Mg ratios, in CAIs confirmed the former-existence of live-^{26}Al in the early solar system [1], numerous data have been obtained for CAIs, chondrules, and plagioclase in both equilibrated ordinary chondrites (EOC) and achondrites. These data (summarized in Fig. 1) indicate (1) the majority of CAIs formed contemporaneously within a short time interval of no more than a few hundred thousand years, (2) chondrule formation began 1-2 Ma after CAI formation and persisted for ~1-3 Myr; and (3) plagioclases in EOC and achondrites processed in parent bodies are at least 4-5 Myr younger than CAIs. These time scales are comparable to those of classes I, II, and III young stars inferred on the basis of infrared observations; (1) ~0.1 Myr for Proto-stars, (2) ~3 Myr for classical T-Tauri stars, and (3) ~10 Myr for weak-lined T-Tauri stars [2]. The ^{26}Al-^{26}Mg chronometer is thus most plausibly interpreted in terms of sequential chain of events – CAIs formed first in the earliest active solar nebula, chondrules next in the quasi-steady proto-planetary disk, and planetary accretion then started a few Myr after the formation of the solar system.

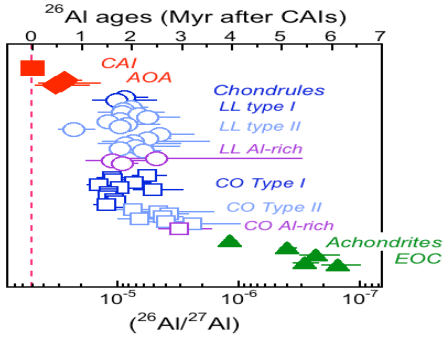

Fig. 1. Summary of ^{26}Al ages from CAIs, chondrules and other meteorites. The initial ^{26}Al/^{27}Al ratios of well correlated isocrhons obtained from CAIs distributed mostly between (4-6) $\times 10^{-5}$ [3]. Other data for individual samples are from [4-16].

Systematic studies of chondrules in LL3.0-3.1 and CO3.0 chondrites indicate contemporary formation in spite of the fact that they formed in distinct isotopic and chemical reservoirs. Chondrules in LL3.0-3.1 show a correlation of the ^{26}Al-^{26}Mg age with bulk Si/Mg and abundances of volatiles, implying that the chemical compositions of chondrule precursors evolved with time from more refractory compositions to volatile ones [10, 17]. Data from CO3.0 chondrites show the tendency that FeO-rich type II chondrules are relatively younger than FeO-poor type I chondrules [11-12].

The high precision Pb-Pb ages: High precision Pb-Pb absolute ages were recently obtained for CAIs and chondrules, after repeated leaching steps to remove non-radiogenic Pb [18]. The average of two CAIs in Efremovka gave the oldest Pb-Pb age of 4567.2±0.6 Myr, while multiple chondrule data from Acfer059 gave the age of 4564.7±0.6 Myr. Thus, these data confirm an ~2 Myr time difference between CAIs and chondrules. Further studies for chondrules from various meteorites are being conducted.

Coherence of the short-lived chronometers: In theory, if the solar system was homogenized, it should be possible to infer the same chronology from any of the various long- and short-lived isotopic chronometers. The various chronometers based on short-lived radionuclides do give approximately the same overall time scale and put the various events in approximately the same order (e.g, Fig. 2), but in detail, there are significant disagreements. Many of these disagreements probably reflect isotopic disturbance of one or more of the systems. Some of them are disturbed or reset very easily. In addition, the nebula may not have been fully homogeneous (cf, the Mn-Cr system [20-22]). In spite of these complications, several systems show that CAIs are the oldest solids, chondrule began to form ~1 Ma later, and meteorite metamorphism and asteroid differentiation required an additional few Ma (Fig. 2)

Constraints from other nuclides: High and variable abundance of the $^{10}Be/^{9}Be$ ($5\text{-}10\times10^{-4}$ [23-25]) inferred from ^{10}B excesses in CAIs requires the production of this short-lived nuclide by high-energy particle irradiation. It has been suggested that CAIs formed closed to the sun where production of ^{10}Be was sufficient, although the contribution of particle irradiation to the other short-lived nuclides, such as ^{26}Al, is considered to be small [25]. Recently, ^{60}Ni excesses from decay of ^{60}Fe were observed in troilite and a radial pyroxene chondrule in UOCs, indicating the initial $^{60}Fe/^{56}Fe$ of the solar system to be 3×10^{-7} or higher [26-28]. This level of ^{60}Fe may require a supernova source that injected other short-lived nuclides into the Sun's parent molecular cloud as well and may have triggered the formation of the solar system.

References: [1] Lee T. et al. (1976) *GRL. 1*, 225-228. [2] Lawson W. A. (1996) *Mon. Not. R. Astron. Soc. 280,* 1071-1088. [3] MacPherson G. J. et al. (1995) *Meteoritics 30,* 365-386. [4] Itoh S. et al. (2002) *LPS XXXIII,* Abstract #1490. [5] Hutcheon I. D. and Hutchison R. (1989) *Nature 337*, 238-241. [6] Russell S. S. et al. (1996) *Science 273*, 757-762. [7] Kita N. T. (2000) *GCA 60*, 3913-3922. [8] McKeegan K. D. et al. (2000) *LPS XXXI*, Abstract #2009. [9] Huss G. R. et al. (2001) *Meteoritics & Planet. Sci. 36*, 975-997. [10] Mostefaoui S. et al. (2002) *Meteoritics & Planet. Sci. 37*, 421-438. [11] Kunihiro T. et al. (2004) *GCA 68*, 2947-2957. [12] Kurahashi E. et al. (2004) *LPS XXXV,* Abstract# 1476. [13] Nyquist L. E. et al. (2003) *EPSL 214,* 11-25. [14] Nyquist L. E. et al. (2003) *LPS XXXIV,* Abstract# 1388. [15] Zinner E. and Göpel C. (2002) *Meteoritics & Planet. Sci. 37,* 1001-1013. [16] Kita N. T. et al. (2003) *LPS XXXIV,* Abstract# 1557. [17] Tachibana S. et al. (2003) *Meteoritics & Planet. Sci. 38*, 939-962. [18] Amelin Y. et al. (2002) *Science 297*, 1678-1683. [19] Lugmair G. W. and Galer S. J. G. (1992) *GCA 56*, 1673-1694. [20] Lugmair G. W. and Shukolyukov A. (1998) *GCA 62*, 2863-2886. [21] Nyquist L. E. et al. (2001) *Meteoritics & Planet. Sci. 36,* 911-938. [22] Shukolyukov A. and Lugmair G. W. (2001) *Meteoritics & Planet. Sci. 36,* A188. [23] McKeegan K. D. et al. (2000) *Science 289*, 1334-1337. [24] Sugiura N. et al. (2001) *Meteoritics & Planet. Sci. 36,* 1397-1408. [25] MacPherson G. J. et al. (2003) *GCA 67*, 3165-3179. [26] Tachibana S. Huss G. R. (2003) *ApJ 588*, L41-L44. [27] Mostefaoui M. et al. (2003) *LPS XXXIV*, Abstract #1585. [28] Huss G. R. and Tachibana S. (2004) *LPS XXXV*, Abstract#1811.

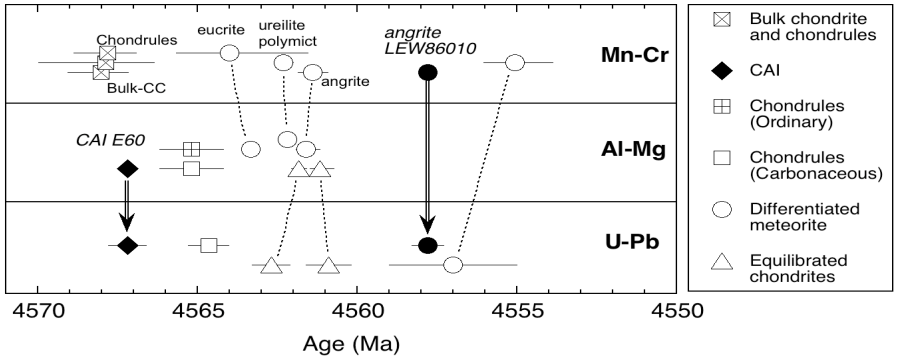

Fig. 2. Comparison of three chronometers. The ^{26}Al and ^{53}Mn ages are converted to absolute ages by using CAIs (4567.2Ma [18]) and LEW86010 (4557.8Ma [19]) as references, respectively.

THE GENETIC RELATIONSHIP BETWEEN REFRACTORY INCLUSIONS AND CHONDRULES. A. N. Krot[1], S. S. Russell[2], G. J. MacPherson[3], G. R. Huss[4], S. Itoh[2], and K. Keil[1] [1]HIGP/SOEST, University of Hawai'i at Manoa, Honolulu, HI 96822, USA (sasha@higp.hawaii.edu), [2]Dept. of Mineralogy, The Natural History Museum, London, SW7 5BD, U.K., [3]Smithsonian Institution, Dept. of Mineral Sciences, Washington DC 20560, USA, [4]Dept. of Geological Sciences, Arizona State University, Tempe, AZ 85287-1404, USA.

Introduction: Chondrules and refractory inclusions [Ca, Al-rich inclusions (CAIs) and amoeboid olivine aggregates (AOAs)] are the major high temperature components of chondritic meteorites formed during transient heating events in the inner solar nebula. Mineralogical, chemical, and isotopic observations, and thermodynamic analysis suggest that refractory inclusions formed in an ^{16}O-rich (Δ^{17}O ~ -20‰) gaseous reservoir at low total pressure (<10^{-4} bar) and high ambient temperatures (near or above the condensation temperatures of forsterite; ~1300 K), and were subsequently isolated (physically or kinetically) from reactions with the high temperature nebular gas [1-6]. Gas-solid reactions (evaporation-condensation) appear to have been the dominant processes during formation of refractory inclusions. Some CAIs (mostly in CV chondrites) experienced extensive melting accompanied by evaporation and mass-dependent isotopic fractionation of Mg and Si [7,8]. Both igneous and non-igneous CAIs are surrounded by ^{16}O-rich multilayered rims (called Wark-Lovering rims) with the outermost layers, composed of Al-diopside and forsterite, formed by gas-solid condensation [9]. Most CAIs show large ^{26}Mg excesses (^{26}Mg*) corresponding to an initial ^{26}Al/^{27}Al ratio [$(^{26}Al/^{27}Al)_I$] of ~4-6×10^{-5} [10-12]. In contrast, most chondrules have low $(^{26}Al/^{27}Al)_I$ ($\leq$1.5×10^{-5}) [10,13-16] and appear to have formed in an ^{16}O-poor (Δ^{17}O > -5‰) gaseous reservoir [17] at low (<1000 K) ambient temperatures and high total pressure [18] or dust/gas ratios [19]. Multiple episodes of melting of pre-existing solids accompanied by evaporation-recondensation are believed to have been the dominant processes during chondrule formation [20]. Here, we review the major isotopic, mineralogical, and chemical constraints on the genetic relationship between chondrules and refractory inclusions.

^{207}Pb-^{206}Pb Ages: The ^{207}Pb-^{206}Pb age of CAIs from Efremovka (CV) and Allende (CV) is 4567.2±0.6 Ma [21-23]. ^{207}Pb-^{206}Pb ages of chondrules range from 4566.7±1.0 Ma for Allende to 4564.7±0.7 Ma for Acfer 059 (CR) to 4562.7±0.5 Ma for Gujba (CB) [24]. These observations suggest that chondrule formation started shortly after or may be even contemporaneously with CAI formation and continued for at least 4.0±1.5 Myr. The duration of CAI formation remains unknown.

^{26}Al-^{26}Mg Ages: The observed differences in $(^{26}Al/^{27}Al)_I$ between most CAIs (~4-6×10^{-5}) and chondrules ($\leq$1.5×10^{-5}) may indicate that CAIs predate formation of chondrules by $\geq$ 1-2 Myr [10,13-16]. This chronological interpretation is based on the assumption that ^{26}Al has a stellar origin and was injected and homogenized in the solar nebula over a time scale that was short compared to its half-life (~ 0.73 Myr) [10]. The alternative, non-chronological interpretation assumes a local origin of ^{26}Al by energetic particle irradiation near the proto-Sun, resulting in radial heterogeneity of ^{26}Al distribution [25]. According to this model, CAIs and chondrules formed contemporaneously in different locations near the proto-Sun. Compound CAI-chondrule objects, oxygen isotopes and bulk trace element abundances of CAIs and chondrules (see below) are generally consistent with the chronological interpretation.

Oxygen Isotopes: AOAs and most CAIs are ^{16}O-enriched (Δ^{17}O ~ -20‰) compared to chondrules (Δ^{17}O > -5‰), suggesting formation in isotopically distinct gaseous reservoirs [2,5]. Some igneous CAIs are ^{16}O-depleted to a level observed in chondrules and characterized by low $(^{26}Al/^{27}Al)_I$ (<5×10^{-6}), indicating that they experienced melting and oxygen isotope exchange in an ^{16}O-poor gaseous reservoir, possibly contemporaneously with chondrule formation [26]. Two Type I chondrules from the CV chondrite Mokoia with relatively ^{16}O-poor bulk compositions (Δ^{17}O ~ -5‰) contain abundant olivine grains displaying a wide range of O-isotopic compositions (Δ^{17}O up to -25‰), suggesting that these chondrules formed by melting of ^{16}O-rich precursors in an ^{16}O-poor gaseous reservoir and experienced incomplete oxygen isotope exchange [27]. Uniformly ^{16}O-rich chondrules are exceptionally rare [28].

These observations have been recently interpreted in terms of isotopic self-shielding during UV photolysis of CO in the initially ^{16}O-rich (Δ^{17}O ~ -25‰) protoplanetary disk or parent molecular cloud [26,29,30]. According to these models, the UV photolysis preferentially dissociates C^{17}O and C^{18}O in certain zones of the protoplanetary disk or the parent molecular cloud. If this process occurs in the stability field of water ice, the released atomic ^{17}O and ^{18}O are incorporated into water ice, while the residual CO gas becomes enriched in ^{16}O. The inner solar nebula had initially solar H_2O/CO ratio and was ^{16}O-rich. During this time, the ^{16}O-rich CAIs and AOAs, and some chondrules formed. Subsequently, the inner solar nebula became H_2O-enriched and ^{16}O-depleted, because meter-size icy bodies, which were

enriched in $^{17,18}O$, agglomerated outside the snowline (~5 AU), drifted rapidly towards the Sun and evaporated. During this time, most of the chondrules and ^{16}O-depleted igneous CAIs formed. Correlated Mg and O isotope studies of chondrules and igneous CAIs are required to test this model.

Compound CAI-chondrule Objects: Compound objects composed of chondrules and CAIs or AOAs have been reported in several chondrite groups (CR, CV, CO, CH, H) and ungrouped carbonaceous chondrites (Acfer 094, Adelaide) [31-33]. Such objects provide the best evidence for a genetic relationship between refractory inclusions and chondrules and are discussed in detail below. We note, however, that the vast majority of refractory inclusions appear to have not been affected by chondrule-forming processes, indicating that they were either absent from the chondrule-forming regions at the time of chondrule formation or chondrule-forming events in a specific nebular region were localized and limited [3,5].

Relict CAIs and AOAs are rare in ferromagnesian chondrules, but ubiquitous in Al-rich (>10 wt% Al_2O_3) chondrules [31-34]. Relict CAIs show clear textural evidence for resorption by host chondrule melts resulting in dissolution of their outermost Wark-Lovering rim layers. Relict CAIs and AOAs are ^{16}O-enriched compared to the host chondrules, suggesting that, like most refractory inclusions, they formed in an ^{16}O-rich gaseous reservoir. Hibonite ($CaAl_{12}O_{19}$) in a relict CAI from Adelaide high $(^{26}Al/^{27}Al)_I$ of $(3.7\pm0.5)\times10^{-5}$; in contrast, melilite ($Ca_2Mg_xAl_{2-2x}Si_{1+x}O_7$) in this CAI and anorthite ($CaAl_2Si_2O_8$) in the host chondrule show no evidence for $^{26}Mg^*$ [$(^{26}Al/^{27}Al)_I < 5\times10^{-6}$]. Grossite ($CaAl_4O_7$) in a relict CAI from PAT91546 (CH) has low $^{26}Mg^*$ with $(^{26}Al/^{27}Al)_I = (1.8\pm1.0)\times10^{-6}$. Three other relict CAIs and their host chondrules from Acfer 094, Acfer 182 (CH) and Sharps (H3.4), have no detectable $^{26}Mg^*$ [$(^{26}Al/^{27}Al)_I < 4\text{-}6\times10^{-6}$]. Based on these observations, we infer that relict CAIs formed at least 2 Myr before their host chondrules and subsequently experienced assimilation by chondrule melts that resulted in partial or complete resetting of their ^{26}Al-^{26}Mg system.

Relict chondrules in CAIs are very rare (only 3 have been described so far). The outer portions of igneous, anorthite-rich (Type C) CAIs from Allende – ABC and TS26 – contain coarse forsteritic olivine-low-Ca pyroxene chondrule fragments which appear to have been dissolved in the CAI melts and are surrounded by haloes of high-Ca pyroxene; the host CAIs lack Wark-Lovering rim layers [35]. We infer that these CAIs experienced incomplete late-stage melting in a chondrule-forming region with addition of chondrule-like material. This interpretation is consistent with low $(^{26}Al/^{27}Al)_I$ in TS26 ($<2.5\times10^{-6}$) [36] and ABC $<2.5\times10^{-6}$ [37]. Another chondrule-bearing CAI from Y-81020 (CO) has a melilite-rich core surrounded by a very fine-grained mantle composed of Al-diopside and anorthite-normative mesostasis and enclosing several igneously-zoned pyroxene grains ranging in composition from enstatite ($MgSiO_3$) to augite ($CaMgSi_2O_6$) [38]. The melilite and pyroxene grains are similarly ^{16}O-depleted, whereas the fine-grained mantle is ^{16}O-rich. It is inferred [38] that pyroxene grains are relict chondrule fragments incorporated into the host CAI prior to its final melting in the CAI-forming region. We note, however, that the lack of Wark-Lovering rim layers around the host CAI and the fast cooling rates (>100°C/hr) during its crystallization inferred by [38] may indicate instead that this compound CAI-chondrule object experienced late-stage melting in an ^{16}O-rich gaseous reservoir during chondrule formation. Magnesium isotopic compositions of the host CAI may provide a reasonable test of both models, but have not been measured yet.

Trace Elements: Many CAIs have fractionated rare earth element (REE) patterns, indicating the important role of high temperature gas-solid fractionation during their formation [6]. Some chondrules exhibit highly-fractionated, Group II-like REE patterns, consistent with the presence of CAI materials among their precursors and, hence, earlier formation of some CAIs [39].

References: [1] Aléon et al. (2002) *MAPS, 37,* 1729. [2] Krot et al. (2002) *Science, 295,* 1051. [3] Krot et al. (2002) *MAPS, 37,* 1451. [4] Krot et al. (2004) *Chem. Erde,* in press. [5] Scott E.R.D., Krot A.N. (2004) In *Treatise on Geochemistry,* 143. [6] MacPherson G.J. (2004) In *Treatise on Geochemistry,* 201. [7] Grossman et al. (2000) *GCA, 64,* 2879. [8] Davis A.M., Richter F.M. (2004) In *Treatise on Geochemistry,* 407. [9] Wark D.A., Boynton W.V. (2001) *MAPS. 36,* 1135. [10] McKeegan K.D., Davis A.M. (2004) In *Treatise on Geochemistry,* 431. [11] Galy et al. (2004) *LPS XXXV,* #1790. [12] McKeegan et al. (2004) *MAPS, 39,* A66. [13] Kita et al. (2000) *GCA, 64,* 3913. [14] Russell et al. (1996) *Science, 273,* 757. [15] Kurahashi et al. (2004) *LPS XXXV,* #1476. [16] Huss et al. (2001) *MAPS, 36,* 975. [17] Krot et al. (2004) *LPS XXXV,* #1389. [18] Galy et al. (2000) *Science, 290,* 1751. [19] Alexander C.M.O'D., Wang J. (2001) *MAPS, 36,* 419. [20] Connolly H.C.Jr., Desch S.J. (2004) *Chem. Erde, 64,* 95. [21] Chen et al. (1981) *EPSL, 52,* 1. [22] Göpel et al. (1991) *Meteoritics, 26,* 338. [23] Amelin *et al.* (2002) *Science, 271,* 1545. [24] Amelin *et al.* (2004) *GCA, 68,* A759. [25] Gounelle et al. (2001) *Astrophys. J., 548,* 1051. [26] Krot et al. (2004) *MAPS, 39,* A56. [27] Jones et al. (2004) *GCA,* in press. [28] Kobayashi et al. (2003) *Geochem. J., 37,* 663. [29] Yurimoto H., Kuramoto K. (2004) *Science,* in press. [30] Lyons J.R., Young E.D. (2004) *LPS XXXV,* #1970. [31] Krot et al. (2002) *MAPS, 37,* 155. [32] Krot A.N., Keil K. (2002) *MAPS, 37,* 91. [33] Krot et al. (1999) *LPS XXX,* #1511. [34] Yurimoto H., Wasson J.T. (2002) *GCA, 66,* 4355. [35] Krot et al. (2004) unpubl. [36] Wark D.A. (1987) *GCA, 51*, 221. [37] MacDougall et al. (1981) *LPS X*, 643. [38] Itoh S., Yurimoto H. (2003) *Nature, 423,* 728. [39] Misawa K., Nakamura N. (1996) In *Chondrules and the Protoplanetary Disk,* 99.

Contemporaneous chondrule formation between ordinary and carbonaceous chondrites.

E. Kurahashi[1,2], N. T. Kita[2,3], H. Nagahara[1], Y. Morishita[2], [1]Department of Earth and Planetary Science (Bldg.#1), University of Tokyo, Hongo, Bunkyo-ku, Tokyo 113-0033, Japan, [2]Micro-scale Isotope Geochemistry Group, Geological Survey of Japan, AIST, Tsukuba Central 7, Tsukuba 305-8567, Japan, [3]University of Wisconsin, (E-mail: kurahashi-erika@aist.go.jp)

Introduction: Chronometer using a short-lived extinct-nuclide ^{26}Al (half-life, $t_{1/2}$=0.73Ma) that decays to ^{26}Mg (^{26}Mg*) has been applied to early solar system materials in chondrites to obtain their relative formation ages. Many ^{26}Al-^{26}Mg analyses have been performed on chondrules in least equilibrated ordinary chondrites (OC). ^{26}Al ages of 15 FeO-rich ferromagnesian chondrules (FeO/(FeO+MgO)>0.1 in olivine or pyroxene; Type II) in LL3.0 Semarkona and LL3.1 Bishunpur suggest the range from 0.8(-0.3/+0.4) to 2.5(-0.4/+0.7) Myr after CAIs formations [1-4]. Two FeO-poor ferromagnesian chondrules (FeO/(FeO+MgO) < 0.1 in olivine or pyroxene; Type I) in the same chondrites show 1.7(-0.5/+0.8) and 1.8(-0.3/+0.5) Myr after CAIs formations [2, 4]. The age of an aluminum-rich (Al-rich) chondrule (Al_2O_3 > 20wt %) in LL3.1 Krymka represents 2.5(-0.7/+2.9) Myr after CAIs formations [5]. The ^{26}Al ages show a relationship with the bulk chemical compositions [6], in which younger chondrules tend to be richer in silica and volatile elements.

Contrary to ordinary chondrites, ^{26}Al ages measured for ferromagnesian chondrules in primitive carbonaceous chondrites (CC) are very limited. The ages of 6 Type II chondrules in the most pristine CO3.0 Yamato-81020 are from 2.1(-0.4/+0.7) to 3.2(-0.6/+1.3) Myr after CAIs formations [7, 8]. The age of one Al-rich chondrule in CV3 Axtell shows 2.8 (-0.4/+0.6) Myr after CAIs formations [9]. Two anorthite-rich chondrules that contain large anorthite region in unique Acfer094 and CV3 Efremovka show 1.5(-0.3/+0.4) and 2.5(-0.5/+0.9) Myr after CAIs formations, respectively [10]. Only one Type I chondrule has been dated for ^{26}Al ages in CV3 Axtell, 1.7(-0.6/+1.7) Myr after CAIs formations [9], which is because of the fine textures and lack of phases with high Al/Mg ratios (>100). Since most chondrules in CC consist of Type I chondrules (~ 90%), we have specifically focused on formation ages of common Type I chondrules in CC [11]. We also examined bulk chemical compositions of chondruls in CC to discuss the relationship with their formation ages.

Analytical Technique: The Al-Mg isotopic analysis was performed using a secondary ion mass spectrometer (SIMS) Cameca IMS-1270 at the Geological Survey of Japan (GSJ, AIST). The analytical procedure is similar to [2], except that we used O^- primary ion beam with reduced sizes of 3 μm for anorthite (0.02-0.03nA) in a single collector mode, and 5 μm for olivine and pyroxene (0.3-0.4nA) in a multi-collector mode. Although O^{2-} ion have higher sputtering rate relative to O^- ion, we used O^- ion because of low generation rate for O^{2-} ion from an ion source. Mass resolution power was set to 3500 for mono-collector mode and 2200 for multi-collector mode.

Bulk chemical compositions of individual chondrules using about 500 points quantitative analyses were performed by an electron microprobe (JEOL JXA-8800/8900 at the University of Tokyo and GSJ). Detail analytical procedures are shown in [6].

Results and Discussions:

^{26}Al ages. We examined fourteen Type I, two Type II and one Al-rich chondrule for ^{26}Al-^{26}Mg isotopic analyses. We found clear ^{26}Mg-excesses in all chondrules, though most Type I chondrules have low Al/Mg ratios (Al/Mg=20-40) [11]. The initial ^{26}Al/^{27}Al ratios, $(^{26}Al/^{27}Al)_0$, are $(0.51+/-0.22)\times10^{-5}$ to $(1.41+/-0.33)\times10^{-5}$ for Type I, $(0.74+/-0.36)\times10^{-5}$ and $(0.78+/-0.17)\times10^{-5}$ for Type II, and $(0.31+/-0.14)\times10^{-5}$ for Al-rich chondrule. Assuming that ^{26}Al was homogeneously distributed in the early solar nebula, the relative formation ages of chondrules are calculated with a canonical ratio of 5×10^{-5} [12]. The results show that the formation ages of Type I are 1.3(-0.2/+0.3) to 2.4(-0.4/+0.6) Myr after CAIs formations. In particular, nine out of the fourteen Type I chondrules are concentrated from 1.5 to 1.8 Myr after CAIs formations (Fig. 1). The ages of Type II are 2.0(-0.2/+0.3) and 2.0(0.4/+0.7) Myr after CAIs, and that of Al-rich chondrule is clearly younger than Type I, 2.9(-0.4/+0.6) Myr after CAIs formations. Figure 1 summarizes relative ^{26}Al ages of chondrules in both OC and CC, which are selected from the least equilibrated chondrites. The chondrule forming period of Type I chondrules in CC is consistent with those of ferromagnesian chondrules in OC, 1.0 to 2.5 Myr after CAIs formation. Thus, Type I chondrules in CC formed contemporaneously with ferromagnesian chondrules in OC. However, the formation ages of Type II chondrules in CC are younger (>2.0 Myr after CAIs formations) than Type I chondrules in CC and ferromagnesian chondrules in OC. According to petrological observations, some FeO-rich olivine grains in Type II include FeO-poor region at the core, whereas FeO-

poor olivine grains in Type I do not contain FeO-rich region. Therefore, Type II chondrules might have been formed later than Type I chondrules in CC forming region, including FeO-poor olivine in Type I as a relict mineral.

From spectral observations of asteroids, it is widely known that reflectance spectra of C-type asteroids inferred as parent bodies of CC are distributed in the middle of the main asteroid belt, near 3AU, whereas S-type asteroids inferred as parent bodies of OC are concentrated in the inner main belt. If OC and CC chondrules were formed in the individual regions, the chemical and isotopic difference between chondrules in OC and CC should have been achieved in the chondrule forming region (or reservoir) or the chondrule formation time in the early solar nebula. The results of the present study that the range of the formation ages of ferromagnesian chondrules in CC is almost the same as OC suggest that the difference between chondrules in CC and OC should be the mainly spatial difference in the early solar nebula.

Relationship between ^{26}Al ages and bulk chemical compositions. We also examine the bulk chemical compositions of individual chondrules in CO3.0 Yamato-81020. The bulk chemical compositions of Type I chondrules show wide variations of MgO (28.8-46.2wt %), Al_2O_3 (1.0-7.3), CaO (1.0-7.6), SiO_2 (40.1-55.3) and FeO (0.9-8.1). The relationship between bulk chemical compositions and ^{26}Al ages of ferromagnesian chondrules in OC have been reported by [6], that younger chondrules tend to be richer in silica and volatile elements. This relationship can be explained by evaporation and recondensation in an open system during chondrule formation [6]. However, we do not observe any correlation between bulk chemical compositions and formation ages of Type I chondrules in CC (Fig. 2). We also found no correlation among texture, size distribution, bulk chemical compositions of both refractory and volatile elements, and formation ages of Type I chondrules in CC. Unlike ferromagnesian chondrules in OC, therefore, Type I chondrules in CC can not be explained by simple evaporation and recondensation. Considering the absence of the relationship among ages, textures, and bulk chemical compositions of individual Type I chondrules in CC, the chondrules could be evolved from pre-existing solid precursors with a wide variety of chemical compositions.

References: [1] Hutcheon I. D. and Hutchison R. (1989) *Nature*, 337, 238-241. [2] Kita N. T. et al. (2000) *GCA*, 64, 22, 3913-3922. [3] McKeegan K. D. et al. (2000) *LPSXXXI*, abstract#2009. [4] Mostefaoui S. et al. (2002) *M&PS*, 37, 421-438. [5] Huss G. R. et al. (2001) *M&PS*, 36, 975-997. [6] Tachibana S. et al. (2003) *M&PS*, 38, 939-962. [7] Yurimoto H. and Wasson J. T. (2002) *GCA*, 66, 4355-4363. [8] Kunihiro T. and Wasson J. T. (2004) *GCA* (in print) [9] Srinivasan G. et al. (2000) *M&PS*, 35, 1333-1354. [10] Hutcheon I. D. et al. (2000) *LPSXXXI*, abstract#1869. [11] Kurahashi E. et al. (2004) *LPSXXXV*, abstract#1476 [12] MacPherson G. J. et al. (1995) *Meteoritics*, 30, 365-386. [13] Anders E. and Grevesse N. (1989) *GCA*, 53, 197-214.

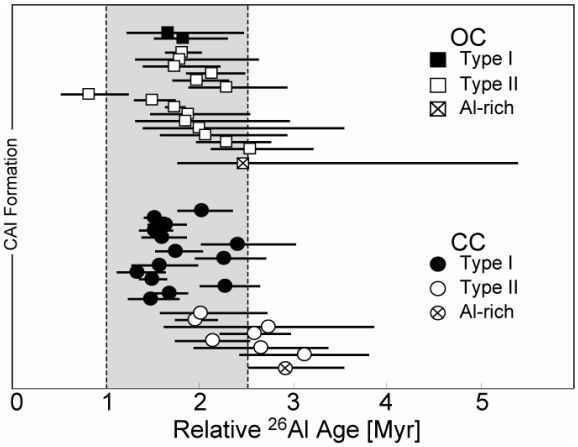

Figure 1. Relative ^{26}Al ages of chondrules in least equilibrated OC and CC. The data are from [1-5, 7-11, and this study]. The shaded area is 1.0 to 2.5 Myr after CAIs formations.

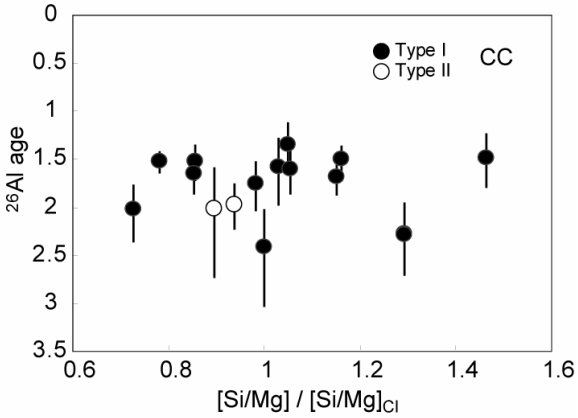

Figure 2. Relationship between ^{26}Al ages and Si/Mg ratio of bulk chemical compositions normalized CI composition [13] of Type I chondrules in CO3.0 Yamato-81020.

CHONDRULES AND ISOLATED GRAINS IN THE FOUNTAIN HILLS BENCUBBINITE. A. R. La Blue[1], D. S. Lauretta[1], and M. Killgore[2]. [1]Lunar and Planetary Laboratory, Univ. of Arizona, Tucson, AZ 85721, USA, arlablue@lpl.arizona.edu, lauretta@lpl.arizona.edu. [2]Southwest Meteorite Laboratory, Payson, AZ 85547, USA.

Introduction: The Fountain Hills (FH) meteorite was recently classified as a Bencubbin-like (CB_a) chondrite, which are part of the CR clan [1]. The FH O-isotopic composition is indistinguishable from CB_a chondrites. Metal and silicate compositions are consistent with the CB_a classification. Significant differences between FH and the other CB_a chondrites were noted. These include abundant porphyritic chondrules and complete lack of sulfide minerals. We are furthering this investigation by analyzing silicate chondrules and isolated grains in FH to determine more about its composition, thermal history, and implications for chondrule formation in the early solar system.

Analytical Techniques: A petrographic thin section of the FH chondrite was surveyed with optical microscopy and BSE imaging. Mineral compositions were determined using electron microprobe analysis.

Results: Chondrule diameters range from 250 to 3,500 μm, averaging 1,200 μm. Porphyritic and barred-olivine chondrules are abundant. A few small granular chondrules are present. Representative porphyritic (Fig. 4), barred (Fig. 5), and granular (Fig. 6) chondrules are described. The porphyritic chondrule contains large phenocrysts of olivine ($Fo_{96\text{-}97}$ with 0.2 wt.% CaO, 0.1 wt.% Al_2O_3, and 0.5 wt.% Cr_2O_3). Pyroxene ($En_{77}Wo_{19}$ with 3.7 wt.% Al_2O_3, 0.8 wt.% TiO_2, and 1.0 wt.% Cr_2O_3) is concentrated in the outer portion of the chondrule. Mesostasis is recrystallized anorthite containing 0.1 wt.% Na_2O, 0.2 wt.% FeO, and 1.0 wt.% MgO. The barred chondrule contains parallel laths of olivine ($Fo_{96\text{-}97}$) with interstitial anorthite. Low-Ca pyroxene ($En_{93}Wo_3$ with 1.4 wt.% Al_2O_3, 0.3 wt.% TiO_2, and 0.8 wt.% Cr_2O_3) occurs on the outer edge. The granular chondrule is composed predominantly of low-Ca pyroxene with variable composition ($En_{91\text{-}95}$ with 0 – 0.5 wt.% Na_2O, 0 – 0.1 wt.% K_2O, 1.3 – 2.9 wt.% CaO, 0.9 – 3.0 wt.% Al_2O_3, 0.1 – 0.3 wt.% TiO_2, and 0.8 – 1.0 wt.% Cr_2O_3). Minor amounts of olivine ($Fo_{96\text{-}97}$) are present.

An isolated chromian spinel grain (Fig. 1 and 2) was characterized. The spinel has a uniform Mg# = 94. However, it is zoned in Cr and Al with Cr contents increasing from core to rim (Fig. 3). The grain is rimmed by anorthite and the rim is 50 μm thick. Olivine with composition Fo_{97} occurs in contact with this grain. Application of the olivine-spinel geothermometer developed by Sack and Ghiorso [2] yields 878 °C using the composition of the spinel closest to the olivine. Cr-Al interdiffusion data for a spinel of composition $(Mg_{0.51}Fe_{0.49})(Al_{0.73}Cr_{0.27})_2O_4$ have recently been measured at 21.4 kb and 1125 °C [3]. These data suggest that $D_{Cr\text{-}Al}$ is ~$0.04*D_{Fe\text{-}Mg}$. Using this relationship and the Arrhenius relation for $D_{Fe\text{-}Mg}$ in spinel [4] we estimate $D_{Cr\text{-}Al}$ in spinel at 878 °C. A reasonable fit to the data was obtained by treating the system as an isothermal diffusion problem. This analysis suggests a heating duration of ~40,000 years to establish the Cr-Al zoning profiles in the FH spinel grain.

Discussion: FH is similar to CB chondrites. However, it is distinct from the other members of this group in several ways. Bencubbinites contain 60-70 vol.% metal whereas ~25 vol.% of FH is metal. It is not present in chondrules in bencubbinites and we have located metal phases inside silicate chondrules from FH. The metal inclusions are small (< 1 μm) but visible in reflected light. There is no report of CAIs in Bencubbinites. Spinel is rare but noticeable in FH (Figs. 1 and 7). FH $\delta^{15}N$ data [1] also does not match other Bencubbinites. Lastly, porphyritic chondrules are absent in CB chondrites but abundant in FH. These factors indicate that FH is a unique CB chondrite.

FH also shares some characterisitics with CR chondrites. Both have abundant Fe-Ni metal but metal is concentrated in chondrules in CRs instead of in the matrix as seen in Fountain Hills. CR chondrites contain a variety of chondrule textural types including porphyritic and barred as does FH. $\delta^{15}N$ data for FH is much closer to the CRs than to the CBs. Since the mineral composition of FH does not fully categorize it as either a CB or a CR, we suggest that FH may be transitionary between the CB and the CR chondrites, thus reinforcing the link between these chondrite groups.

The formation of porphyritic chondrules requires preservation of nucleation sites in chondrule melts. The presence of abundant porphyritic chondrules in FH suggests that these chondrules formed either by: (1) incomplete melting of solid precursors or (2) melt formation in the presence of abundant dust grains. The complete lack of fine-grained matrix in FH seems to rule out (2). The lack of sulfide minerals and low alkali abundances are consistent with FH chondrule formation in a high-temperature region of the solar nebula. However, direct condensation of chondrule melts is inconsistent with observed chondrule textures. FH chondrules may have formed by processing of an earlier generation of CB chondrules as suggested by [5] for other CB_a chondrites.

Acknowledgments: We thank K. Domanik for assistance with the microprobe, J. Ganguly for providing diffusion data, M. Ghiorso for the Excel version of the geothermometer, and T. J. McCoy for highly informative talks and inspiration. This work was supported by NASA grant NNG04GF65G (PI: DSL). **References:** [1] Lauretta et al. (2004) *LPSC* #1255. [2] Sack and Ghiorso (1991) *Am. Min.* **76**, 827-847. [3] J. Ganguly, personal communication, 7/27/2004. [4] Liermann and Ganguly (2002) *GCA* **66**, 2903-2913. [5] Krot et al. (2004) *MAPS* **39**, A56.

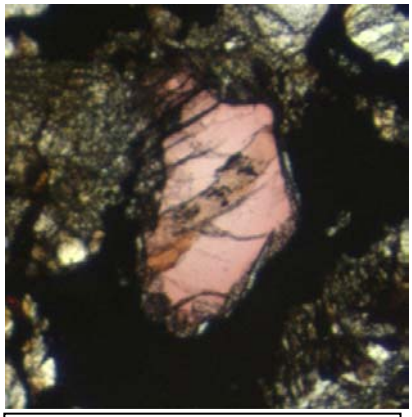

Figure 1. Plane-pol. optical image of spinel grain. FOV=900 μm.

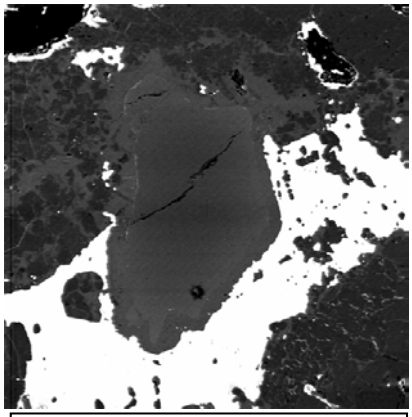

Fig. 2. BSE image of spinel grain in Fig. 1. FOV = 900 μm

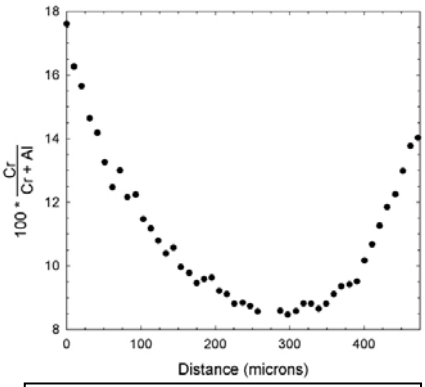

Fig. 3. Compositional variation of spinel (from bottom to top as shown in Fig. 2)

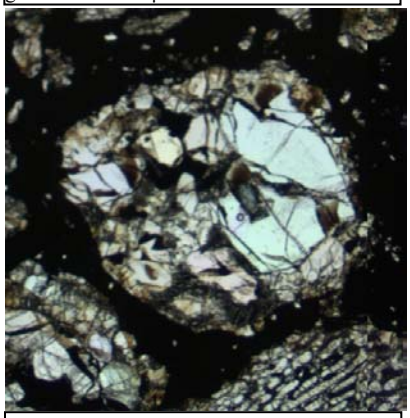

Fig. 4. Plane-pol. optical image of porphyritic chondrule. Dia = 1,035 μm

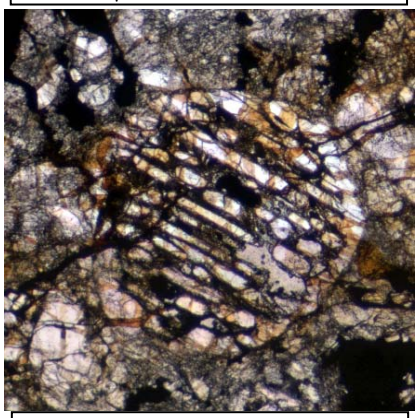

Fig. 5. Plane-pol. optical image of barred chondrule. Diameter = 1,070 μm

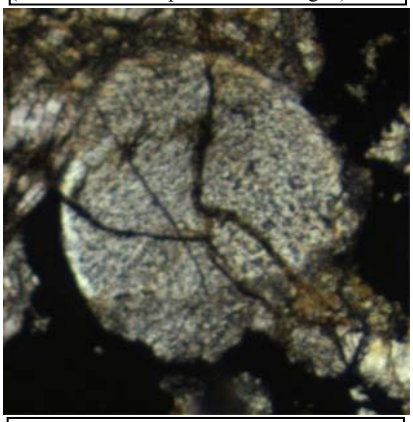

Fig. 6. Plane-pol. optical image of granular chondrule. Diameter = 930 μm

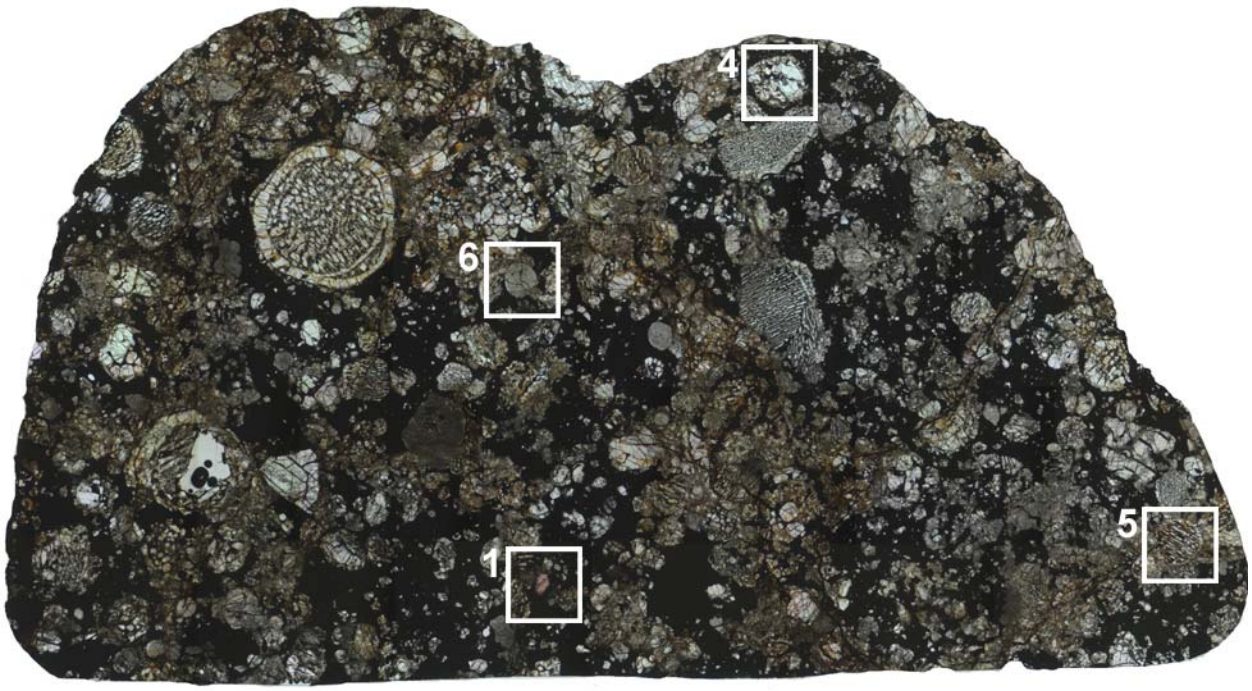

Fig. 7. Plain polarized map of Fountain Hills in thin section. Location of chondrules and spinel grains in Figs. 1, 4-6 are indicated. FOV = 3.5 cm

IMPLICATIONS OF CHONDRULE FORMATION IN A GAS OF SOLAR COMPOSITION. D. S. Lauretta, M. J. Drake, and M. Stimpfl, Lunar and Planetary Laboratory, University of Arizona, Tucson, AZ 85721, USA. Email: lauretta@lpl.arizona.edu

Introduction: It is widely believed that chondrules formed in the solar nebula. If this is true then they must have been exposed to a gas of near-solar composition. Here, we explore some implications of chondrule formation in such an environment. The equilibrium distribution of major gas species in a solar composition gas is shown for temperatures relevant to chondrule formation in Fig.1 at a total pressure of 10^{-5} bars. We use the abundances of [1] with a portion of the total O removed to form major silicate minerals. It is estimated that few chondrules with liquidus temperatures over 2023 K were completely melted, and few with liquidus temperatures under 1673 K were incompletely melted [2]. However, [3] showed that a short heat pulse, with a peak temperature well above the liquidus, can also produce porphyritic chondrule textures. As a result, the maximum temperature of chondrule formation is estimated to be ~2373 K. Chondrule precursors are thought to have equilibrated with the nebular gas down to 650 K, the 50% condensation temperature for S in a canonical solar nebula [4]. We focus on the most abundant species in the gas phase: H_2, CO, H_2O, and the S-bearing species H_2S, HS, and S.

H_2: Many type-I chondrules contain large Fe-based metal grains. Some of these grains are trapped at the chondrule boundary, with a significant surface area exposed to any external fluid. If chondrules formed in the solar nebula than these metal grains would have been exposed to H_2(g). At the highest temperatures at which chondrules are thought to have formed (2273 K) [3], significant concentrations of H(g) may have also been present. The ability of metals to absorb hydrogen has been known since the mid 1800s [5]. The properties of metal-hydrogen systems have been the subject of intense research because small concentrations of H in metal results in significant changes in mechanical and metallurgical properties, particularly the brittleness of stainless steels and other industrial metals [6]. Within a metal, hydrogen molecules are dissociated and hydrogen atoms occupy interstitial sites in the host-metal lattice. Hydrogen atoms jump from one interstitial site to a neighboring vacant one and diffuse this way over large distances through the metal, resulting in rapid H saturation in a metal grain. The concentration of H in metal (X_H) is expressed as: $X_H = \sqrt{P_{H_2}} \cdot e^{-\frac{\Delta S^{nc}}{k_b}} \cdot e^{\frac{\Delta H}{k_b T}}$ [7]. In this equation P_{H2} is the partial pressure of H_2(g), ΔS^{nc} is the non-configurational entropy of solution, k_b is Boltzmann's constant, ΔH is the enthalpy of solution, and T is temperature. Values for ΔS^{nc} and ΔH are from [8]. We calculated the abundance of H in pure Fe and Ni metals in contact with H_2(g) as a function of temperature (Fig. 2). If chondrules formed in an ambient solar composition gas at 10^{-5} bars total pressure, then metal grains at chondrule boundaries should contain 1 – 3 ppm H. Increasing the total pressure (and hence the H_2 partial pressure) to 10^{-3} bars increases H concentrations to 10 – 30 ppm. Such an increase in pressure is predicted by shock wave models for chondrule formation [9]. These results do not take into account the effect of H(g), which is likely to increase the concentration of H. Furthermore, these calculations are for pure, perfect metallic crystals. Defects in metallic microstructures act as hydrogen traps that significantly increase the solubility of H and decrease its mobility [6]. Once in these defects sites, it is very difficult to remove H from metal; a major problem for the steel industry but a potential advantage for cosmochemistry. We propose a direct test of nebular formation of chondrules by measuring the abundance and isotopic composition of H in metal grains at chondrule boundaries. Such measurements will establish whether or not chondrules form in the presence of H_2(g) and constrain the partial pressure of this species.

CO: At temperatures relevant to chondrule formation CO(g) is the primary carrier of both C and O (Fig. 1). Chondrule melts in the presence of this molecule must have had significant interaction with the vapor. If the initial composition of a chondrule melt is more oxidizing than the surrounding gas then CO(g) will serve as a reducing agent. Recent experiments by [10] illustrate the nature of the reduction reaction. FeO-bearing silicate melts in the presence of CO(g) undergo an internal reaction in which divalent iron is converted to metallic iron plus electron holes. Nanometer-scale iron-metal grains form at the melt-vapor interface. Molecular oxygen released from FeO reduction participates in the conversion of CO to CO_2 at the melt surface. This reaction releases electrons, which fill the electron holes created by Fe reduction. The reduction interface propagates inward and the distance from chondrule surface increases throughout the duration of heating. Electron holes created in the interior of the melt droplet diffuse toward the melt surface, charge-balanced by a counterflux of Mg^{2+} cations, which is the rate-limiting factor for the overall reduction reaction. The cation-to-oxygen ratio increases with reaction progress, resulting in reduction of the melt. It is likely that H_2(g) serves a similar capacity but experimental studies of this reaction have not been performed.

H_2O: Ion probe determinations of H_2O concentrations of chondrules from primitive chondrites yield mean concentrations of 500 – 2100 ppm in olivine [11]. The distribution of D/H ratios is similar to that of matrix minerals suggesting that hydrated minerals, such as phyllosilicates, may have been a component of chondrule precursors. However, experimental simulations of chondrule formation using hydrous silicates as precursors yield high percentages of vesicles [12]. Since vesicles are rare in chondrules, such materials have been excluded as precursors.

Recent studies on the role of H_2O adsorption in the solar nebula may resolve this controversy [13]. We modeled the adsorption of H_2O on olivine surfaces using Monte Carlo simulations and an iterative process allowing the surface to reach a steady state saturation at each temperature. Water molecules not only interact with the substrate by means of weak bonds (~5kJ/mole) but also establish H bonds with other H_2O molecules present in a monolayer [14]. The results of these calculations show that significant amounts of H_2O can be absorbed on olivine surfaces below 700 K. At 400 K, a complete monolayer is stable. Based on studies of agglomeratic olivine chondrules, thought to represent chondrule precursors, we can infer that chondrule precursor materials were dominated by olivine crystals 2-5 μm in diameter [15]. Each adsorbed water molecule occupies 10 $Å^2$, thus a 5-μm olivine grain is capable of adsorbing the equivalent of 1000 ppm H_2O at 400 K. A 2-μm grain can adsorb over 2000 ppm H_2O. These values are consistent with those measured by [11]. Sulfur condensation occurs at ~700 K in a canonical nebula and is 100 % condensed by 400 K. It is noteworthy that chondrules containing silicates with high FeO contents are typically associated with high sulfide abundances. It is possible that S condensation is accompanied by H_2O adsorption, which results in oxidizing melts, allowing any remnant Fe metal to oxidize and become incorporated into silicates. Chondrules devoid of sulfides are composed of low-FeO silicates. Precursors of these objects may not have equilibrated with the nebular gas at low temperatures and thus escaped H_2O adsorption and sulfide formation.

H_2S, HS, and S: Sulfur condenses through the corrosion of Fe-based metal. The temperature at which this takes place is dependent on the bulk S/H ratio of the gas phase. For solar composition this occurs below 700 K [4]. However, several lines of evidence point towards chondrule formation in dust-rich regions of the solar nebula [16]. Increasing the S/H ratio of the vapor by a factor of 300 leads to sulfide formation at T > 1100 K and is pressure dependent [17]. Sulfide formation is extremely rapid [4]. Thus, chondrule-associated metal, particularly grains exposed at chondrule boundaries could not escape sulfurization unless they formed in S-depleted regions or were removed from contact with the gas on extremely rapid timescales (hours to days). H_2S is structurally similar to H_2O. Thus, H_2S may adsorb on grain surfaces in a manner analogous to that described for H_2O above.

References: [1] Lodders (2003) *Ap. J.* **591**, 1220. [2] Radomsky and Hewins (1990) *GCA* **54**, 3475. [3] Connolly et al. (1998) *GCA* **62**, 2725. [4] Lauretta et al. (1996) *Icarus* **122**, 288. [5] Graham (1866) *Phil. Trans. Roy. Soc. (London)* **156**, 399. [6] Dos Santos and De Miranda (1997) *J. Mat. Sci.* **32**, 6311. [7] Wipf (2001) *Physica Scripta* **T94**, 43. [8] Fukai (1993) *The Metal-Hydrogen System*, Springer-Verlag. [9] Ciesla and Hood (2002) *Icarus* **158**, 281. [10] Everman and Cooper (2003) *J. Am. Ceram. Soc.* **86**, 487. [11] Deloule et al. (1998) *GCA* **62**, 3367 [12] Maharaj and Hewins (1994) *GCA* **58**, 1335. [13] Stimpfl et al. (2004) *MAPS* **39**, A99. [14] de Leeuw N.H. et al. (2000) *Phys. Chem. Min.* **27**, 332. [15] Weisberg and Prinz (1996) In *Chondrules and the Protoplanetary Disk*, 119-128. Cambridge Univ. Press. [16] Hood and Ciesla (2001) *MAPS* **36**, 1571. [17] Lauretta et al. (2001) *GCA* **65**, 1337.

Fig. 1 – Equilibrium gas distribution

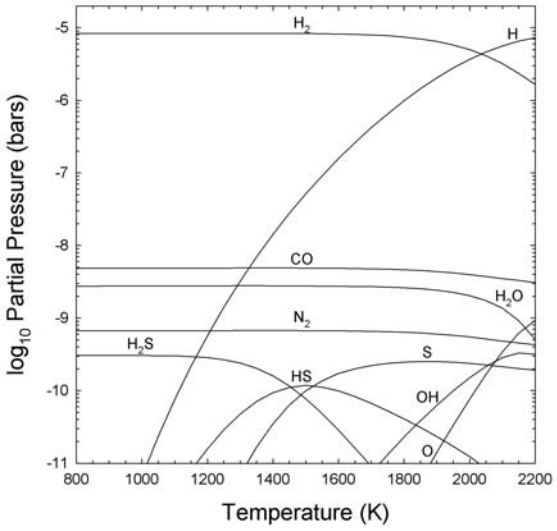

Fig. 2 – Minimum H concentration in metal

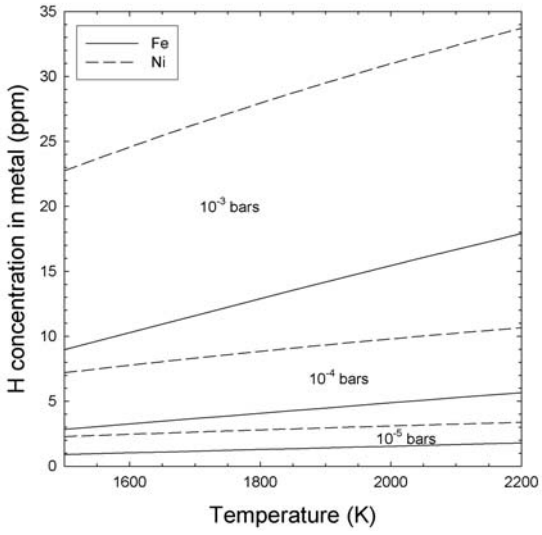

IMPLICATIONS OF METEORITIC ^{36}CL ABUNDANCE FOR THE ORIGIN OF SHORT-LIVED RADIONUCLIDES IN THE EARLY SOLAR SYSTEM. L. A. Leshin[1, 2], Y. Guan[1], and Y. Lin[3], [1]Department of Geological Sciences, [2]Center for Meteorite Studies, Arizona State University, Tempe AZ 85287-1404, USA, [3]Inst. of Geology and Geophysics, Chinese Academy of Sciences, Beijing 100029, China. (laurie.leshin@asu.edu).

Introduction: Short-lived, now extinct radionuclides detected in primitive meteorites have revealed important information about events in the earliest history of our solar system. They can be used as fine-scale chronometers to trace processes in the solar nebula and on meteorite parent bodies [1]. The relative abundances of different short-lived isotopes in the early solar system can also be used to constrain the local galactic environment of solar system formation because the different production mechanisms (*i.e.*, supernova or AGB stars vs. "local production" scenarios) result in different abundance patterns of short-lived radionuclides. Finally, the different chemical affinities (e.g., volatile vs. refractory) of short-lived radionuclides provide an opportunity to track unique chemical processes in the early solar system. Thus, investigation of short-lived radionuclides, including the search for evidence of "new" short-lived isotopes (those not positively detected previously) has the potential to shed light on many important questions in cosmochemistry. Recently, we reported the first direct evidence for the presence of ^{36}Cl in meteorites by detecting its *in situ* decay product --^{36}S excess, in alteration assemblages of a Ca-Al-rich inclusion (CAI) from the Ningqiang carbonaceous chondrite [2]. ^{36}Cl has a half-life of 0.3 million years (My) and decays to either ^{36}Ar (98.1%, β^-) or ^{36}S (1.9%, ε and β^+) [3]. Here we combine the evidence for live ^{36}Cl with ^{26}Al-^{26}Mg systematics and petrologic observations of the CAI to report the "canonical" ^{36}Cl abundance, and we explore the implications of the presence of live ^{36}Cl for models for the origin of short-lived radionuclides in our solar system.

Results and Discussion: Alteration assemblages, consisting of sodalite ($Na_8Al_6Si_6O_{24}Cl_2$) and nepheline ($Na_4Al_4Si_4O_{16}$), were studied in three CAIs from the Ningqiang carbonaceous chondrites and two EH3 enstatite chondrites – EET87746 and ALH 77295. Sulfur isotopes were analyzed in the ASU GeoSIMS lab, along with correlated investigation of the ^{26}Al-^{26}Mg system. The sodalite contains high Cl (7.5 wt%) with no detectible sulfur (<0.06 wt% from the electron probe), and therefore represents the best available phase to search for evidence of now decayed ^{36}Cl.

The fine-grained alteration assemblages in the two CAIs from the enstatite chondrites showed no resolvable ^{36}S excess because of their low ^{35}Cl/^{34}S ratios (<100). Ion images revealed the presence of fine-grained hot spots of ^{34}S, suggesting the presence of tiny sulfides, which would mask evidence of ^{36}Cl. Four alteration assemblages in the Ningqiang CAI (NQJ1-1#1) with high ^{35}Cl/^{34}S ratios (up to 57,000) showed clear ^{36}S excesses that correlate with ^{35}Cl/^{34}S ratios. The inferred $(^{36}Cl/^{35}Cl)_o$ ratios (±2σ) are: $(4.6 \pm 0.6) \times 10^{-6}$, $(5.1 \pm 1.0) \times 10^{-6}$, $(7.7 \pm 2.5) \times 10^{-6}$, and $(1.1 \pm 0.2) \times 10^{-5}$, respectively. The two assemblages with the highest Cl/S ratios yield the best determination of the initial $(^{36}Cl/^{35}Cl)_o$ ratios of ~5×10^{-6} in sodalite.

The inferred $(^{36}Cl/^{35}Cl)_o$ ratios $[(5–11) \times 10^{-6}]$ of the alteration assemblages of the Ningqiang CAI are about 4 to 8 times higher than a previous estimate $(1.4 \pm 0.2) \times 10^{-6}$, which derived from measurements of ^{36}Ar excess in matrix of the Efremovka carbonaceous chondrite [4]. There are two possible explanations for the difference. First, the vast majority (94-96%) of ^{36}Ar in meteorites is a mixture of a trapped component, a spallation component, and the decay of cosmogenic ^{36}Cl (i.e., ^{36}Cl produced by recent irradiation by cosmic rays). Estimation of ^{36}Ar excess from the decay of short-lived ^{36}Cl is highly uncertain, because it only can be done after subtraction of these components, especially the most abundant trapped component. Furthermore, recent study of isotopic compositions of noble gases in meteorites showed a large variation of ^{38}Ar/^{36}Ar ratios due to experimental artifact, requiring a reassessment for the *entire* reported ^{36}Ar excess [5]. Thus, the most likely explanation is that the previous report of ^{36}Cl decay products was inaccurate. However, it is possible that the difference may represent a time interval between the alteration of the CAI and formation of Cl-bearing phases in Efremovka matrix. Assuming homogeneous distribution of ^{36}Cl, the difference corresponds to a time interval of 0.6-1.2 My.

A previous petrographic and mineralogical study of the Ningqiang CAI [6] showed that sodalite and nepheline are the products of secondary processes that altered the primary minerals in the inclusion. Therefore, the $(^{36}Cl/^{35}Cl)_o$ ratios in-

ferred from the sodalite analyses cannot represent the initial value at the time when CAIs formed. To deduce the "canonical" $(^{36}Cl/^{35}Cl)_o$ value, the time interval between the formation and alteration of the Ningqiang CAI was examined using the ^{26}Al-^{26}Mg system in each individual mineral phase, and petrographic relationships among the CAIs in Ningqiang [6]. Although "canonical" ^{26}Al levels were detected in the unaltered melilite-spinel-rich crust, consistent with previous observations in Ningqiang CAIs, neither anorthite nor the alteration assemblages in the mantle of NQJ1-1#1 show resolvable ^{26}Mg excess, providing a maximum inferred $(^{26}Al/^{27}Al)_o$ ratio of $\sim 0.7 \times 10^{-5}$. Assuming the $(^{26}Al/^{27}Al)_o$ ratios of melilite and sodalite reflect a temporal difference, then sodalite formed at least 1.5 – 2 My after the formation of melilite. Using this time difference and the best $(^{36}Cl/^{35}Cl)_o$ value ($\sim 5 \times 10^{-6}$) of sodalite, the "canonical" $(^{36}Cl/^{35}Cl)_o$ ratio at the time when CAIs first formed is then inferred to be $\geq 3 \times 10^{-4}$.

This $(^{36}Cl/^{35}Cl)_o$ value can be used to constrain the source of short lived radionuclides and the setting of solar system formation. If from a stellar source, supernova model predictions of the $(^{36}Cl/^{35}Cl)_o$ value range from 3×10^{-6} to 2×10^{-4} [7], whereas low-mass AGB star models suggest much lower values ($\leq 7.85\times 10^{-7}$ - 2.4×10^{-6})[8,9]. The initial $(^{36}Cl/^{35}Cl)_o$ ($\geq 3 \times 10^{-4}$) at CAI formation estimated in this study is clearly significantly higher than the suggestion from the AGB star models, but consistent with the predicted values from a supernova source.

Alternatively, in a local irradiation model an upper limit of $(^{36}Cl/^{35}Cl)_o = 1.3\times10^{-4}$ has been predicted [10], which, although below our lower limit, is at least broadly consistent with the observation from this study. However, the volatile nature of chlorine and the observation of ^{36}Cl in sodalite are probably not compatible with the theory of local irradiation origin. According to the models of Shu *et al.* [e.g., 11, 12], intense irradiation of the proto-Sun evaporated Mg-Fe-silicate dustballs to form CAIs, and simultaneously produced short-lived radionuclides (*e.g.* ^{10}Be, ^{26}Al, ^{41}Ca and ^{53}Mn) through the bombardment of CAI materials by energetic particles from the Sun. After their formation, CAIs bearing short-lived radionuclides were ejected to distant locations where chondrites accreted. Sodalite, a product of secondary alteration at relatively low-temperature, formed after the CAI primary phases, and in a different environment. Therefore, in the local irradiation model, ^{36}Cl itself would have to be produced in a gaseous phase very close to the proto-Sun by intense irradiation, and then a mechanism to transport the gaseous ^{36}Cl, coupled with solids, from the CAI formation region to distant chondrite forming regions must be invoked. Finally, the transported gaseous ^{36}Cl would have to be incorporated later into alteration assemblages. According to the local irradiation model [11], however, gases and small particles would be thrown into interstellar space with finite escape speeds, decoupled from the large CAIs that fell back to the disk. Therefore, the observation of ^{36}Cl in this study presents a serious challenge to the local irradiation models in which the irradiation takes place, and the CAIs form, very near the young Sun. Rather, it is more consistent the hypothesis that the solar system formed in proximity to a massive star which supplied the short-lived isotopes to the forming solar system when it went supernova [e.g., 13]

Unlike other short-lived radionuclides (*e.g.* ^{26}Al, ^{41}Ca, and ^{53}Mn), chlorine is a volatile element, and it is closely associated with secondary alteration observed in CAIs, chondrules and matrix. The timing (and location) is an important issue in understanding volatile-rock interactions commonly observed in most major components of primitive meteorites. Because of its short half-life, ^{36}Cl may serve as a new chronometer with fine resolution especially for low temperature events in the nebula and/or on asteroidal bodies. The mere observation of ^{36}Cl in sodalite suggests that secondary alteration of at least this CAI occurred relatively shortly after CAI formation. However, new work to follow up this discovery, analyzing Cl-bearing phases from other meteorite groups and in other petrographic settings, is needed. The data could reveal an important record of nebular and parent body alteration, help trace the earliest history of volatiles in our solar system, and shed light n the origin of the short-lived radionuclides in the solar system.

References: [1] E. Zinner (2003) *Science* **300**, 265. [2] Lin Y. et al (2004) *LPSC XXXV,* # 2084. [3] P. M. Endt (1990), *Nuclear Physics* **A521**, 1-830. [4] S. V. S. Murty et al. (1997) *Ap. J.* **475**, L65. [5] V. K. Rai et al. (2003) *GCA* **67**, 4435. [6] Y. Lin & M. Kimura, (1998) *MAPS* **33**, 435. [7] G. J. Wasserburg et al. (1998) *Ap. J.* **500**, L189. [8] R. Gallino et al. (2004) *New Astron. Rev.* **48**, 133. [9] M. Busso et al. (1999) *Ann. Rev. Astron. Astrophys.* **37**, 239. [10] I. Leya et al. (2003) *Ap. J.* **594**, 605. [11] F. H. Shu et al. (1996), *Science* **271**, 1545. [12] F. H. Shu et al. (1997) *Science* **277**, 1475. [13] J.J. Hester et al., (2004) *Science* **304**, 1116.

SIZE SORTING AND THE CHONDRULE SIZE SPECTRUM. Kurt Liffman[1, 2], [1]CSIRO/MIT P.O. Box 56, Highett, VIC 3190 AUSTRALIA, Kurt.Liffman@csiro.au, [2]Centre for Stellar and Planetary Astrophysics, Monash University, Clayton, VIC 3150.

Introduction: Since the first proposal in 1877 [1] there have been at least twenty different theories proposed for explaining the formation of the components, such as chondrules, that are observed in primitive meteorites [2].

In this paper, we investigate the jet flow model of chondrule formation. We assume that chondrules were formed in a bipolar jet flow that was produced by the interaction between primordial Sun and the inner edge of the solar nebula at the very earliest stages of the formation of the solar system. In this jet model [3-5], chondrules and refractory inclusions were formed and ejected from the inner solar nebula by a bipolar jet flow. In principle, a portion of the ejected particles can then travel across the face of the nebula, where the increase in the disk height allows some of the chondrules and refractory inclusions to reenter the outer regions of the solar nebula at hypersonic speeds [6].

The jet model can be used to investigate the observed size sorting of chondrules and metal grains within the primitive chondritic meteorites. If one compares the radii (a) and densities ( ) of metal or metal-troilite grains (which we denote by M) and silicate chondrules (denoted by C), it has been suggested that the equation

$$\rho_C a_C = \rho_M a_M \qquad (1)$$

is approximately true for some chondrite classes [7]. This and related findings, have been taken as evidence that the chondrules, metal grains and metal-troilite grains were aerodynamically size-sorted in the solar nebula [8], [9].

Why Use the Jet Model?: The jet flow model has produced a number of successful predictions. For example, Liffman [3] argued that chondrule formation occurred over a 10^6 to 10^7 year time scale. This has subsequently been verified (*e.g.*, [10]). Liffman [3] also argued that chondrules were produced by an ablation mechanism, where pre-chondrule droplets were produced by the shear interaction between a streaming gas flow and molten material. Kadono and Arakawa [11] experimentally tested this hypothesis and obtained a size spectrum of droplets that was similar to the chondrule size spectrum. They also obtained a required chondrule formation ram pressure of about 0.1 atm - similar to that given in [3]. Liffman and Brown [5] suggested that significant amounts of heated, refractory dust would have been formed in the outflow region and spread across the solar nebula. This prediction is consistent with the subsequent observed presence of annealed, crystalline dust in comets [12].

A constraint on the chondrule formation process is rim chronology, where igneous, coarse-grained rims are surrounded by fine-grained rims, but not the other way around [13]. In the jet model, igneous rims are formed at the base of the jet flow, while fine-grained rims are formed when the chondrule rams into the solar nebula [6], after the chondrule has been ejected from the jet flow. So, we should expect, and see, coarse-grained rims surrounded by fine-grained rims.

Suppose we adopt another chondrule formation model, *e.g.*, the shock model. A shock wave can, in principle, give the sequence of igneous rim followed by a fine-grained rim [14]. However, if the first shock wave were later followed by one or more weaker shocks then one might expect a sequence of transition rims where a fine-grained rim turns into a coarse grained rim. Such rims are not observed.

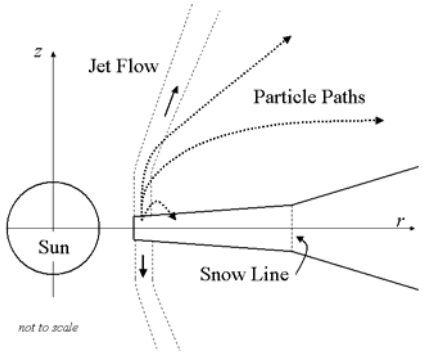

Figure 1: Schematic depiction of the model used in the Monte Carlo simulation. Particles are placed into the base of the outflow and ejected by the flow.

Results from the Monte Carlo Code: To investigate size sorting, we constructed a model solar nebula, complete with outflow. In this model, it was assumed that the protoSun had a mass equal to one solar mass and a radius equal to two solar radii. The outflow mass loss rate was set to 10^{-9} solar masses/year. A schematic of the system is shown in Figure 1.

The size spectrums of the metal and chondrule particles that are injected into the flow is shown in Figure 2. Particles were injected into the flow at 0.073 AU from the Sun and the average Fe/Si ratio was approximately solar.

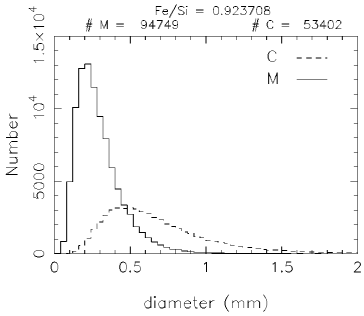

Figure 2: Initial size spectrum of silicate chondrules (C) (broken line) and metal grains (M) (unbroken line). In this simulation, 94,749 metal grains and 53,402 chondrules were injected into the flow.

Case 1, Constant Flow Speed: In our first example of the processing that occurs once material is ejected from the flow, we injected particles into an outflow with a set constant flow speed of 173 km s^{-1}, which was 1.5 times the Keplerian speed at the base of the flow. This type of flow produced significant size sorting (Figure 3), with Fe/Si ratios up to 1.7 times solar (Figure 4).

We suggest that this example may represent a possible formation scenario for CB chondrites,

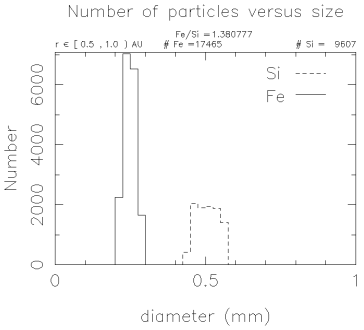

Figure 3: Size spectrum of particles that stop at a distance of 0.5 to 1.0 AU from the Sun.

which show strong size sorting and unusually high metal abundance.

Case 2, Variable Flow Speed: We set the outflow speed to be completely random between 115 and 254 km s^{-1}. For this case, size sorting disappeared, log-normal size distributions for both chondrules and metal grains were obtained for all distances from the Sun and the Fe/Si ratio was approximately solar (Figure 5).

The variable flow case may be more applicable to the ordinary chondrites, where the H, L and LL Fe/Si ratios may have been set by the chondrule precursor material.

For both the constant and variable flow rates, the number of particles stopping at a distance *r* from the Sun declined as a function of *r*. We suspect that this is a geometric effect.

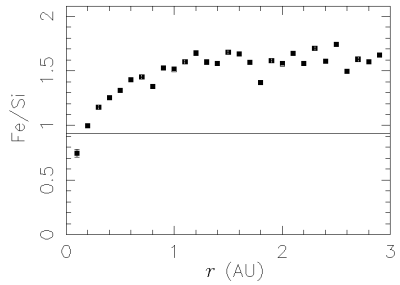

Figure 4: Fe/Si ratio versus distance from the Sun for the case of a constant speed jet flow. The unbroken line represents the solar Fe/Si ratio.

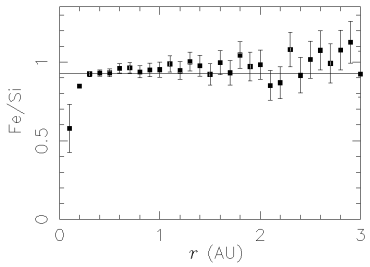

Figure 5: Fe/Si ratio versus distance from the Sun for the variable flow case.

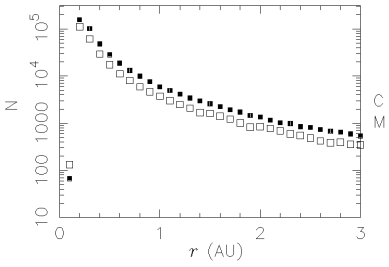

Figure 6: Number of chondrules and metal grains as a function of distance from the Sun.

References: [1] Sorby H. C.(1877) *Nature*,15, 495. [2] Grossman, J. N. (1988) *Meteorites and the Early Solar System*, 680. [3] Liffman, K. (1992) *Icarus,* 100, 608. [4] Shu F., et al. (1996) *Science*, 271, 1545. [5] Liffman, K. and Brown M.J.I. (1996) *Chondrules and the Protoplanetary Disk*, 285. [6] Liffman, K. and Toscano M., (2000) *Icarus*, 143, 106. [7] Skinner, W.R. and Leenhouts J. M. (1993) *LPSC* XXIV, 1315. [8] Dodd, R. T. (1976) *EPSL*, 30, 281. [9] Kuebler, K. E., *et al.* (1999) *Icarus*, 141. [10] Russell S. *et al.* (2005) *Meteorites and the Early Solar System II*, submitted. [11] Kadono T. and M. Arakawa (2004) *Icarus*, in press. [12] Nuth III J. A.(2001) *American Scientist*, 89, 228. [13] Grossman, J. N., *et al.* (1988) *Meteorites and the Early Solar System*, 619. [14] Connolly, H. C. Jr, and Love S. G. (1998) *Science*, 280, 62.

Comparative study of refractory inclusions from different groups of chondrites. Y. Lin[1], M. Kimura[2], B. Miao[1], and D. Dai[3]. [1]Institute of Geology and Geophysics, Chinese Academy of Sciences, Beijing 100029, China, linyt@mail.igcas.ac.cn. [2]Faculty of Science, Ibaraki University, Mito 310-8512, Japan. [3]Guangzhou Institute of Geochemistry, Chinese Academy of Sciences, Guangzhou, China.

Introduction: Previous study of refractory inclusions from the Ningqiang carbonaceous chondrite demonstrates that most inclusions are gas-solid condensation assemblages with bulk compositions following the predicted condensation trajectory [1]. Studies of refractory inclusions from enstatite chondrites [2-6], and those from unequilibrated ordinary chondrites (UOCs) [7] suggest similar sources of refractory inclusions to those in carbonaceous chondrites. As a part of our systematic study on refractory inclusions from various groups of chondrites, we report here the petrography and mineral chemistry of 24 refractory inclusions from 16 UOCs and 27 from 3 carbonaceous chondrites. Our preliminary results confirm a similar condensation origin of refractory inclusions in these meteorites.

Refractory inclusions from carbonaceous chondrites: Three new Antarctic carbonaceous chondrites, *i.e.* GRV 020025 (CM2), GRV 021579 (CO3) and GRV 022459 (CV3), have been studied in this work, with a total of 27 refractory inclusions found in three polished thin sections. The section of GRV 020025 contains 11 refractory inclusions. Six of the refractory inclusions (80-500 μm in size) are loose assemblages of concentrically zoned objects each having a fine-grained spinel core, a needle-shaped phyllosilicate mantle and a Ca-pyroxene rim. They are referred to as Type A-like inclusions, with assumption of phyllosilicates replacing pre-existing melilite. Another 4 refractory inclusions (70-240 μm in size) are also assemblages of concentric objects, each consisting mainly of a spinel core and a Ca-pyroxene rim. These inclusions are referred to as spinel-pyroxene-rich. In addition, one spinel spherule (80 μm in diameter) was found in GRV 020025. It contains predominant spinel, with minor perovskite enclosed in spinel and a thin and irregular rim of fine-grained alteration products. GRV 021579 contains similar types of refractory inclusions as GRV 020025, except for feldspathoids as main alteration products instead of phyllosilicates. Four of the refractory inclusions (50-170 μm in size) are referred to as Type A-like, with a core consisting of small grains of spinel in fine-grained alteration assemblages and a Ca-pyroxene rim. Other 8 refractory inclusions (80-300 μm in size) are spinel-pyroxene-rich, each having a spinel core and a Ca-pyroxene rim. Forsterite was found as an outermost layer in 3 of them. There is a spinel spherule (100 μm in diameter) in GRV 021579, too, which has a spinel-fassaite intergrown core and a Ca-pyroxene rim. GRV 022459 contains only three Type A-like inclusions (80-520 μm in size), consisting of spinel + melilite cores and Ca-pyroxene rims. Melilite is only partially replaced by fine-grained anorthite, feldspathoids, and hedenbergite.

Although almost all refractory inclusions in both GRV 020025 and GRV 021579 are heavily altered, spinel in these inclusions is typical of FeO-poor (<0.79 wt%, except for one analysis of 1.24 wt%). In contrast, spinel in the three refractory inclusions in GRV 021579, which are less altered than those in the other two meteorites, contains high FeO (up to 21 wt%), and is ZnO-bearing (<0.20 wt%). Ca-pyroxene rims have compositions of Al-rich diopside, and the Al_2O_3 content shows an increasing trend towards the cores of the refractory inclusions. The TiO_2 contents are less than 2.3 wt%, positively correlated with Al_2O_3.

Refractory inclusions from ordinary chondrites: A survey for refractory inclusions has been conducted on 16 polished thin sections of different UOCs, with discovery of a total of 24 refractory inclusions. These meteorites are 5 H-chondrites, 10 L-chondrites, and 1 LL-chondrite. Distribution of refractory inclusions is highly heterogeneous, with 7 refractory inclusions found in Y-791428 (H3), but none in other 8 chondrites (1 H-chondrite, 6 L-chondrites and the LL-chondrite). Similar to those in the above carbonaceous chondrites, most refractory inclusions (13 out of 24) in these UOCs can be referred to as Type A-like, consisting of small grains of spinel in fine-grained Na-rich matrix. However, the Ca-pyroxene rim is found only in two of them. Ten of other refractory inclusions are fragments of spinel, without Ca-pyroxene rims. Another refractory inclusion is a fragment of fassaite (~100 μm in size), with fine-grained spinel and perovskite at one side.

All grains of spinel in the refractory inclusions from these UOCs are typical of FeO-rich (13.2-25.3 wt%) and ZnO-bearing (0.49-2.01 wt%), and both are correlated. Many spinel grains contain high Cr_2O_3 (up to 23.5 wt%). The fassaite fragment is highly Al_2O_3-rich (23.0-23.6 wt%), with TiO_2 content increasing from 1.27 wt% at one side to 3.72 wt% at the other side that encloses spinel and perovskite.

Discussion

Alteration of refractory inclusions. Almost all refractory inclusions in both the UOCs and the carbonaceous chondrites are heavily altered. Melilite is one of the most common major minerals in Ca-Al-rich inclusions in carbonaceous chondrites, but only a few grains survived in GRV 022459 (CV3) and none in the other two carbonaceous chondrites neither in all UOCs. It is likely that melilite has been replaced by the fine-grained assemblages during alteration. Furthermore, the alteration seems related with the chemical groups of chondrites. The cccurrence of phyllosilicates in the refractory inclusions in GRV 020025 (CM2) is consistent with aqueous alteration reported in other CM chondrites [8]. Although alteration of the other refractory inclusions is typical of anhydrous, spinel is FeO-poor in GRV 021579 (CO3), FeO-bearing in GRV 022459 (CV3), and highly FeO-rich in all UOCs, suggestive of different oxygen fugacities of their forming locations in the solar nebula. This is consistent with the previous observations of refractory inclusions in ordinary chondrites [9] and enstatite chondrites [6].

Pre-altered assemblages of refractory inclusions. As discussed above, the absence of melilite in these refractory inclusions is likely due to secondary alteration. With this assumption, pre-altered mineral assemblages of the Type A-like inclusions could be melilite-spinel, similar to fluffy Type A inclusions [10]. This is consistent with the occurrence of small spinel grains in the alteration matrix, analogue to spinel grains enclosed in melilite in fluffy Type As. Different from the occurrence of spinel-pyroxene-rich inclusions in the carbonaceous chondrites, spinel fragments were found in the UOCs, probably due to collision loss of Ca-pyroxene rims of the latter. This is consistent with the common absence of Ca-pyroxene rims of Type A-like inclusions in the same meteorites. It is obvious that most of the refractory inclusions can be referred to as type A-like or spinel-pyroxene-rich, regardless of their different chemical groups. This observation and the previous results [1,6,9] demonstrate similar refractory inclusions in various groups of chondrites. Many differences (*e.g.* abundance and alteration assemblages) can be contributed to secondary processes (*e.g.* size-sorting, transportation, and alteration under different conditions).

Constraints on refractory inclusion formation. Our previous study of refractory inclusions in the Ningqiang meteorite demonstrates that most of them are non-molten, and have bulk compositions following the predicted condensation trajectory [1]. This is confirmed by the extended studies of refractory inclusions in UOCs [9] (and this work), enstatite chondrites [6] and carbonaceous chondrites (this work). Alternative origin of refractory inclusions is the X-wind model [11,12], which can explain the systematically different abundances of the short-lived nuclides between refractory inclusions and chondrules. However, refractory inclusions are referred to as evaporated residues by the X-wind model, inconsistent with the observation of predominant non-molten refractory inclusions in various groups of chondrites.

Recent discovery of the short-lived, now extinct ^{36}Cl in alteration assemblages in an anorthite-spinel-rich inclusion from the Ningqiang meteorite [13] has another serious challenge to the X-wind model. Allocation of the ^{36}Cl in the alteration assemblages (sodalite) indicates a later incorporation of gaseous ^{36}Cl into the refractory inclusion, requiring a complicated mechanism to transport gaseous ^{36}Cl together with the solid inclusion from near the proto-Sun region to a distant chondrite-accreting location without significant diluted.

Acknowledgements: Ten of the ordinary chondrite polished thin sections were supplied by the National Institute of Polar Research, Japan, and the other samples by the China Polar Research Center. This work was supported by the pilot project of knowledge innovation of Chinese Academy of Sciences (Grant No: KZCX3-SW-123) and the National Natural Science Foundation of China (Grant No. 40025311).

References: [1] Y. Lin & M. Kimura. *GCA.* 2003, **67**, 2251-2267. [2] Y. Guan, et al. *Science.* 2000, **289**, 1330-1333. [3] Y. Guan, et al. *EPSL.* 2000, **181**, 271-277. [4] T. J. Fagan, et al. *MAPS.* 2000, **35**, 771-781. [5] T. J. Fagan, et al. *MAPS.* 2001, **36**, 223-230. [6] Y. Lin, et al. *GCA.* 2003, **67**, 4935-4948. [7] M. Kimura, et al. *NIPR symp. Antarct. Met.* 2000, [8] G. J. MacPherson, et al. In *Meteorites and the early solar system* (*ed.* J. F. Kerridge and M. S. Matthews). 1988, 746-807. [9] M. Kimura, et al. *MAPS.* 2002, **37**, 1417-1434. [10] G. J. MacPherson & L. Grossman. *GCA.* 1984, **48**, 29-46. [11] F. H. Shu, et al. *Science.* 1996, **271**, 1545-1552. [12] F. H. Shu, et al. *ApJ.* 2001, **548**, 1029-1050. [13] Y. Lin, et al. *LPSC.* 2004, **35**, #2084.

IN SITU INVESTIGATION OF Mg ISOTOPE DISTRIBUTIONS IN AN ALLENDE CAI BY COMBINED LA-ICPMS and SIMS ANALYSES. M.-C. Liu[1], K. D. McKeegan[1] and E. D. Young[1,2]. [1]Dept. of Earth and Space Sciences, UCLA, Los Angeles, CA, 90095, (mcliu @ess.ucla.edu), [2]Inst. Geophys. Planet. Phys, UCLA, Los Angeles, CA, 90095

Introduction: The initial abundance of the short-lived radionuclide ^{26}Al (half-life = ~0.73 Ma) in the earliest formed rocks is an important parameter in theories for the origins of all extinct radionuclides in the solar nebula and for possibly developing a high-resolution chronology for solar system formation. For many years since the discovery [1]of the former presence of ^{26}Al in a Calcium-Aluminum-rich Inclusion (CAI) from the Allende meteorite, an initial ^{26}Al/^{27}Al initial ratio of ~5×10^{-5} has been thought to characterize wide regions of the solar nebula at the time of formation of the first solid materials [2]. This so-called "canonical" value has been observed in many CAIs from different meteorites, although most of the data are based on ion microprobe (SIMS) analyses of very Mg-poor minerals, such as anorthite. Recent analyses of Mg isotope compositions of whole CAIs by Inductively Coupled Mass Spectrometry (ICPMS) have suggested that a higher ^{26}Al/^{27}Al ratio of ~7×10^{-5} was closer to the true relative abundance of ^{26}Al at the time of CAI crystallization [3, 4, 5]. In this view, the previous canonical value reflects localized isotopic redistribution during CAI cooling or mild metamorphism several hundred thousand years after formation.

An important test of the intriguing suggestion by Galy and colleagues [3, 4, 5] would be to ascertain whether internal isochron(s) can be observed that might corroborate both the high initial ratio and subsequent disturbance of the Al-Mg system. Because the isotope shifts due to in-growth of radiogenic ^{26}Mg are small in minerals such as pyroxene and spinel, this approach requires high precision analyses. Such investigations have been undertaken independently using the in situ analytical capabilities of a Finnigan Neptune Laser-Ablation ICPMS [6] and a CAMECA ims 1270 Secondary Ion Mass Spectrometer (SIMS) [7,8]. Here we report a coordinated study of Al-Mg systematics in an Allende CAI using both LA-ICPMS and SIMS instruments.

Sample description and methods: Allende MC-1 is a Type-B CAI with small spinel crystals dispersed throughout the inclusion but concentrated around the outer margins, and large Ti-rich pyroxene and melilite (Åk$_{40}$ to ~Åk$_{65}$) crystals in the interior (Fig. 1). Anorthite is absent. The spherical shape of the ~4mm diameter CAI suggests that it crystallized from a melt droplet.

A thick section of MC-1 was prepared by embedding in epoxy and polishing with diamond paste. The methods for laser ablation ICPMS analysis are described by [4]. Sample ablation is achieved by a UV (213nm) laser with spot size ~50-100μm and a fluence of 20 J/cm^2 in a He carrier gas. Mg isotope compositions are referenced to the Dead Sea Mg (DSM3) scale [6] by rapid comparison with a forsterite standard. Because the ablation step is decoupled from ionization, the ICPMS delivers a constant instrumental mass fractionation independent of the mineral phase analyzed, thus it is possible to obtain highly precise and accurate analyses of mass fractionation inherent in CAI minerals.

Ion microprobe analyses were performed at high mass resolving power with a multiple-collector Faraday cup array using the UCLA CAMECA ims 1270. An oxygen primary beam was used to sputter shallow craters of ~20-25 μm diameter from 29 spots (6 spinel, 11 fassaite and 12 melilite) in MC-1. Instrumental mass fractionation is corrected by using Burma spinel and pyroxene glass standards and assuming an exponential mass fractionation law. Mass fractionation corrections for melilite are currently uncertain due to possible matrix effects and the lack of an appropriate standard, but these possible inaccuracies have no adverse effect on the calculation of radiogenic ^{26}Mg. For both ion probe and ICPMS analysis, Δ^{26}Mg* is calculated as δ^{26}Mg - δ^{25}Mg/0.519. Accuracy on Δ^{26}Mg* is comparable between the methods and is typically in the range of 0.1‰.

Results: As with most Type-B CAIs, Mg is mass fractionated favoring the heavy isotopes in the bulk of the CAI by ~6 to 8‰/amu relative to chondritic values. However, the degree of Mg isotope fractionation decreases toward the periphery of the CAI (Fig. 2), indicating exchange of Mg with an external reservoir probably by recondensation of Mg following initial evaporation during the molten stage of CAI formation. Similar behavior has been observed by LA-ICPMS analyses of other CV CAIs [6].

MC-1 shows well-resolved Δ^{26}Mg* excesses in spinel and pyroxene (fassaite) which are well-correlated with Al/Mg (Fig. 3). Melilite also displays Δ^{26}Mg*, but there is evidence for some isotopic disturbance. General agreement between both analysis methods is good. A fit to all data by ICPMS yields a slope equivalent to initial $(^{26}\text{Al}/^{27}\text{Al})_0=(6.3\pm0.8)\times10^{-5}$

with an intercept of 0.05‰ (within error of 0). A fit of the ion microprobe data on spinel and pyroxene, if forced through the origin, yields $(^{26}Al/^{27}Al)_0=(6.0\pm0.9)\times10^{-5}$ (all errors 1σ). Thus, both analysis techniques yield consistent apparent internal isochrons with higher than the traditional 'canonical' $^{26}Al/^{27}Al$ ratio, supporting the hypothesis by Galy and co-workers.

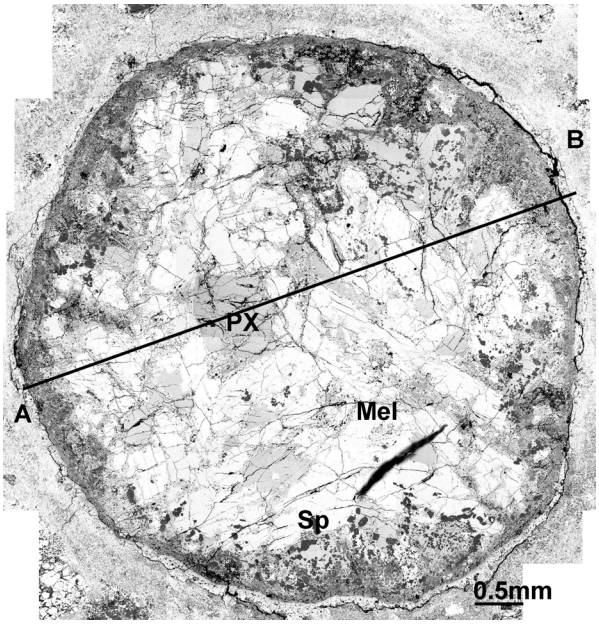

Fig 1. Back-scattered electron micrograph of Allende MC-1. The main constituents in this Type-B CAI are melilite (MEL), fassaite (PX) and spinel (SP).

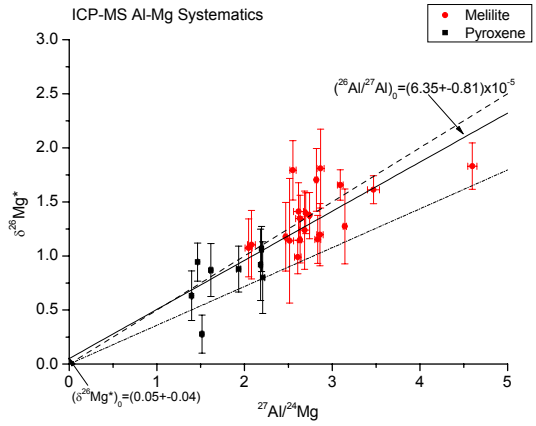

Fig 3. Al-Mg evolution diagram for MC-1 measured by LA-ICPMS. A best fit through all data yields a $^{26}Al/^{27}Al$ initial ratio of 6.35×10^{-5} and an intercept consistent with 0‰. Reference lines are shown corresponding to 7×10^{-5} and 5×10^{-5}.

References: [1] Lee, T. et al., (1976) *GRL, 3*: 41-44. [2] MacPherson G. J., et al. (1995) *Meteoritics* 30, 365-386. [3] Galy, A. et al., (2000) *Science* 290, 1751-1753. [4] Young et al., (2001) *GCA* 66, 983-698. [5] Galy, A. et al., (2004) *LPS XXXV,* Abstract #1790. [6] Simon, J. I. et al, (2004) *LPS XXXV,* Abstract #1668. [7] Taylor, D. J. et al., (2004) *MAPS 37*: A104. [8] McKeegan, K. D. et al., (2004) *MAPS 37*: A66.

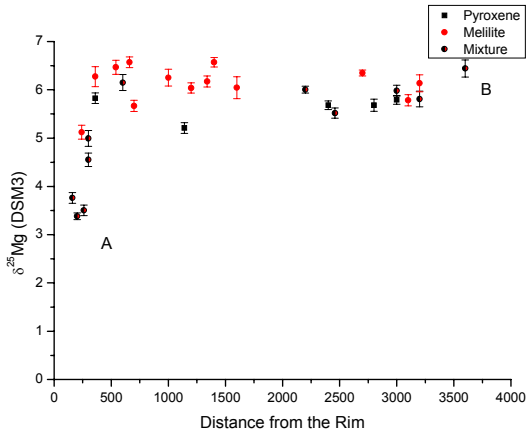

Fig 2. Mg isotope mass fractionation measured by LA-ICPMS in Allende MC-1 as a function of distance along the traverse A-B shown in Figure 1.

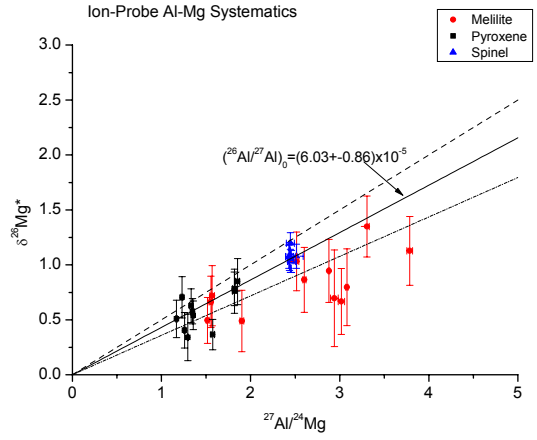

Fig 4. Al-Mg evolution diagram for MC-1 measured by ion microprobe. A best fit through spinel and pyroxene yields a $^{26}Al/^{27}Al$ initial ratio of 6.0×10^{-5} (forced through the origin). Reference lines are shown corresponding to 7×10^{-5} and 5×10^{-5}.

PHOTOCHEMICAL SPECIATION OF OXYGEN ISOTOPES IN THE SOLAR NEBULA. J. R. Lyons[1] and E. D. Young[1,2], [1]Institute of Geophysics and Planetary Physics, Center for Astrobiology, UCLA, Los Angeles, CA 90095-1567, jrl@ess.ucla.edu ; [2]Department of Earth and Space Sciences, UCLA, Los Angeles, CA 90095-1567.

Introduction:

Clayton proposed [1] that self shielding of CO at the X-point of the solar nebula was responsible for the formation of an ^{16}O-poor gas capable of shifting the oxygen isotopes of the rocky component of the inner solar system ~ + 50 ‰ in both ^{17}O and ^{18}O. In this proposed model the most refractory mineral phases (e.g., CAI's) retained their original (interstellar) isotope ratios, and isotope-selective self shielding of CO produced H_2O strongly depleted in ^{16}O. Because isotope-selective self shielding (ISSS) is a temperature dependent process, ISSS at the X-point would have been difficult if the gas temperatures were high [2,3]. ISSS is an excellent mechanism for the formation of distinct oxygen isotope reservoirs, especially in the surface region of the nebula [4-6] or in the parent molecular cloud [7].

We evaluated the self-shielding at the nebula surface by employing a one-dimensional photochemical model to compute time-dependent isotopomer mole fraction profiles. The model has been extended from an earlier version [6] to include a large number of gas-phase and ionic compounds, as well as gas-grain reactions. This extension is necessary to place the present model within the context of existing disk chemistry work [8,9], and allows us to explore isotopic evolution and the O/ ^{18}O ratio of many components of the nebular gas. Radiative transfer is treated in one-dimension only, namely along the normal axis of the disk, rather than along the path from the central protostar. This simplification greatly reduces computational requirements without sacrificing any of the fundamental physical processes, and is likely a fair representation of photodissociation via enhanced far ultraviolet (FUV) radiation in a star-forming region.

Photochemistry in a one-dimensional disk:

We utilized the analytical flared-disk model of Aikawa and Herbst [8] which describes the two-dimensional distribution of H nuclei. Here we present results evaluated at a distance of R = 30 AU from the protosun, where the temperature is 51 K and the H_2 number density is 5 x 10^{10} cm^{-3} in the midplane. We assumed a solar composition nebula for which CO/H_2 = 2 x 10^{-4} by mole.

Non-mass dependent fractionation occurs during photolysis of CO isotopomers:

$$C^{16}O + h\nu \rightarrow C + {}^{16}O$$
$$C^{17}O + h\nu \rightarrow C + {}^{17}O$$
$$C^{18}O + h\nu \rightarrow C + {}^{18}O$$

where photodissociation occurs in the wavelength range 91.2 to 110 nm in the presence of abundant hydrogen [10]. The gas-phase species included are

$$H_2, H, CO, C, CH, CH_2, CH_3, CH_4,$$
$$C_2H, C_2H_2, C_2H_4, C_3H_m, C_4H_n,$$
$$O, OH, H_2O, O_2, HCO, H_2CO, CO_2, CH_3OH$$

and the ion species are

$$C^+, CH_2^+, CH_3^+, CH_5^+, C_2H_3^+, C_3H_m^+, HCO^+, H_3O^+$$

All gas-phase species also exist as molecules bound to grain surfaces. Molecular binding energies to ice-coated grain surfaces are taken from previously published disk models (e.g., [9]). The anomalous fractionation produced during CO photolysis is passed to other oxygen-containing molecular species during chemical reactions.

To follow the time evolution and vertical distribution of molecules in the disk, we solved the coupled one-dimensional continuity and flux equations for each species:

$$\frac{\partial f_i}{\partial t} = \frac{1}{n}\frac{\partial}{\partial z}\left(\nu_t n \frac{\partial f_i}{\partial z} \right) + \frac{P_i}{n} - L_i f_i$$

where f_i is the mole fraction of species 'i', n is the number density of the background gas (mostly H_2), z is the height above the disk midplane, and t is time measured from the initiation of FUV radiation on the disk. Vertical motion is characterized by the turbulent viscosity, $_t$ = cH, where c is the sound speed and H is the vertical scale height in the nebular gas, and $\alpha \leq 1$ is a free parameter commonly used in disk models to describe the strength of turbulent mixing. The vertical scale height is H ~ 0.1R. P_i and L_i are the production rate (molecules cm^{-3} s^{-1}) and loss rate (molecules s^{-1}), respectively, for species 'i'.

To quantify the effects of self and mutual shielding (i.e., shielding of one isotopomer by another), we employed the results of van Dishoeck and Black [10] developed for molecular clouds in the interstellar medium (ISM). Using fits to their derived shielding functions, expressions for the photodissociation rate constant (L_i) for each isotopomer may be determined (not shown here). The effects of dust opacity and absorption by H_2 are also included.

Results:

For a radial distance of 30 AU (51 K), the model was run from time zero to 10^7 years for a range of values of and FUV multiplying factor. Figure 1 (below) shows the time evolution of O and O of several species at the disk midplane for $= 10^{-2}$ and 10 x FUV. Figure 1 demonstrates the formation of ^{16}O-poor O and ^{16}O-rich molecules due to self CO photodissociation.

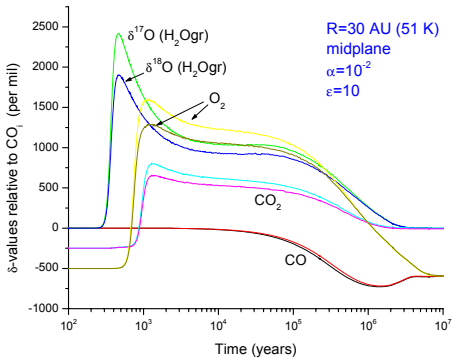

Conversion of photoproduct O to H_2O occurs by reactions on grain surfaces and by ion-molecule reactions. If we add the photodissociation-derived H_2O to the complement of H_2O expected in the collapsing molecular cloud (which has initial isotope values of –50 ‰, -50‰), we obtain the total nebular H_2O. Figure 2 (below) shows the resulting $^{17}O_{smow}$ for total nebular H_2O versus time for a range of FUV fluxes (each curve is labeled with the FUV multiplying factor). The shaded region of the figure shows the range of ^{17}O of initial water (or gas) inferred by Clayton and Mayeda [11] and by Young [12] from analyses of carbonaceous chondrites. For $= 10^{-2}$ an FUV flux ~ 10 x modern sun is optimal for ages < 0.5 Ma. Higher FUV fluxes dissociate too much C^{16}O, reducing the magnitude of the fractionation. For $\alpha \leq 10^{-4}$ all curves fall below the shaded region implying that vigorous mixing was required in the nebula.

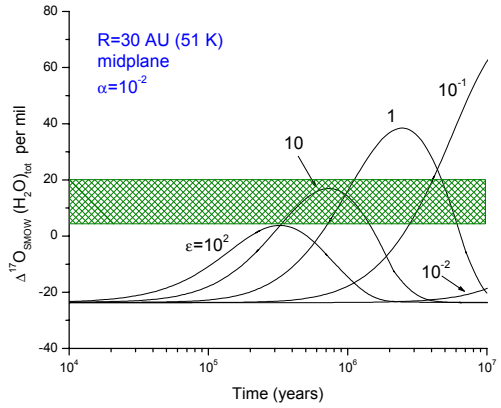

On a 3-isotope plot (not shown), it is seen that lines of slope ~ 1.05 – 1.10 are produced. This results from the model assumption that self shielding by C^{17}O and C^{18}O differs only by the column abundance of these two isotopomers. In making this assumption we have neglected potential line-by-line differences in the absorbing character of the individual isotopomers.

Conclusions: We have used a one-dimensional photochemical model to demonstrate that CO self shielding could have produced mass-independent fractionation in nebula H_2O consistent with that required by analyses of carbonaceous chondrites. The model results are strongly dependent on the vigor of vertical mixing and on the FUV flux incident on the disk. It has not yet been demonstrated that a fractionation line of slope between .95 and 1.0 is produced by CO photodissociation.

References: [1] Clayton R.N. (2002) *LPSC XXXIII,* abstract #1326. [2] Lyons J.R. and Young E.D. (2003) *LPSC XXXIV,* abstract #1981. [3] Navon O. & Wasserburg G.J. (1985), *EPSL 73*, 1-16. [4] Lyons J.R. (2002), *Astrobiology 2*, 532. [5] Young E.D. and Lyons J.R. (2003) *LPSC XXXIV,* abstract #1923. [6] Lyons J.R. and Young E.D. (2004) *LPSC XXXV*, abstract #1970. [7] Yurimoto H. and Kuramoto K. (2002) *Met. Soc*. Abs. # 5149. [8] Aikawa Y. and Herbst E. (1999) *Astron. Astrophys., 351*, 233-246. [9] Willacy K. et al. (1998), *Astron. Astrophys. 338*, 995-1005. [10] van Dishoeck E.F. and Black J.H. (1988) *Astrophys. J., 334,* 771–802. [11] Clayton R.N. and Mayeda T.K. (1984) *Earth Planet. Sci Lett., 67,* 151-161. [12] Young E.D. (2001) *Phil. Trans. R. Soc. Lond. A., 359*, 2095-2110.